Project Review Committee

Each research project will have an advisory committee appointed by the LTRC Director. The Project Review Committee is responsible for assisting the LTRC Administrator or Manager in the development of acceptable research problem statements, requests for proposals, review of research proposals, oversight of approved research projects, and implementation of findings.

The dedication and work effort of the following Project Review Committee members to guide this research study to fruition are acknowledged and appreciated.

LTRC Administrator/ Manager
Zhongjie "Doc" Zhang
Pavement & Geotechnical Research Administrator

Members
Mark Morvant, DOTD
Kim Martindale, DOTD
Artur D'Andrea, DOTD
Murad Abu-Farsakh, DOTD
Michael B Boudreaux, DOTD
Mark Stinson, FHWA
Walid R. Alaywan, DOTD

Directorate Implementation Sponsor
William T. Temple
DOTD Chief Engineer

TECHNICAL REPORT STANDARD PAGE

1. Report No.	2. Government Accession No.	3. Recipient's Catalog No.
FHWA/LA.05/403		

4. Title and Subtitle	5. Report Date
Determination of Interaction between Bridge Concrete Approach Slab and Embankment Settlement	July 2005
	6. Performing Organization Code
7. Author(s)	8. Performing Organization Report No.
C. S. Cai, George Z. Voyiadjis, Xiaomin Shi	
9. Performing Organization Name and Address	10. Work Unit No.
Department of Civil Engineering Louisiana State University Baton Rouge, Louisiana 70803	11. Contract or Grant No. LTRC Project No. 03-4GT State Project No. 736-99-1149
12. Sponsoring Agency Name and Address	13. Type of Report and Period Covered
Louisiana Transportation Research Center 4101 Gourrier Avenue Baton Rouge, LA 70808	**Final Report** February 2003-July 2005
	14. Sponsoring Agency Code

15. Supplementary Notes

16. Abstract

The main objective of this research is to correlate the deformation and internal force of the approach slab with the approach embankment settlements and the approach slab parameters such as length and thickness. Finite element analysis was carried out in the present study. This correlation will be used to evaluate the effectiveness of approach slabs and develop guidelines for their structural design. This information will also help determine when settlement controls are necessary. While flat approach slabs may be used for some short span applications, longer span lengths would require very thick slabs. In such cases, ribbed approach slabs (similar to slab-on-beam bridge decks) are proposed in the present study because they provide advantages over the flat slabs. Based on finite element analysis, internal forces and deformations of ribbed slabs were predicted and their designs were conducted.

In addition, special studies on a few issues that were not included in the original scope of work were conducted. These special studies including investigating (1) the skew angle effects and the applicability of the developed methodology for right approach slabs to skewed approach slabs; (2) the failure mode/mechanism of the approach slab end and the abutment connection; (3) the applicability of the developed methodology to AASHTO LRFD highway loads; and (4) rating of the developed approach slabs in terms of special trucks.

17. Key Words	18. Distribution Statement
Approach span, differential settlement, finite element analysis, bridge rating, slab design	**Unrestricted. This document is available through the National Technical Information Service, Springfield, VA 21161.**

19. Security Classif. (of this report)	20. Security Classif. (of this age)	21. No. of Pages	22. Price
N/A	N/A	150	N/A

Determination of Interaction between Bridge Concrete Approach Slab and Embankment Settlement

by

PI: C. S. Cai, Ph.D., P.E.

Co-PI: George Z. Voyiadjis, Ph.D.

Research Assistant: Xiaomin Shi

Department of Civil Engineering

Louisiana State University

Baton Rouge, Louisiana 70803

LTRC Project No. 03-4GT

State Project No. 736-99-1149

Conducted for

Louisiana Department of Transportation and Development

Louisiana Transportation Research Center

July 2005

ABSTRACT

Soil embankment settlement causes concrete approach slabs of bridges to lose their contacts and supports from the soil. When soil settlement occurs, the slab will bend in a concave manner that causes a sudden change in slope grade near its ends. Meanwhile, loads on the slab will also redistribute to the ends of the slab, which may result in faulting across the roadway at the pavement end of the approach slab. Eventually, the rideability of the bridge approach slab will deteriorate. State Departments of Transportation (DOTs) are spending millions of dollars each year to deal with problems near the ends of approach slabs.

The main objective of this research is to correlate the deformation and internal force of the approach slab with the approach embankment settlements and the approach slab parameters such as length and thickness. This correlation will be used to evaluate the effectiveness of approach slabs and develop guidelines for their structural design. This information will also help determine when settlement controls are necessary.

To investigate the effect of embankment settlements on the performance of the approach slab, a 3-D finite element analysis was conducted to examine the interaction between the approach slab and the embankment soil, and, consequently, the separation of the slab and soil. By analyzing the results obtained from a parametric study, this research established a correlation among the slab parameters, deflections of approach slabs, internal moments of the slab, and the differential settlements. The predicted internal moments of the approach slab make it possible to design the approach slab considering different levels of embankment settlements. A proper design of the approach slab will help mitigate the rideability problems of the slab. Current AASHTO code specifications do not provide clear guidelines to design approach slabs considering the embankment settlements *[1], [2]*.

While flat approach slabs may be used for some short span applications, longer span lengths would require very thick slabs. In such cases, ribbed approach slabs (similar to slab-on-beam bridge decks) are proposed in the present study because they provide advantages over the flat slabs. Based on finite element analysis, internal forces and deformations of ribbed slabs were predicted and their designs were conducted.

In addition, special studies on a few issues that were not included in the original scope of work were conducted. These special studies including investigating (1) the skew angle effects and the applicability of the developed methodology for right approach slabs to skewed approach slabs; (2) the failure mode/mechanism of the approach slab end and the abutment connection; (3) the applicability of the developed methodology to AASHTO LRFD highway loads; and (4) rating of the developed approach slabs in terms of special trucks.

ACKNOWLEDGMENTS

The investigators appreciate the Louisiana Transportation Research Center (LTRC), Louisiana Department of Transportation and Development, for funding this project.

The investigators also want to express their thanks to the entire project committee and those who provided help during the development of the research program.

Special thanks go to Project Manager, Dr. Zhongjie "Doc" Zhang, for his guidance during the process of this project; Mr. Mark Morvant, Associate Director, LTRC, for carefully reviewing the draft report, and Mr. Artur D'Andrea and Ms. Zhengzheng Fu, DOTD bridge engineers, for their very constructive commends and suggestions for this research.

IMPLEMENTATION STATEMENT

The developed methodology, findings, and design aids are targeted at the Louisiana Department of Transportation and Development (LADOTD) design guidelines/specifications and, therefore, the audience will be state highway engineers and professional consulting engineers. The researchers observed that an impediment to successful implementation could be that these engineers may not be willing to sacrifice simplicity for accuracy. Keeping this in mind, the research team has made a reasonable balance between simplicity and accuracy in developing practical formulae/design aids.

The research results have been presented to professional conferences and peer reviewed journals and have received good feedback/comments. The state structural and geotechnical engineers may take a leadership role in implementing the findings into design guidelines. Effort may also be made to introduce the methodology to AASHTO specifications that do not have specific guidelines for designing approach slabs considering differential settlements.

For flat approach slabs with a span length of 20 ft., the major reinforcement (bottom layer in the span direction) should be changed to #7@6". For flat approach slabs with a span length of 40 and 60 ft., the major reinforcement (bottom layer in the span direction) should follow table 16. For ribbed approach slabs with a span length of 60 and 80 ft., the reinforcement of the beam should follow table 21.

The connection detail between the approach slab and the abutment should be changed if a large embankment differential settlement (e.g., more than 6 in.) is expected in order to avoid damage near the connection area. The researchers also recommend removing or loosening those anchoring bolts after the construction and changing the layout of the dowel rebar. The decision to remove the anchoring bolts should also be based on the deformation requirement of the joint; however, information is not currently available on the deformation requirement.

This research is purely based on finite element analysis. Therefore, further field evaluation may be needed to confirm the findings.

TABLE OF CONTENTS

LIST OF TABLES

LIST OF FIGURES

INTRODUCTION

Background

Bridge approaches in Louisiana are normally constructed with reinforced concrete slabs that connect the bridge deck with the adjacent paved roadway. Their function is to provide a smooth transition between the bridge deck and the roadway pavement. However, complaints about the ride quality of bridge approach slabs still need to be resolved. The complaints usually involve a "bump" that motorists feel when they approach or leave bridges. Field observations indicated that either faulting near the slab and the pavement joint or a sudden change in the slope grade of the approach slab (as shown in figure 1) causes this "bump." The faulting and change of slope are partly due to the bending of the slab as the embankment settles *[3]*.

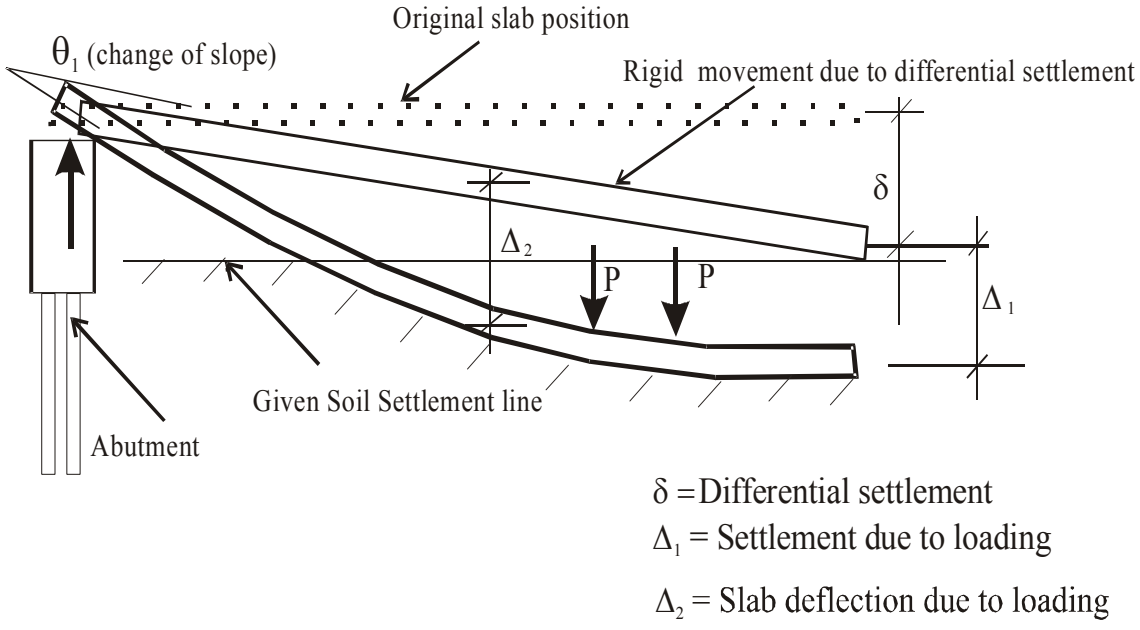

Figure 1

Illustration of approach slab and its interaction with soil

Concrete approach slabs can lose their contacts and supports from soil due to various reasons. The major reason is the settlement of embankment soil on which the slabs are built (figure 1). When settlement occurs, the slabs will bend in a concave manner that causes a sudden change in the slope grade of the approach slab. Traffic load and the self-weight of the

slab will also redistribute to the ends of the slab and vertical faulting or bump across the roadway may occur. Eventually, the rideability of the bridge approach slabs will deteriorate.

Although the bump-related problems have been commonly recognized and the causes identified, no unified engineering solutions have emerged, primarily because of the number and complexity of the factors involved.

LADOTD has launched a major effort to solve this problem by changing the design of approach slabs where differential settlement is expected. The objective is to find a feasible solution that allows the approach slabs to be strong enough to lose a portion or all of their contact supports without detrimental deflection. In this solution, the flexural rigidity (EI) of the approach slabs will be increased by increasing the moment of inertia at the slab's cross sections, therefore allowing some embankment settlement without a decrease in ride quality. This solution requires a thorough understanding of the interaction among bridge approach slab, bridge abutment, and underneath embankment settlement.

The main objective of this research is to establish correlations, such as that between the approach embankment settlement and the approach slab's faulting and deflection. This research also seeks to help LADOTD design engineers develop a solution to resolve the stated problem.

Literature Review

Several comprehensive studies on approach slab performance have been sponsored over the years by various state Department of Transportation (DOTs). A study conducted at the California DOT by Stewart identified the original ground subsidence and fill settlement as primary causes of approach maintenance problems *[4]*. The resulting recommendations included using select fill material for a distance of 150 ft. from the bridge, waterproofing the approach embankment, and using approach slabs 30 ft. long. The proposed approach slab should be doweled into the backwall to ensure a watertight joint. In addition, the slab should be cantilevered over the wingwalls to minimize surface water infiltration.

A study conducted by the Washington State DOT summarized findings from various state DOTs and recommended guidelines for the use and construction of approach slabs *[5]*. While promoting the use of approach slabs in general, the researchers recommended that a design geotechnical engineer be responsible for assessing the need on a site-specific basis. The study also called for the use of select granular fill and stringent inspections of the placement and compaction of the abutment backfill. The main causes of bridge approach distress were traced to consolidation of foundation soils, compression of embankment fill, and a localized soil settlement near the approach-abutment interface attributable to inadequate compaction.

Research conducted by Mahmood indicated that the type of abutment affects the magnitude of approach settlement *[6]*. The study recommended the use of various ground improvement techniques, including wick drains and surcharging, to mitigate the foundation soil settlement. The use of lightweight fill materials was also proposed as a means of reducing the vertical loading exerted on the foundation soil.

Wahls summarized that the performance of a bridge approach is affected by the design and construction of the bridge abutment and foundation *[7]*. The major bridge-approach problems are directly related to the relative settlement of the approach slab and the bridge abutment. The causes of bridge-approach settlements are one or more of the following: time-dependent consolidation of the embankment foundation, time-dependent consolidation of approach embankment, poor compaction of abutment backfill caused by restricted access of standard compaction equipment, erosion of soil at the abutment face, and poor drainage of the embankment and abutment backfill. Hence, the approach-slab design and the type of abutment and foundation affect the performance of the approach slab. The differential settlement can be minimized by the sequence of construction of the embankment, approach pavement, abutment, and superstructure. The design of the approach slab may minimize the effects of the embankment settlement on the performance of the bridge-approach system.

Chini et al. summarized critical items in the design and construction of bridge approaches *[8]*. They recommended particular materials and construction techniques for approach embankments. These recommendations included removal and replacement of compressible

foundation soils, dynamic compaction, surcharging, use of select borrow fill material, and minimum compaction requirements of 95 percent of the Standard Proctor, along with increased construction inspection.

A NCHRP synthesis report on the settlement of approach slabs recommended more stringent requirements for fill material specifications and inspection practices *[9]*. The study concluded that close cooperation among geotechnical, structural, pavement, construction, and maintenance engineers correlates with lower reported incidences of excessive approach settlement. The synthesis identified some factors that tend to minimize the bump, such as abutment and embankment on strong soil, a long approach slab, well-compacted fills or stabilized fills, appropriate fill material, effective drainage, low embankments, good construction practice and inspection, and adequate waiting period between fill placement and paving. The study also concluded that the use of approach slabs minimizes or eliminates the problem of the bump.

Hoope conducted a literature review regarding issues involved in using, designing, and constructing approach slabs *[10]*. The research emphasized that the presence of an approach slab has no effect on the magnitude of differential settlement. The study summarized the practice of various DOTs regarding the use, design, and construction of approach slabs and compared them with those used by the Virginia Department of Transportation. It cited that half of the respondents quoted a commonly used slab length of 20 ft. with a thickness ranging from 8 to 17 in. The study also concluded that every DOT uses unique criteria that govern the use, design, and construction of bridge approach slabs. Other research projects were also carried out by different investigators *[11], [12],[13],[14],[15]*.

Recently, Nassif et al. conducted a numerical analysis on New Jersey's approach and transition slabs by using springs to simulate the interaction of soil and structure *[17]*. The study identified the probable causes of approach slab cracking, location of cracks, and factors influencing cracks development and recommended new design alternatives that could reduce or eliminate crack in bridge approach and transition slabs. The research concluded that, among the parameters that affect the cracking as well as the overall behavior of the approach

and transition slabs (i.e. (1) concrete compressive strength, f_c', (2) the steel rebar yielding stress, f_y, (3) the steel rebar nominal cross sectional area, A_s, (4) the concrete slab thickness, and (5) soil settlement or void development), slab thickness is the most effective parameter in reducing the tensile stresses in the critical elements. The researcher also provided some new design proposals for NJDOT: (1) constant thickness of the approach slab and (2) embedded beams design. The soil structure interaction was modeled by linear springs, and the soil settlement in the model was simulated by removing springs from various locations. However, the spring model of soil structure interaction cannot simulate the contacting and separating process due to the slab deformation caused by external loads.

Briaud et al. recommended a maximum allowable change in approach slope of 1/200 *[18]*, based on studies by Wahls *[7]* and Stark et al. *[11]*. Long et al. also proposed a relative gradient of less than 1/200 to ensure rider comfort and a gradient of between 1/100 and 1/125 as a criterion for initiating remedial measures *[19]*.

In summary, the majority of the previous research can be categorized as (1) syntheses of practice, (2) identification of the sources of differential settlement, (3) soil improvement, and (4) numerical analysis. The previous numerical study of the interaction between approach slab and embankment modeled by spring cannot simulate the real interaction of soil and the deformed slab due to dead load and truck load.

There are no guidelines in the AASHTO code specifications regarding the structural design of approach slabs. The LADOTD design manual specifies minimum reinforcement requirements, but it does not specify how to conduct the structural design. Therefore, there is a need to establish design alternatives with construction guidelines to mitigate the problem.

OBJECTIVE

The main objective of this research is to correlate the deformation and internal force of the approach slab with the approach embankment settlements and the approach slab parameters such as length and thickness. This correlation will be used to evaluate the effectiveness of approach slabs and develop guidelines for their structural design. This information will also help determine when settlement controls are necessary.

As stated earlier, the “bump”-related problem is a complicated phenomenon. Consequently, another objective is to better understand the mechanism of the formation of the bumps and faulting. The research results will help develop an instrumentation and field monitoring scheme that will be used to verify the established correlation and eventually lead to the solution of the stated problem.

SCOPE

The scope of this research is divided into the following four parts.

Literature review: The current practice regarding the interaction among bridge approach slab, bridge abutment, and embankment settlement as well as the related topics were examined and reviewed to better understand the mechanism of the formation of the bumps and faulting. Analytical modeling techniques of soil were also reviewed in this task.

Investigation of Interaction between Embankment Settlement and Approach Slab: Using a three dimensional (3-D) finite element model, the interaction between the slab and the supporting embankment was analyzed and the mechanism and magnitude of the slab's deformation was determined. Meanwhile, the effects of differential settlements on the performance of approach slabs, excessive stress distribution of embankment soil, and approach slab design were also analyzed. In addition, a parametric study was conducted by changing the slab section thickness and span length in order to establish the relationship between the slab parameters and the differential settlements.

Development of Design Aid: Based on the results from the parametric study, a correlation among the slab parameters (including length and thickness), deflection of approach slabs, internal moments of the slab, and the differential settlements between abutments and their approach embankment was established.

Ribbed Approach Slab: Flat approach slabs may be used for some short span applications. However, a large span length would require a very thick slab. In such a case, ribbed approach slabs (similar to slab-on-beam bridge decks) are proposed in the present study because they provide advantages over the flat slab. The ribbed approach can also be hopefully used to replace

the current pile-supported approach slab (PSAS) for some span ranges. Based on the 3-D finite element analysis, internal force and deformation of ribbed slab were predicted. The predicted internal forces provide design engineers a scientific basis to properly design the approach slab considering different levels of embankment settlements.

In addition, special studies on a few issues that were not included in the original scope of work were conducted. These special studies including investigating (1) the skew angle effects and the applicability of the developed methodology for right approach slabs to skewed approach slabs; (2) the failure mode/mechanism of the approach slab end and the abutment connection; (3) the applicability of the developed methodology to AASHTO LRFD highway loads; and (4) rating of the developed approach slabs in terms of special trucks.

METHODOLOGY

The present finite element analysis simulates the interaction of the approach slab and the embankment soil by assuming a given differential settlement of embankment, as shown in figure 1. The actual embankment settlement will be determined on a case-by-case basis for each specific bridge. Since the left end of the slab sits on the relatively stiffer abutment and the right end on the relatively weaker soil or sleeper slab, the assumed differential settlement results in a linear gap (with a triangle shape) between the approach slab and the embankment soil.

Interaction between Approach Slab and Embankment Soil

Finite Element Modeling

Geometry Models. Before using the finite element modeling, embankment geometry, abutment type, embankment fill type, and approach slab type need to be studied and particular geometries and configurations decided. These parameters are determined by the LADOTD design specifications or common practice in the State of Louisiana. A typical configuration of a concrete abutment constructed on a cut slope embankment used in the present study is shown in figure 2.

In this 3-D finite element analysis, 20, 40, and 60 ft. long approach slabs were studied. Flat slabs were used for simpler applications. The width of slab, which is typically 40 ft., is fit for a typical two-lane highway. A sleeper slab, which provides an additional transition to the roadway pavement, as shown in figure 2, is used in this model to minimize the possibility of differential settlement at the approach slab-roadway interface.

The dimensions of the approach slab, sleeper slab, abutment, embankment, and subgrade soil are defined in figure 2 and listed in tables 1 and 2. The sleeper slab dimensions (4 ft. in width and 2 ft. in thickness) are larger than the current ones in Louisiana (3 ft. in width and 1 ft. in thickness) since larger force is expected. However, actual sizes need to be designed/checked once the

reaction forces are available, which is not within the scope of this work. The dimensions of L5, W2, and H5 will be decided based on a sensitivity study through a finite element analysis.

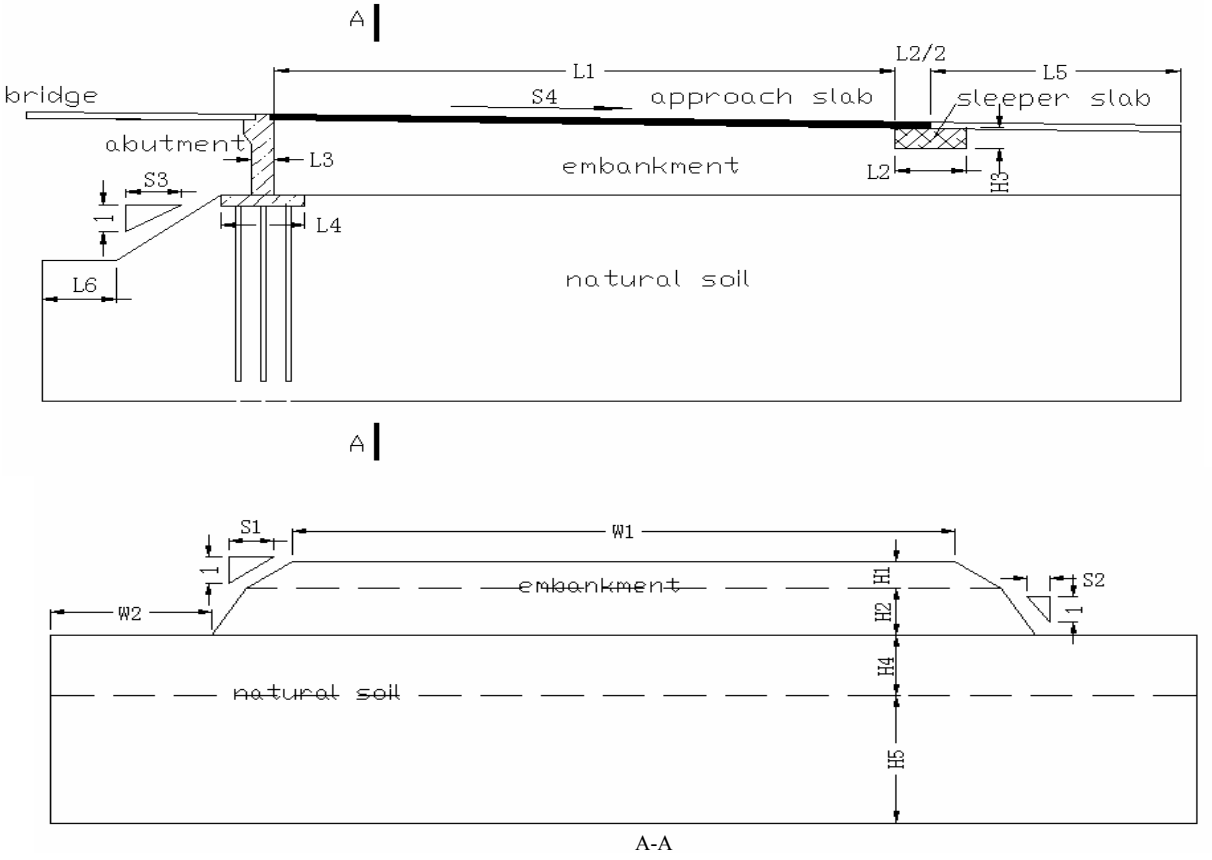

Figure 2
Sketch of bridge abutment

Table 1
Dimension of approach slab, sleeper slab and abutment

	approach slab		sleeper slab		Abutment	
	L1(ft.)	S4	L2(ft.)	H3(ft.)	L3(ft.)	L4(ft.)
Range	40, 60	2%	4	2	2	4

Table 2
Dimension of embankment and natural soil

Embankment Soil						Natural Soil				
W1(ft.)	H1(ft.)	H2(ft.)	S1	S2	L5	W2(ft.)	H4(ft.)	H5(ft.)	S3	L6
45	4	5	6	4	-	-	5	-	2	10

A 3-D finite element model was established as shown in figure 3. Eight-node hexahedron elements (ANSYS© Solid 45) were used to form the finite element mesh. A contact and target pair surface element available in the ANSYS© element library was used to simulate the interaction between the soil and slab. This surface element is a compression-only element and can thus model the contacting and separating process between the slab and soil *[20]*. When the soil is in tension, the slab and soil will separate automatically.

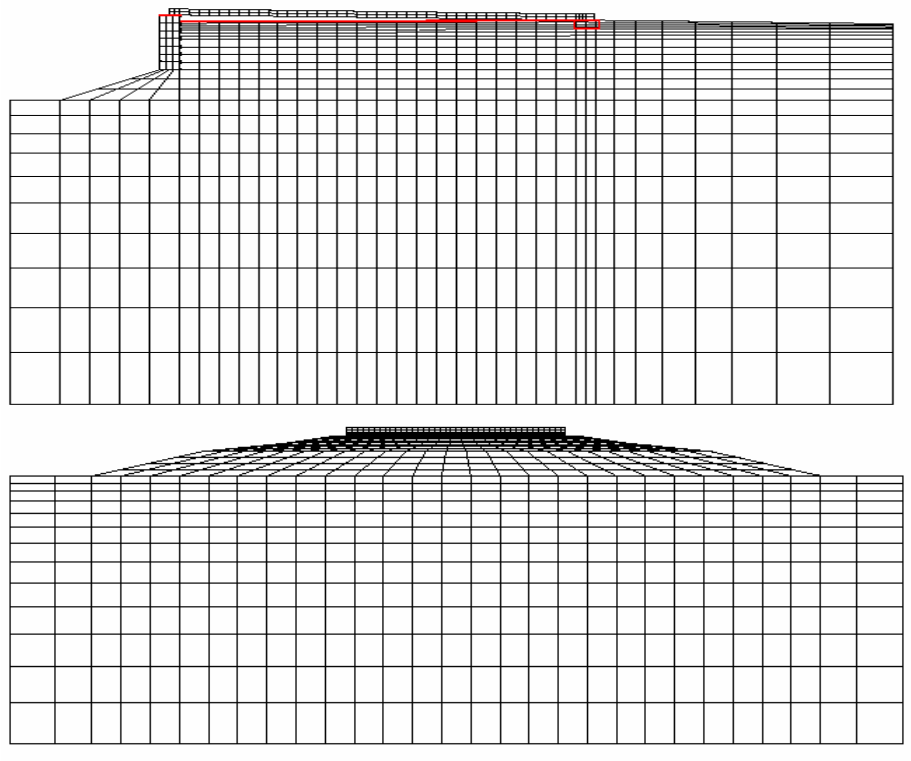

Figure 3
Typical finite element mesh

Material Models and Parameters: The soil profile under the approach slab consists of compacted embankment and silty clay subgrade soil, which is typical for Louisiana. The elastoplastic model is used to characterize the soil response under dry conditions. The Drucker-Prager (DP) material model is applicable to granular (frictional) material such as soils, rock, and concrete. The Drucker-Prager model is used to define the yield criteria for both embankment soil and subgrade soil in the following form:

$$f(I_1, J_2) = \sqrt{J_2} - \alpha I_1 - k = 0 \quad (1)$$

where I_1 and J_2 are the first invariant and second deviatoric invariant of the stress tensor, and α and *k* are material constants, which are related to the constants C and φ. The C and φ are material parameters that represent the cohesion coefficient and internal friction angle, respectively, and can be determined from test results.

Soils used as embankment fill in Louisiana should satisfy the LADOTD design specifications as follows *[21]*:

Usable Soils: Usable soils shall have a PI of 25 or less, an organic content of 5 percent or less and a maximum silt content of 65 percent.

Selected Soils: Selected soils are natural soils with a maximum PI of 20, maximum Liquid Limit of 35, a maximum organic content of 5 percent, and a maximum silt content of 65 percent.

Headers: Headers are that portion of the embankment within 500 feet (150 m) of a bridge end. Headers shall be constructed for their full height with usable soils having a minimum PI of 12 and a maximum PI of 25. No lime treatment to the soil to meet the PI requirements will be permitted.

According to the two soil classification systems-AASHTO and USCS, soils mentioned above can be classified into the types indicated in table 3.

Table 3
Soil classification

		Usable soil	Selected soil	Headers
PI		≤25	≤20	12≤PI≤25
LL			≤35	
Silt Content		≤65%	≤65%	≤65%
Organic Content		≤5%	≤5%	≤5%
Soil Classification System	AASHTO	-	-	A-2-6 or A-6 A-2-7 A-7
	USCS	-	-	CL

Considering the approach fill used in Louisiana and parameters recommended and used in relative reports (See Appendix A), ranges of material parameters as shown in table 4 are proposed to be used in the present finite element analysis.

Table 4
Material parameters

	E psi (MPa) Elastic modulus	υ Poisson ratio	c psi (kPa) Cohesion	φ(°) Friction angle	γ pcf (kg/m^3) Density
Embankment Soil	37700 (260)	0.3	11.6 (80)	30	127.4 (2000)
Natural Soil	4360 (30)	0.3	7.25 (50)	30	95.6 (1500)

Load. The AASHTO truck loads were applied on the slab in addition to the dead load of the slab. The two HS20 truck loads were moved along the slab length to produce the worst loading scenario for the slab deflection and internal bending moments. The 40-ft. slab width could accommodate three trucks. Doing so will need to apply multiple presence reduction factor and it was found that the two trucks are more critical and thus used in the analysis.

Determination of Boundary Conditions

The soil underneath the approach span is theoretically semi-infinite. A sensitivity analysis was conducted to decide how far the boundaries - laterally, vertically, and longitudinally - should be included in the finite element model. Three parameters, W2, L5, and H5 as shown in figure 2 were investigated in the sensitivity study. Using material parameters shown in table 4, effects of these three geometric parameters were modeled to determine the boundary conditions:

(1) W2 was varied from 5, 10, 15, 20, 25, 30, to 45 ft. for fixed L5 =30 ft. and H5 = 30 ft.;
(2) L5 was varied from 10, 20, 30, 40, 50, to 120 ft. for fixed H5 = 30 ft. and W2 = 25 ft.;

(3) H5 was varied from 5, 10, 20, 30, 35, 40, 50, 60, 100, to 200 ft. for fixed W2 = 25 ft. and L5 = 30 ft..

For each case, two truck loads (HS 20) on two lanes (closest wheel distance between the two trucks is 4 ft. based on AASHTO specifications) and slab self-weight were applied to the approach slab. In this sensitivity study, a 2 ft. differential settlement between abutment and approach slab was used to model the extreme case in which the approach slab and embankment soil have essentially no contacts.

The deflection of the approach slab and the vertical stress in embankment soil under sleeper slab for the three conditions are shown in figures 4 and 5. These figures clearly demonstrate that the W2 condition has insignificant effects on the results. When L5 is larger than 40 ft., the results for both deflection and soil stress barely change. When H5 is larger than 50 ft., its effect on deflection reduces, but still slightly impacts, the magnitude of the soil stress. From the sensitivity analysis above and considering the computational efficiency, the boundary condition for the slab-soil interaction analysis was determined as: W2 = 15 (ft.); L5 = 40 (ft.); H5 = 50 (ft). Based on the Saint-Venant Principle, different settlement scenarios should not significantly affect this sensitivity study. Therefore, these boundary dimensions and slab dimensions were used in the analyses of different settlements described in the following sections unless otherwise specified.

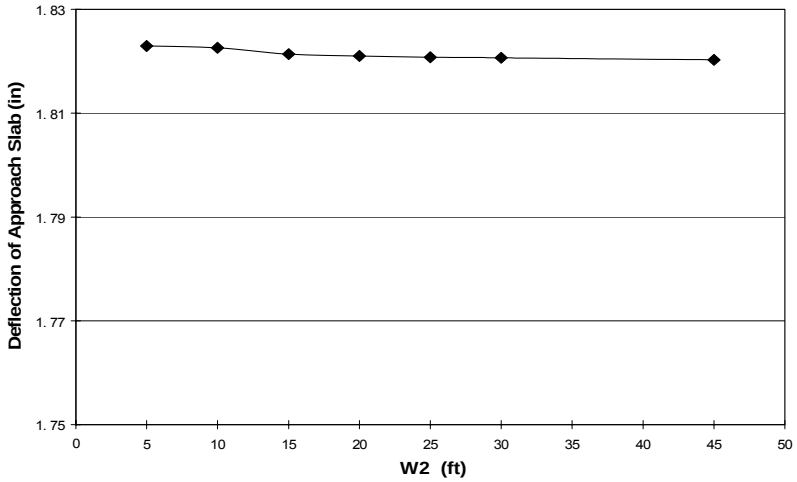

(a) Deflection versus w2

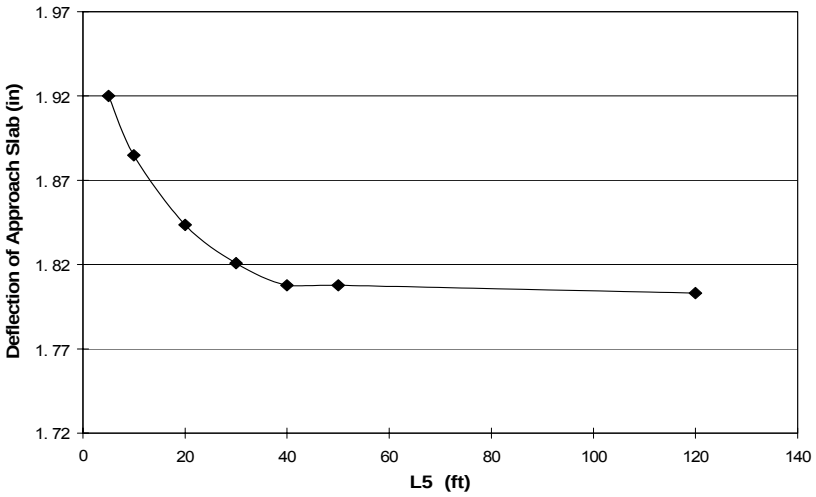

(b) Deflection versus L5

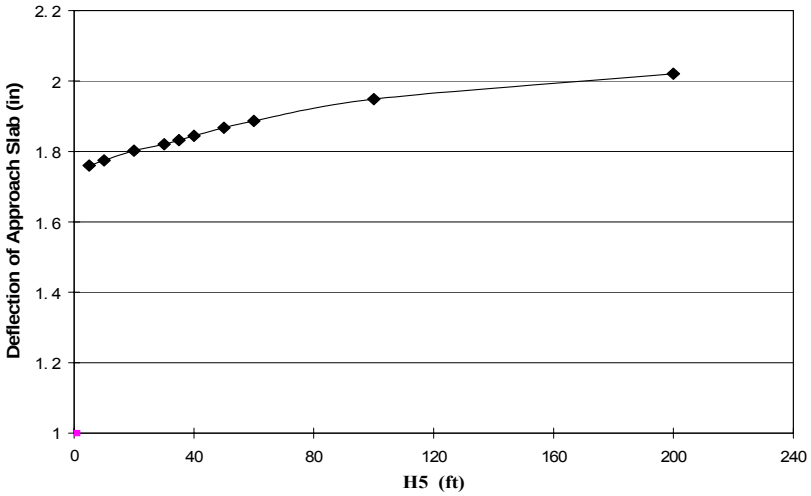

(c) Deflection versus H5

Figure 4
Effects of parameters on deflection of approach slab

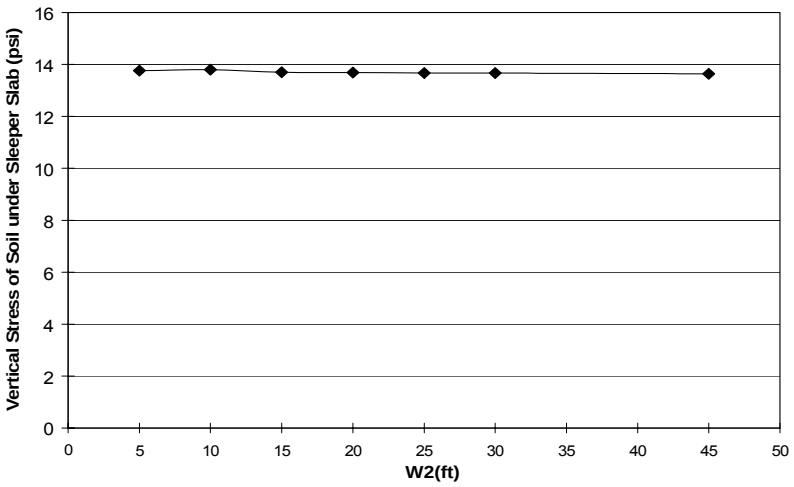

(a) Stress versus W2

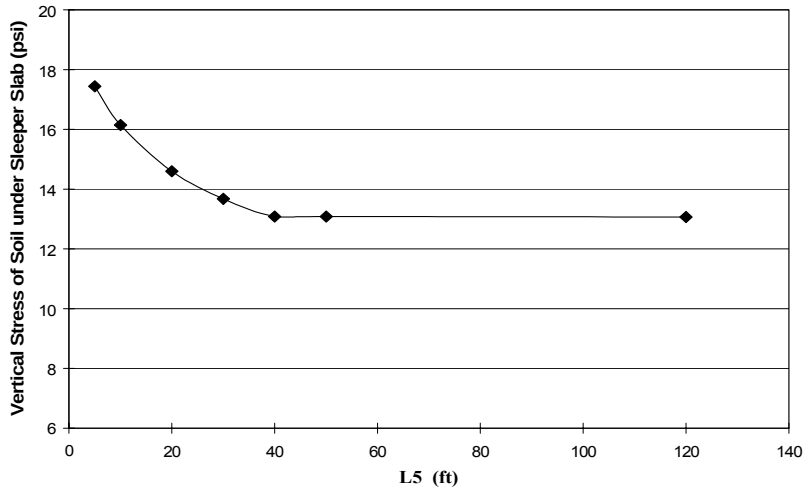

(b) Stress versus L5

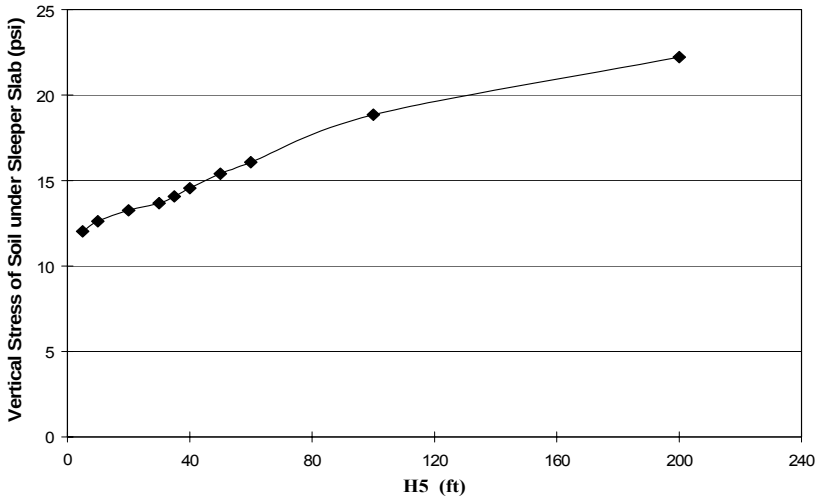

(c) Stress versus H5

Figure 5

Effects of parameters on vertical stress of soil

After the dimensions (i.e., boundaries) of the finite element model were decided, a parametric study was conducted to examine the mechanism of interaction between the embankment soils and the approach slab under different embankment settlements. The maximum deflections and internal moments of the approach slab under different settlements were obtained by moving the truck loads along the slab. In the finite element analysis for a given embankment settlement, the dead load (*DL*) was applied first; followed by the dead load and live loads (*DL+LL*) applied together. The live load effects (*LL*) were then calculated with the total effect by subtracting the dead load effect, i.e., (*DL+LL*) – (*DL)*. This procedure is necessary since the loading sequence affects the contacting and separating process between the slab and the soil. Therefore, the live load cannot be applied independently without including the dead load for a proper nonlinear solution.

Effect of Settlement on Performance of Approach Slabs

As shown in figures 6 and 7, the magnitude of the slab's maximum deflections and internal moments increases with the increase of the embankment settlements. When the differential settlement increases from 6.0 in. to a larger value, almost no change occurs in the deflection and internal moment of the approach slab. The settlement no longer affects the performance of the slab since the approach slab almost completely loses its contact with the soil and performs as a simple beam. With a L/800 as live load deflection control that is typically used in bridge engineering, the allowable live load deflection will be 40/800 = 0.05 ft. = 0.6 in., which corresponds to an allowable embankment settlement of about 5 in. as shown in figure 6.

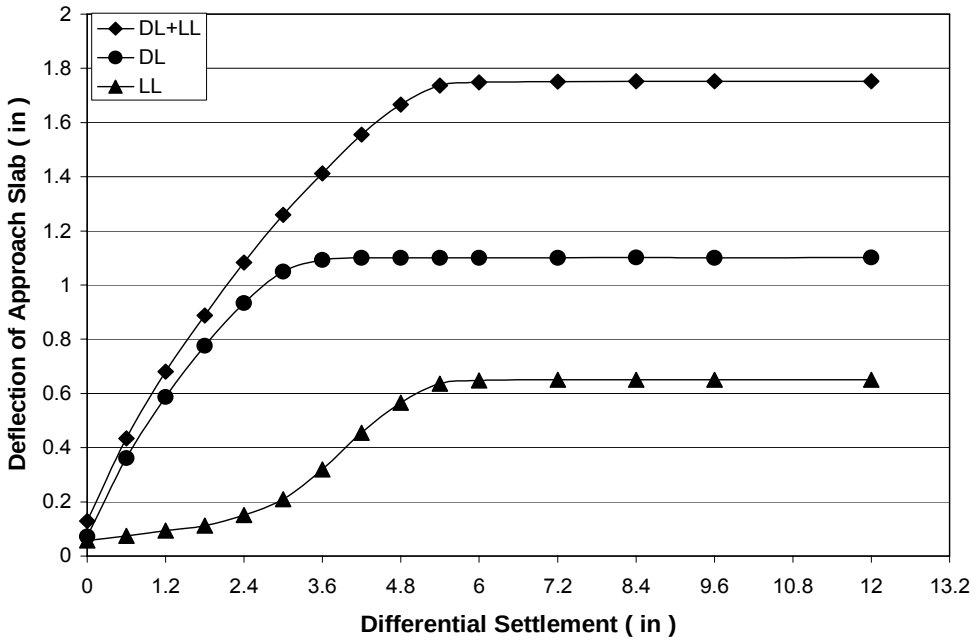

Figure 6
Deflection of approach slab versus settlement

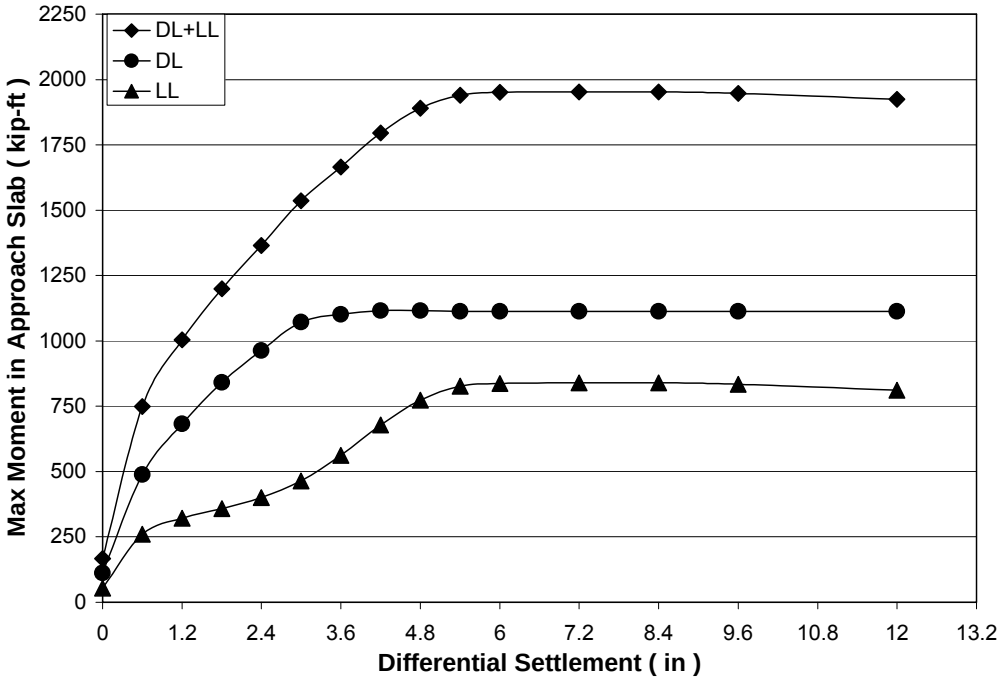

Figure 7
Internal moment of approach slab versus settlement

Effect of Settlement on Soil

Similarly, as shown in figure 8, the maximum vertical stress of the embankment soil under the sleeper slab continues to increase with the increase of the differential settlement. Since the slab loses more support from the soil as the settlement increases, a larger portion of the slab self-weight and truck loads is distributed to the sleeper slab and eventually to the soil under the sleeper slab. In comparison with the slab deflection and internal moments (figures 6 and 7), the stress in the soil continues to increase even when the settlement exceeds 6.0 in., but at a reduced rate. A typical vertical stress distribution along the span for the soil under the approach slab and under the sleeper slab is shown in figure 9.

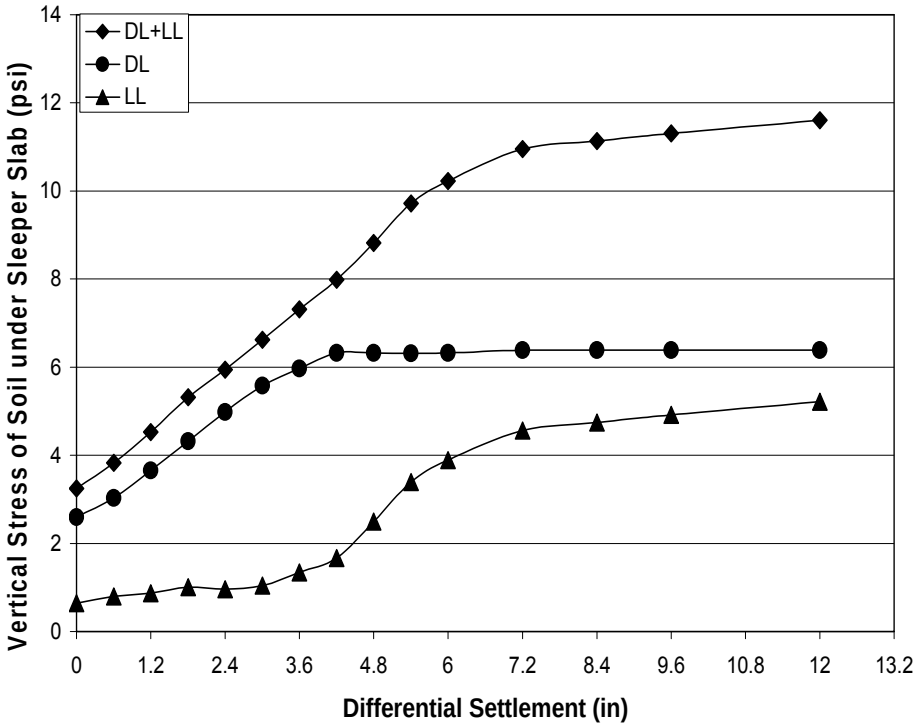

Figure 8
Vertical stress of soil under sleeper slab versus settlement

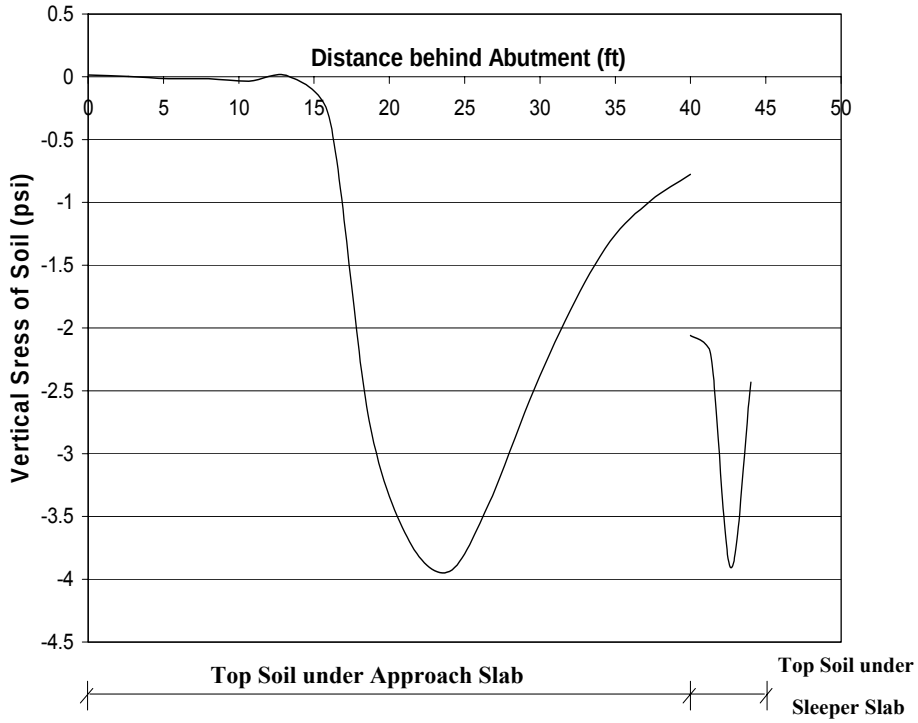

Figure 9
Stress distribution in soil near interface
(Settlement = 0.6 in.)

As discussed earlier, the differential settlement between the two ends of the approach slab forms a gap between the approach slab and the embankment. Due to the action of truck loads and slab self-weight, the approach slab deforms downward and is supported by the embankment at the contacting points.

Figure 10 shows the assumed settlement lines of the embankment and the predicted deflection shape of the slab under different differential settlements (In the finite element analysis, the differential settlement was modeled by changing the soil line instead of specifying two different elevations of the slab ends). The figure clearly exhibits the contact area between the slab and embankment near the sleeper slab and the gap near the abutment. As the settlement increases, the gap becomes deeper and longer, and the contact area decreases. If the settlement is large enough, the slab and embankment have no contact, and the slab loses the support from the embankment,

except near the sleeper slab. Thus, the deflection and internal moment of the approach slab will not change with the increase of the embankment settlement as indicated in figures 6 to 8.

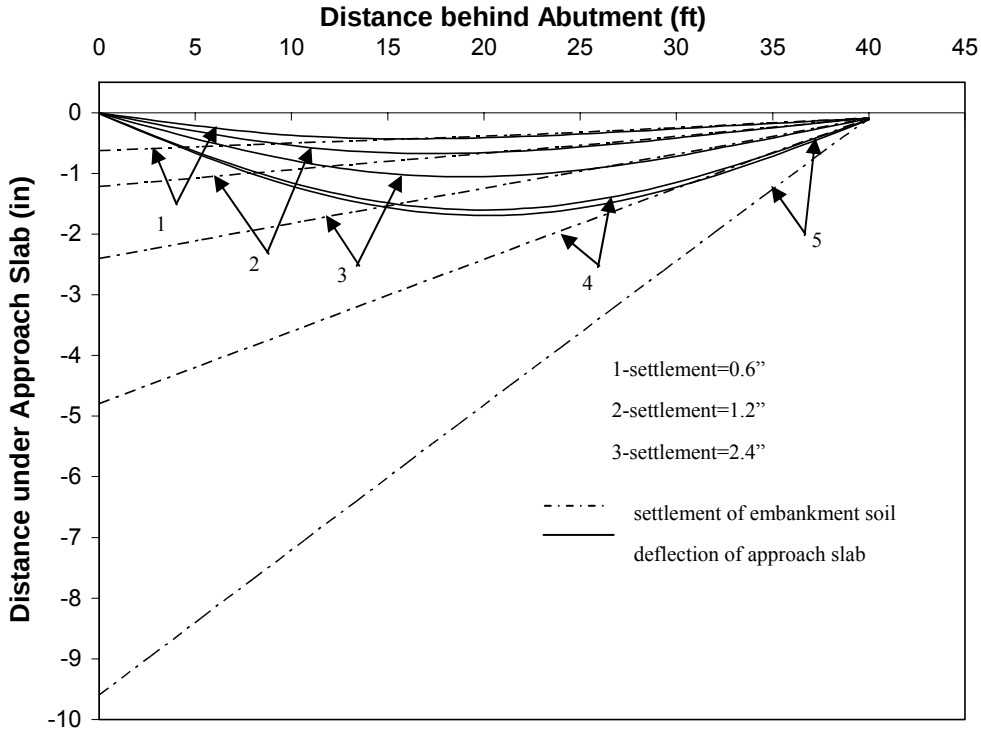

Figure 10
Interface between approach slab and embankment soil

Figures 11 to 14 show the 3-D stress distribution contours of finite element analysis in the soil and approach slab for 0.6, 1.2, 2.4 and 6.0 in. differential settlements. As the settlement increases, the approach slab behavior resembles that of a simply supported beam. Correspondingly, the maximum stress region in the slab moves towards the mid-span and the soil stress below the sleeper slab increases.

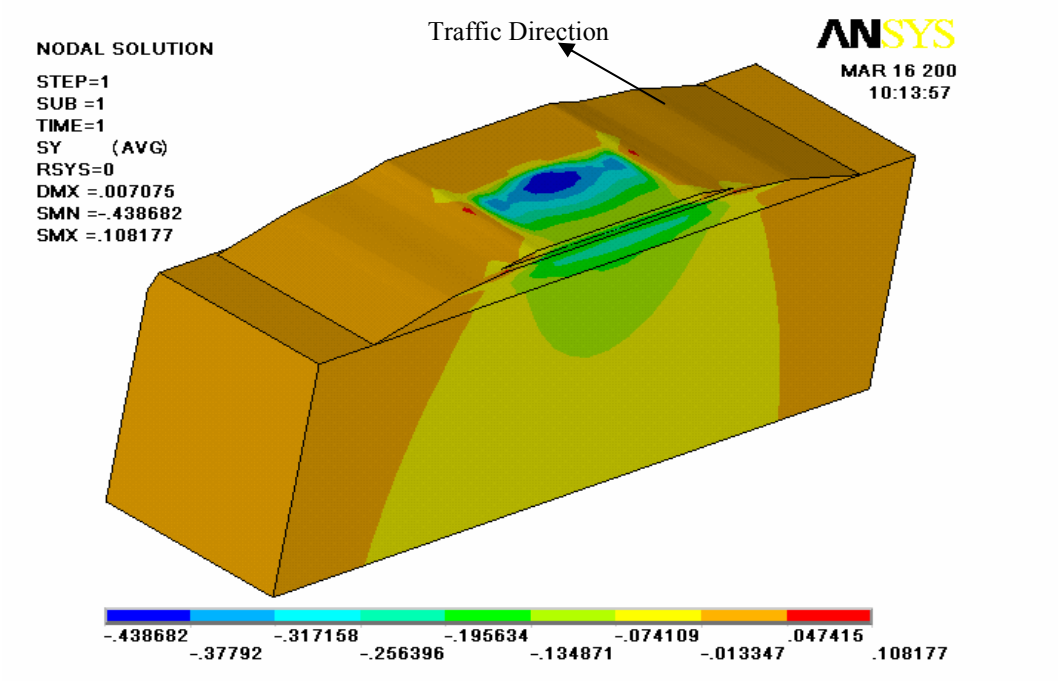

(a) Vertical stress distribution in embankment soil (ksf)

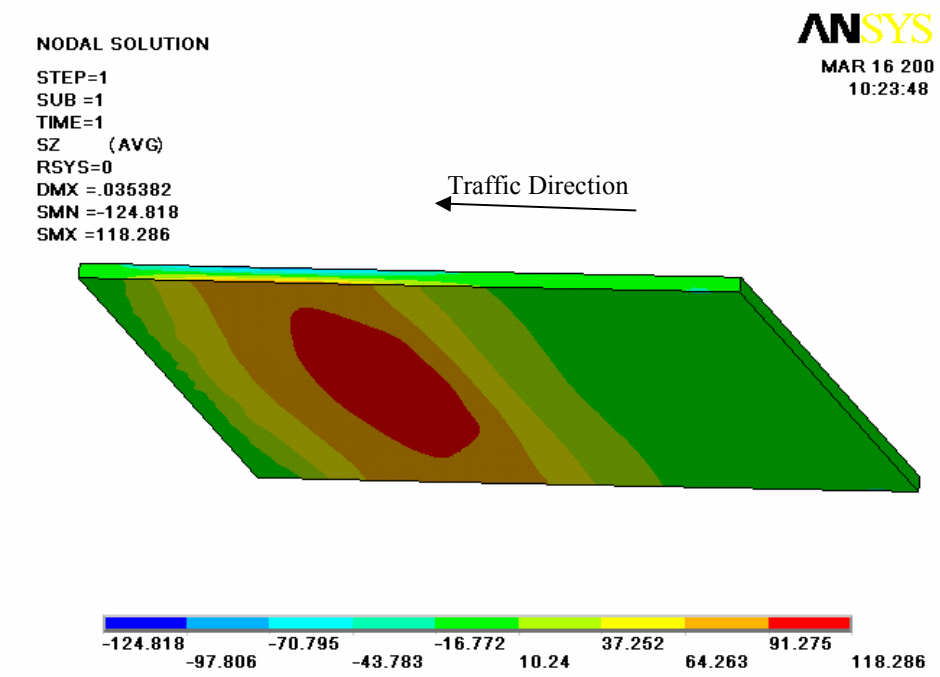

(b) Longitudinal stress distribution in slab (ksf)

Figure 11
Stress distribution in soil and slab (settlement = 0.6 in.)

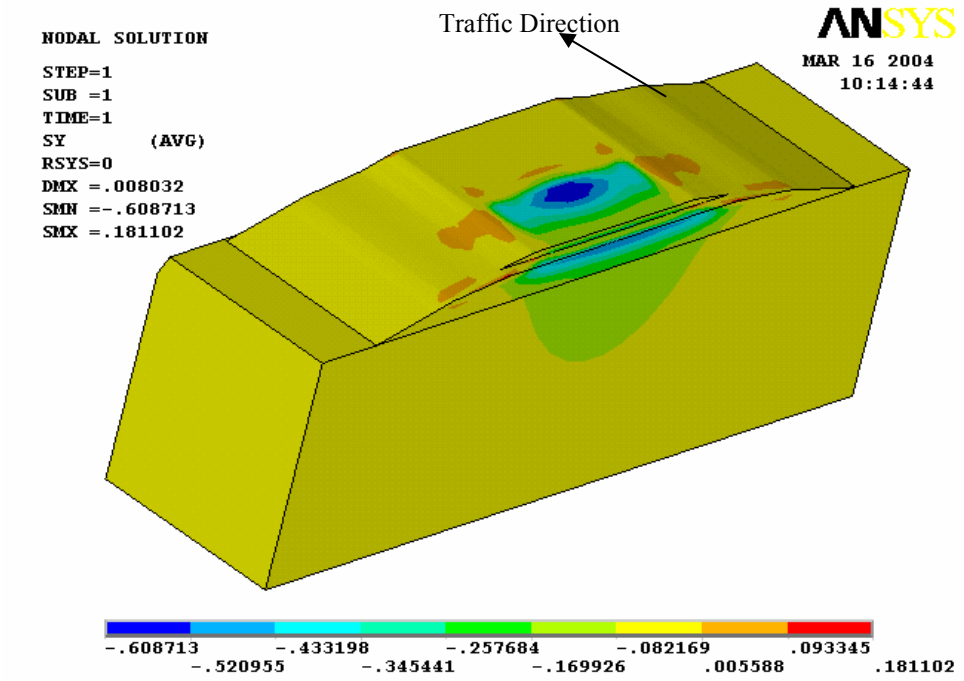

(a) Vertical stress distribution in embankment soil (ksf)

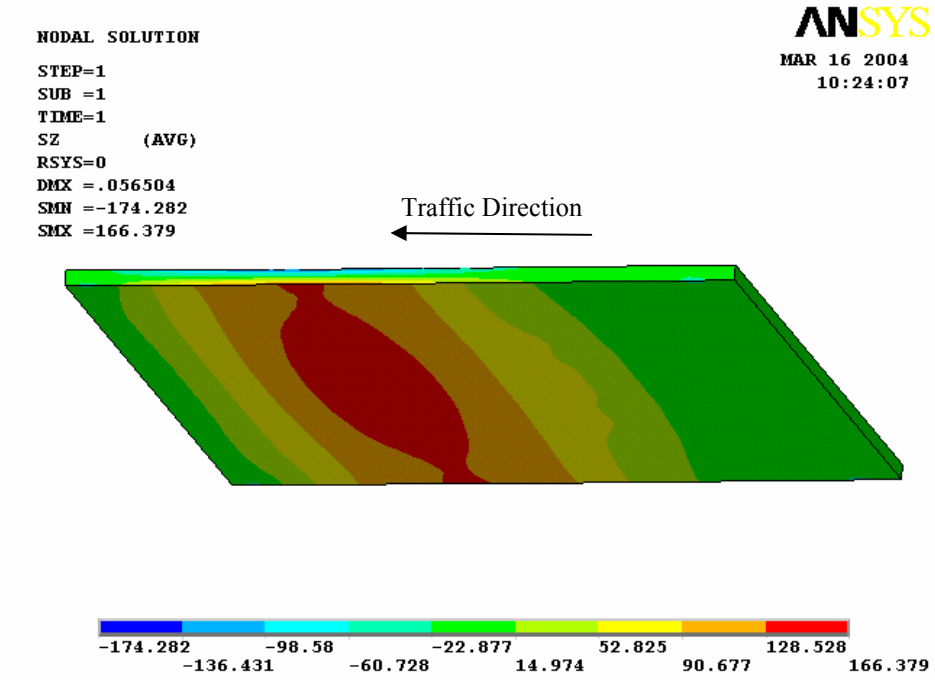

(b) Longitudinal stress distribution in slab (ksf)

Figure 12
Stress distribution in soil and slab (settlement =1.2 in.)

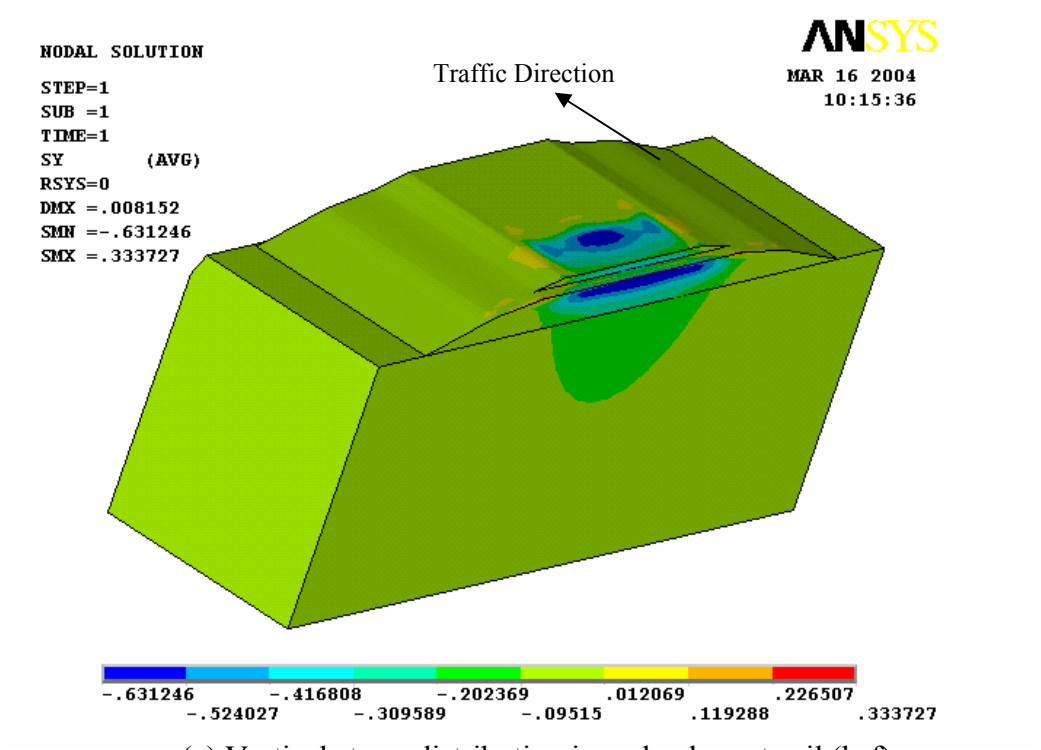

(a) Vertical stress distribution in embankment soil (ksf)

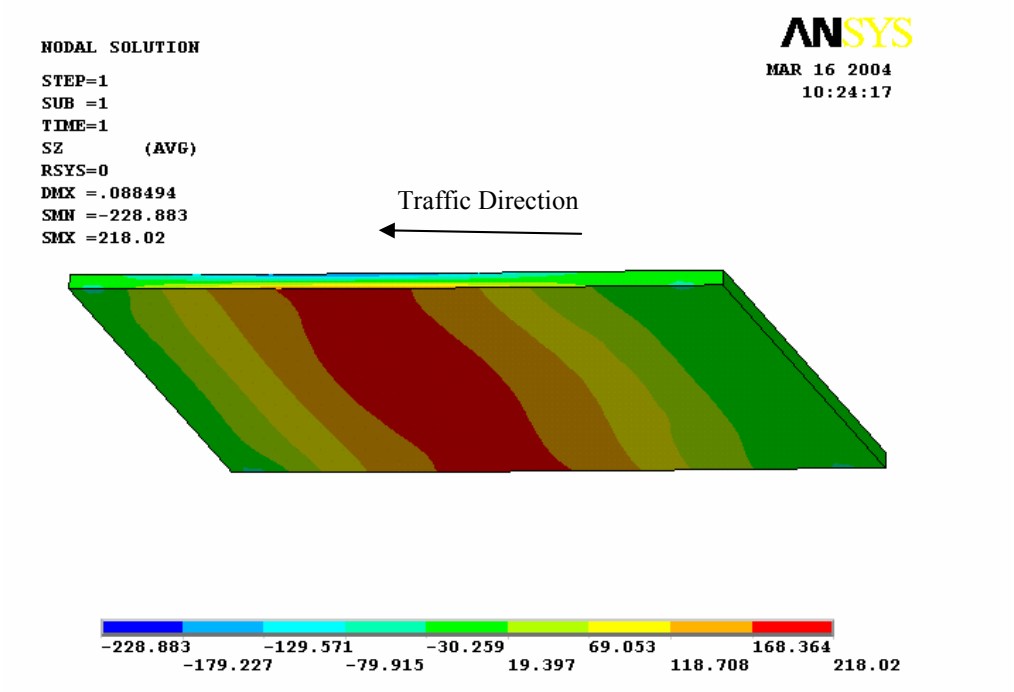

(b) Longitudinal stress distribution in slab (ksf)

Figure 13
Stress distribution in soil and slab (settlement = 2.4 in.)

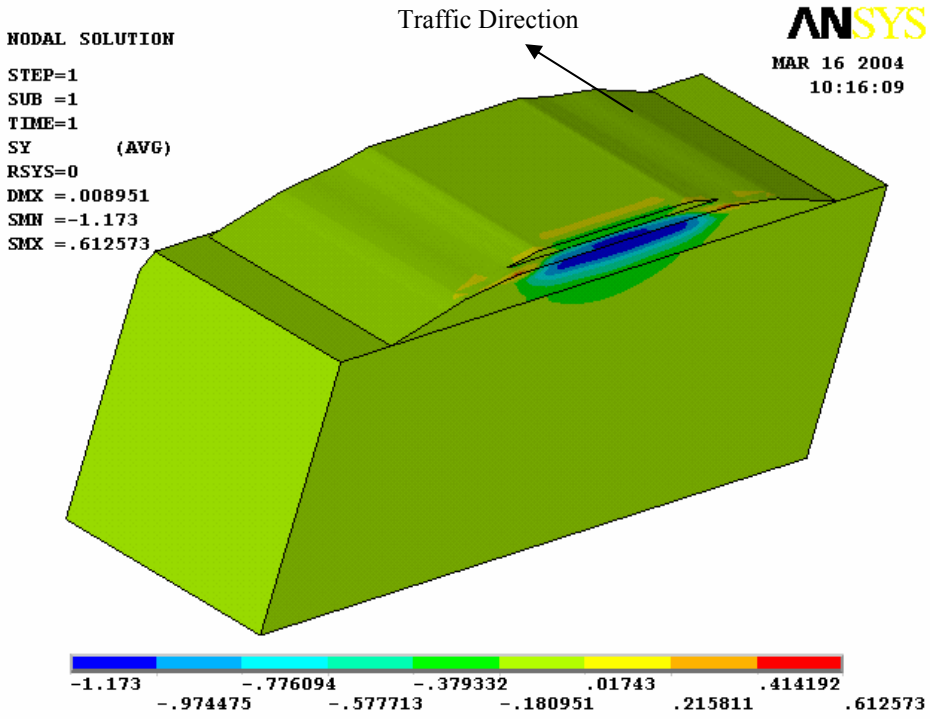

(a) Vertical stress distribution in embankment soil (ksf)

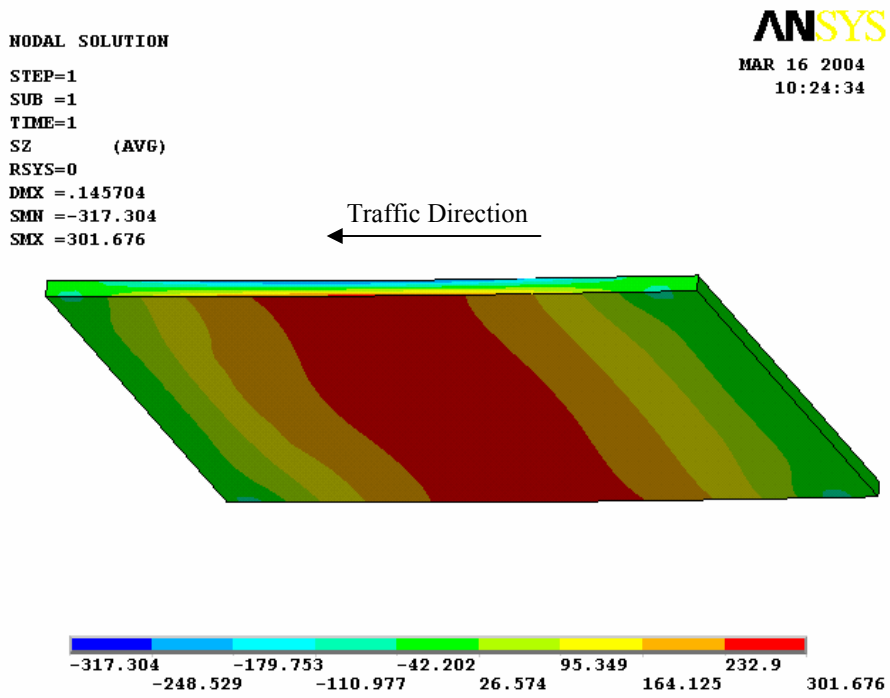

(b) Longitudinal stress distribution in slab (ksf)

Figure 14

Stress distribution in soil and slab (settlement = 6.0 in.)

Effects of Embankment Settlements on Slab Design

Since the increase of the embankment settlement results in a separation of the slab from the soil and a subsequent increase of the internal moment in the approach slab, the slab must be designed to provide enough strength for an expected embankment settlement. To this end, the results from the finite element analysis were used to evaluate the structural design of the approach slabs that are used by the LADOTD. Currently, the LADOTD standard drawing calls for #6@6" for the bottom reinforcement of the approach slab *[21]*.

When the approach slab is subjected to bending, the stresses induced by the concentrated loads are not uniformly distributed over the whole width of the slab. If the width of the slab is large, only a part of the slab is effective in resisting a given bending load. The non-uniform distribution of the stresses in the slab means that a simple beam theory cannot be applied for the slab analysis without some modifications or verifications. Therefore it is convenient, for design purposes, to consider a slab width (an effective width), which, if uniformly stressed, would represent the same amount of flexural resistance as the real slab. The effective width in slabs may be affected by the following parameters: (1) position of load, (2) ratio of the span length of the slab to its width, and (3) type of loading.

For the simply supported slab, the case of the two trucks applied at the mid-span was chosen as the basic loading type, and a uniformly distributed dead load was considered. By moving the trucks along the transverse direction of the slab, the critical scenario was observed when the trucks move to one side of the slab. The effective width w_e is defined as:

$$w_e = \frac{\int_0^w \sigma_y dx}{\sigma_{y\max}} \qquad (2)$$

where σ_y = bending stress in section, σ_{ymax} = maximum bending stress in section, and w = width of the slab.

For an approach slab that is 40 ft. long, 40 ft. wide, and 12 in. thick, the effective widths, w_e, for the truck loads on the side of the slab were calculated by varying the differential settlement from 0.6 to 7.2 in. The effective width corresponding to one truck load is plotted in figure 15. As expected, the dead load is much more uniformly distributed across the bridge width, and, thus, the effective width is larger than that of the live load. The effective width per truck was also determined to be 11.8 ft. per AASHTO code (2002) for simply supported slabs, which is within the range of the prediction. Therefore, when no more accurate information is available, the effective width specified in the AASHTO specifications can also be used for the partially supported approach slabs. As shown in figure 15, when the differential settlement is small, then the predicted effective width for live loads is smaller than that specified in the codes. This implies that using the code effective width is not conservative for design. However, small settlement is not the critical condition. For larger settlement (about 3 in. in this case), the code effective width is more conservative than the predicted values.

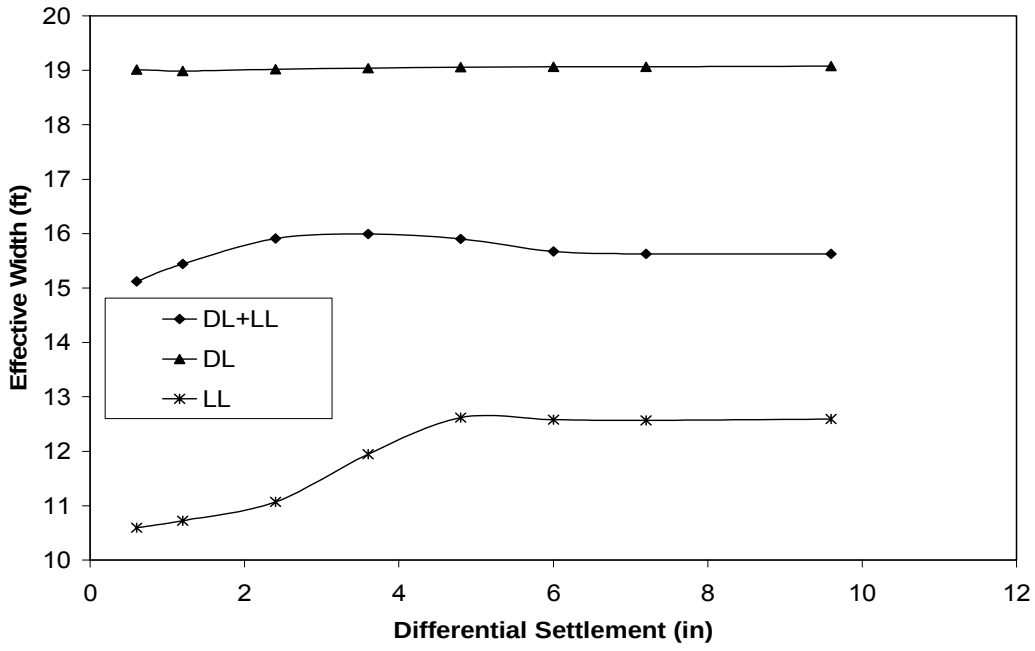

Figure 15
Effective width of slab versus differential settlement

Checking the strength of the approach slab was conducted according to the AASHTO Standard Specifications (AASHTO 2002), namely, with load factors of 1.3 for dead load, 2.17 for live load, and 1.3 for impact factor, with an equivalent slab width of 11.8 ft. The results of the reinforcement design considering the effects of different differential settlements are shown in table 5.

Table 5
Design of approach slab

Settlement (in.)	M (kip-ft.)			ρ	ρ_{max}	A_s ($in.^2/ft.$)	Reinforcement (2)
	DL	LL	1.3DL +2.17(LL+IM)				
0	33.2	27.1	119.6	0.0019	0.0214	0.23	#4@10.0”
0.6	144.0	130.5	555.4	0.0095	0.0214	1.14	#6@ 4.5”
1.2	202.3	183.9	716.9	0.0127	0.0214	1.52	#6@ 3.5”
1.8	248.3	179.0	822.1	0.0148	0.0214	1.78	#7@ 4.0”
2.4	284.2	200.6	935.3	0.0173	0.0214	2.08	#8@ 4.5”
3.0	316.2	232.0	1065.6	0.0204	0.0214	2.45	#10@6.0”
3.6	325.1	281.3	1216.2	0.0243	0.0214	NA(1)	NA
4.2	329.3	339.4	1385.5	0.0293	0.0214	NA	NA
4.8	329.3	386.9	1519.5	0.0341	0.0214	NA	NA
5.4	328.4	413.5	1593.4	0.0372	0.0214	NA	NA
6.0	328.4	418.7	1608.1	0.0379	0.0214	NA	NA
7.2	328.4	419.9	1611.5	0.0381	0.0214	NA	NA
8.4	328.4	420.0	1611.8	0.0381	0.0214	NA	NA

Note: (1) The required reinforcement ratio ρ exceeds the allowed maximum reinforcement of flexure, i.e., $\rho > \rho_{max} = 0.75\rho_b$, meaning that section dimension needs to be increased.

(2) Some rebar size listed above may not be practical for a slab with a thickness of 12 in.

It is interesting to observe in table 5 that when the settlement is zero, the required reinforcement at the bottom of the slab is 0.23 $in.^2/ft.$ and it increases to 1.14 $in.^2/ft.$ when the settlement increases to 0.6 in. This indicates that the current design (LADOTD 2002), 0.88 $in.^2/ft.$, is good only for the case of zero settlement and is not adequate for a settlement larger than 0.6 in. When the embankment settlement increases, more reinforcement is required. When the settlement exceeds 3.0 in., then the required reinforcement ratio, ρ, will exceed the allowed maximum reinforcement ratio, ρ_{max}, namely 75 percent of the balanced reinforcement ratio (AASHTO 2002). In this case, either the slab thickness should be increased or soil should be improved to control the settlement within the allowable limit.

Development of Design Aids for Approach Slab

Two extreme cases are currently used in practical design of approach slabs. The first case assumes the slab is in full contact with the soil and does not consider differential settlement. This assumption may result in an unconservative design. In the other extreme case, an approach slab is designed as a simple beam, assuming a complete separation between the slab and the embankment except for at the two ends. This assumption, while conservative, will definitely result in an uneconomical design. In many real cases, the slab is in partial separation and partial contact with the soil along the span length. Analysis of interaction between the slab and soil shows that partial supports provided from the embankment soil to the concrete slab will reduce the internal force of the slab. The previous section showed how finite element procedures could help design approach slabs for a given embankment settlement. In this section, parametric studies were conducted to develop a design aid to make a simpler design procedure so that engineers do not need to use complicated finite element analysis in a routine design.

Parametric Analysis

A parametric study was conducted by changing the slab thickness and length to establish the relationship between the slab responses, parameters, and the corresponding differential

settlements, which can be used in routine design. The slab parameters, length (L) and thickness (h), were investigated in the parametric study for the following cases: (1) h was varied from 1, 1.5, to 2 ft. for the fixed L = 40 ft.; and (2) h was varied from 1.5, 2.25, to 3 ft. for the fixed L = 60 ft.

As shown in figures16 to 18, with the increase of embankment settlements, the magnitude of the maximum internal moments, deflections, and rotation angles in the slab increases to some constant values. For example, with L = 40 ft. and h = 12 in., a settlement increase from 6.0 in. to larger values, creates almost no change in the internal moment, deflection, and rotation angle since the approach slab has essentially become a simply-supported beam. For the same differential settlement, the approach slab thickness (h) increases as the deflection in the slab decreases. Smaller deflections of the approach slab reduce the contact area between the slab and embankment soil. As a result, the value of the differential settlement beyond which the settlement ceases to affect the slab behavior decreases (figures16 to 18).

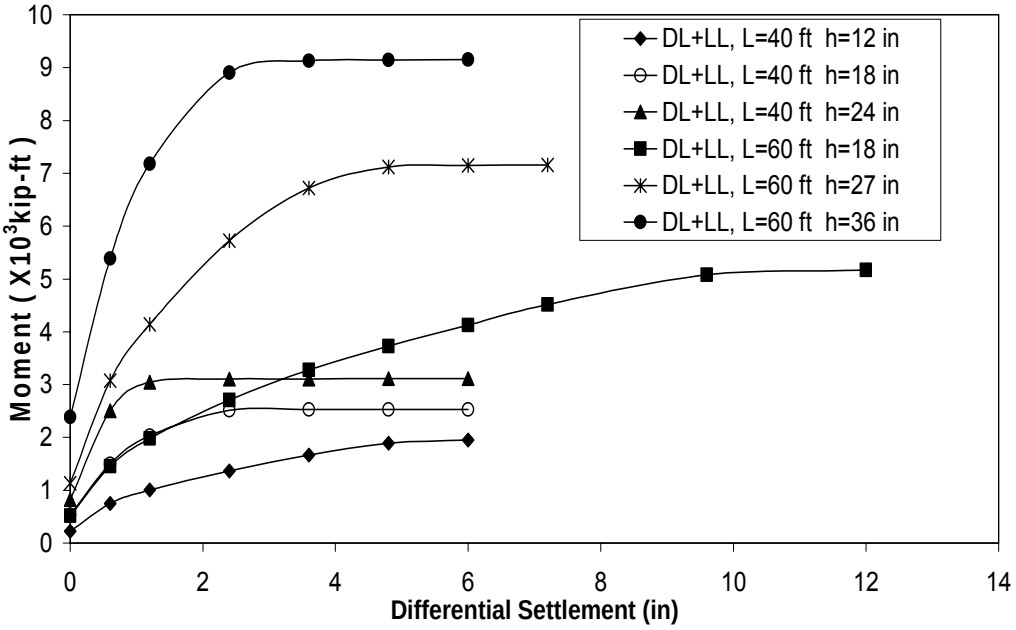

Figure 16
Internal moment of slab versus differential settlement

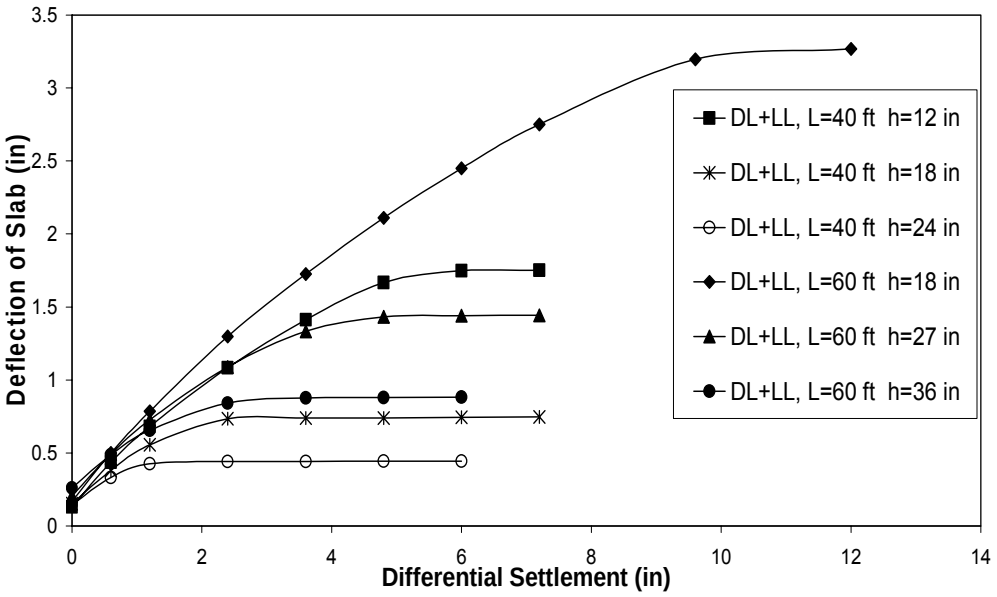

Figure 17
Deflection of slab versus differential settlement

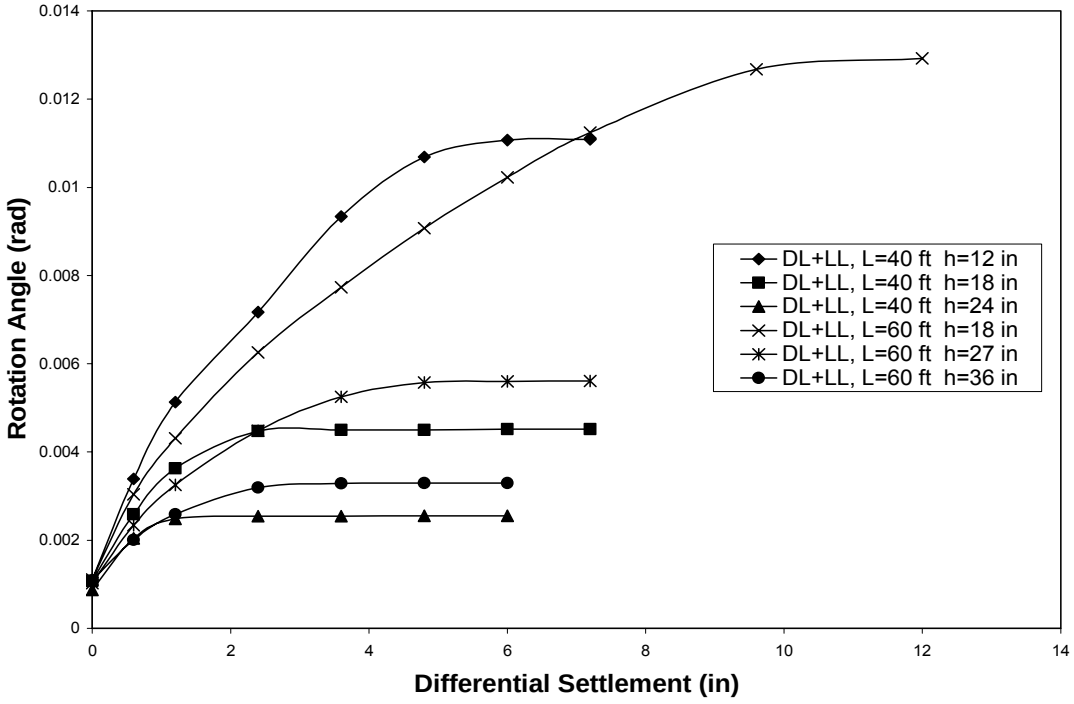

Figure 18
Rotation angle of slab versus differential settlement

Regression Analysis

By analyzing the results from the finite element analysis, this study established a correlation among the slab parameters, deflection and rotation angle of the slab, internal moment of the slab, and the differential settlement. The results are then normalized with respect to a traditional simply-supported (pin and roller supports) beams, i.e., a beam without considering the contact between the slab and the soil, and without considering the elastic deformation at the beam end supports. Engineers can conveniently obtain the slab response, such as deflections, rotation angles and moments, by multiplying the slab response of the simply-supported beam with a computed coefficient.

The parameters obtained from the finite element analysis fit the curve of exponential function, i.e., $f(x) = A - B \times e^{cx}$. The unknown coefficients A, B, and C can be computed by doing a least square curve fitting, which minimizes the sum of the squares of the deviations of the data from the model.

The predicted maximum internal moments in approach slabs due to the total load (dead load plus live load without considering dynamic impact effect) and dead load only are normalized. They are represented in figure 19 and can be expressed by an exponential function with a regression analysis as follows:

$$M_T = \left(0.9629 - 0.7945 e^{-1.5795 \times 10^7 \left(\frac{\delta h^2}{L^4}\right)} \right) M_{T0} = K_{TM} M_{T0} \quad (3)$$

$$M_D = \left(0.9538 - 0.8080 e^{-2.1938 \times 10^7 \left(\frac{\delta h^2}{L^4}\right)} \right) M_{D0} = K_{DM} M_{D0} \quad (4)$$

where M_T = maximum moment of the approach slab due to the total load; M_D = maximum moment of the approach slab due to the dead load; δ = differential settlement (ft.); h = thickness of the approach slab (ft.); L = length of the approach slab (ft.); K_{DM} and K_{TM} are moment

coefficients that are self-evidenced in the equations; M_{T0} = maximum moment of a simply-supported beam due to the total load; and M_{D0} = maximum moment of a simply supported beam due to the dead load.

The maximum internal moment in approach slab due to live load is then calculated as:

$$M_L = K_{TM} M_{T0} - K_{DM} M_{D0} \tag{5}$$

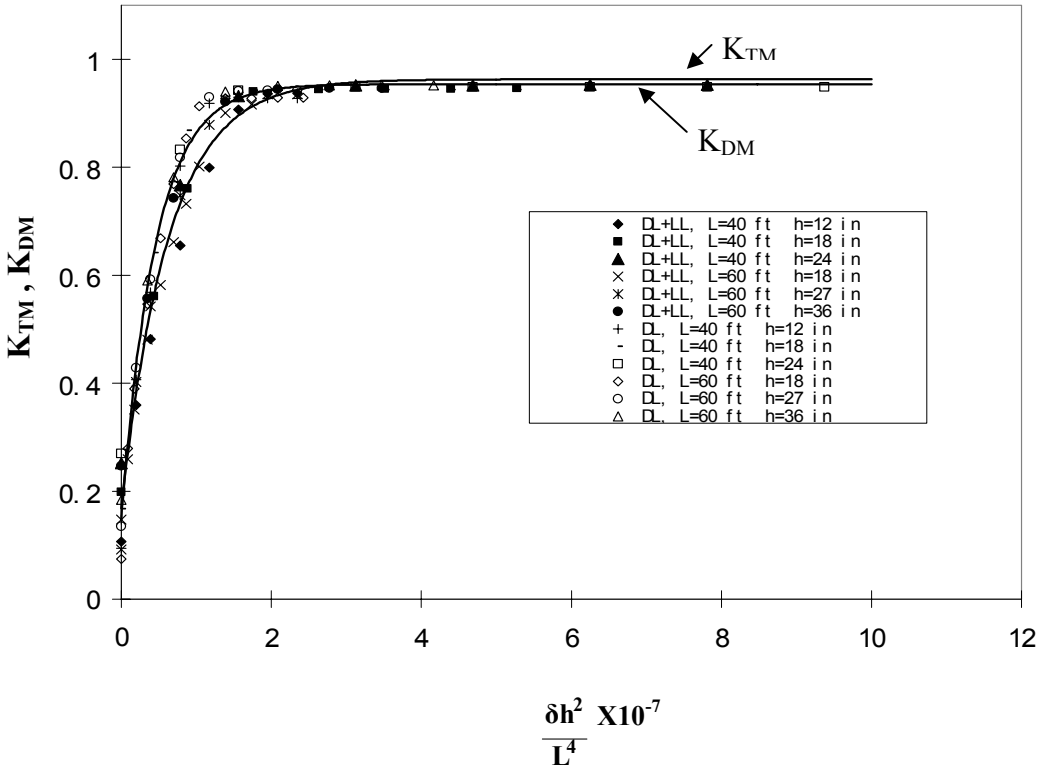

Figure 19
K_{TM} and K_{DM} curve

Similarly, the maximum deflections (Δ_2 in figure 1, including both the slab deflection and load-induced support deformation) in the approach slab due to the total load and dead load only are represented by the curves shown in figure 20 and can be expressed by an exponential function as:

$$d_T = \left((2.9359 - 2.5443e^{-1.3475\times10^7(\frac{\delta h^2}{L^4})}) \times (\frac{h}{L})^{0.3} \right) d_{T0} = K_{Td} d_{T0} \quad (6)$$

$$d_D = \left((3.0003 - 2.5895e^{-1.8194\times10^7(\frac{\delta h^2}{L^4})}) \times (\frac{h}{L})^{0.3} \right) d_{D0} = K_{Dd} d_{D0} \quad (7)$$

where d_T = maximum deflection of the approach slab due to the total load; d_D = maximum deflection of the approach slab due to the dead load; K_{Dd} and K_{Td} are deflection coefficients that are self-evidenced in the equations; d_{T0} = maximum deflection of an simply supported beam due to the total load; and d_{D0} = maximum deflection of an simply supported beam due to the dead load.

The maximum deflection in the approach slab due to live load is then calculated as:

$$d_L = K_{Td} d_{T0} - K_{Dd} d_{D0} \quad (8)$$

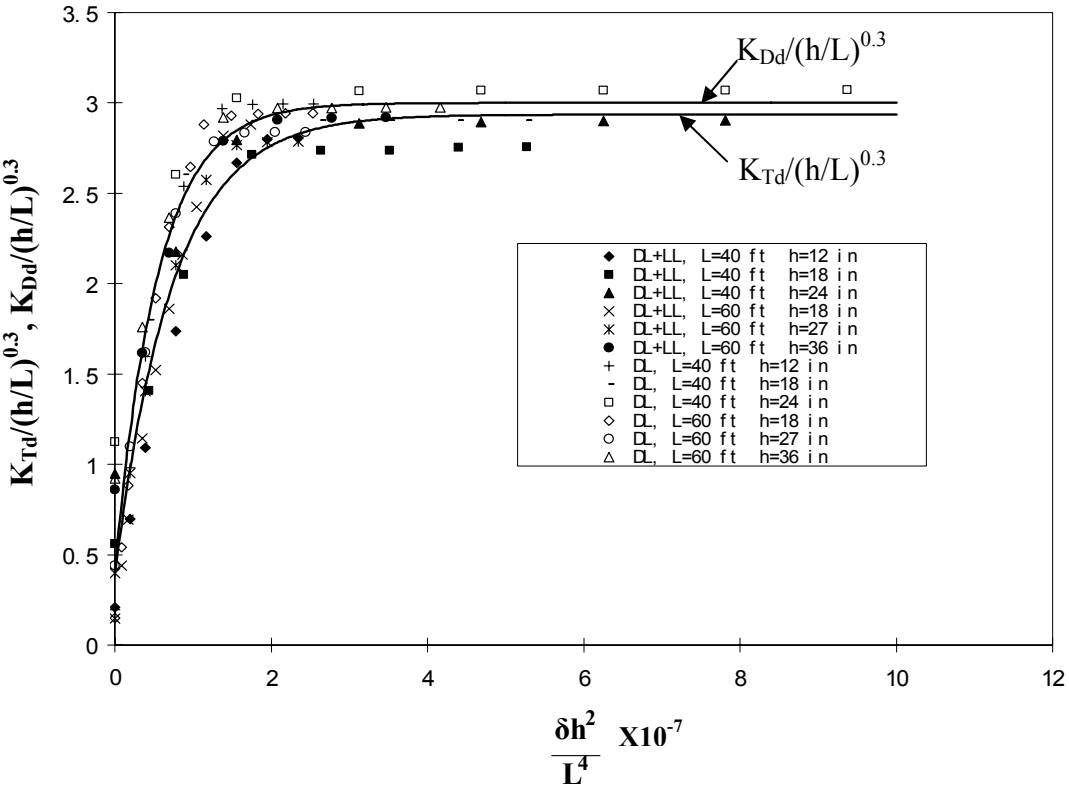

Figure 20
K_{Td} and K_{Dd} curve

Finally, the end rotation angle also shown in figure 1 is represented in figure 21 and the formulas are obtained as:

$$\theta_T = \left((1.8547 - 1.5177e^{-1.4462\times10^7(\frac{\delta h^2}{L^4})}) \times (\frac{h}{L})^{0.2} \right) \theta_{T0} = K_{T\theta}\theta_{T0} \qquad (9)$$

$$\theta_D = \left((1.8378 - 1.4904e^{-2.0574\times10^7(\frac{\delta h^2}{L^4})}) \times (\frac{h}{L})^{0.2} \right) \theta_{D0} = K_{D\theta}\theta_{D0} \qquad (10)$$

where θ_T = maximum rotation of the approach slab due to the total load; θ_D = maximum rotation of the approach slab due to the dead load; $K_{D\theta}$ and $K_{T\theta}$ are moment coefficients that are self-

evidenced in the equations; θ_{T0} = rotation angle of a simply-supported beam due to the total load; and θ_{D0} = rotation angle of a simply-supported beam due to the dead load.

The maximum rotation angle in the approach slab due to live load is then calculated as:

$$\theta_L = K_{T\theta}\theta_{T0} - K_{D\theta}\theta_{D0} \tag{11}$$

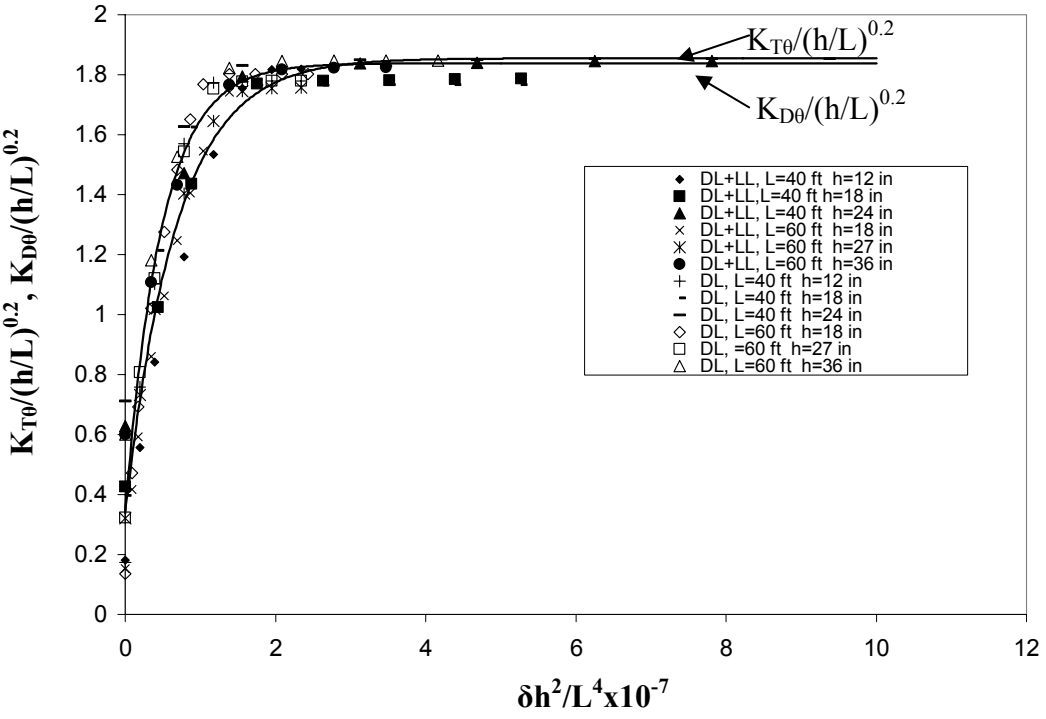

Figure 21
$K_{T\theta}$ and $K_{D\theta}$ curve

This information will help the engineers to make decisions in selecting a more appropriate/economical solution. For example, engineers can choose to control the excessive settlement by improving embankment fills or foundations, or to select a stiffer approach slab to accommodate the deformations and settlements. This information can also be used for structural evaluation and design. The current LADOTD Bridge Design Manual does not require structural

calculations in the approach slab design, and standard reinforcement are specified in the standard drawings.

All the above results of the approach slab were obtained based on an elastic analysis without considering cracking, and the contribution of reinforcement in concrete was ignored (since reinforcement makes an insignificant contribution before concrete cracks). The example in the Appendix shows how to calculate the internal force, deflection, and rotation angle of cracked reinforced concrete approach slabs from the results obtained above. This approach is consistent with the current practice in bridge engineering, namely using an elastic analysis to predict the internal force and deflection first and then considering cracking in the strength design and the long-term deflection calculation.

Ribbed Slab

For approach embankments sitting directly on weak foundation soils, 120 ft. (30 m) long pile-supported approach slabs (PSAS) are often used in Louisiana, hopefully to achieve a reasonable transition as shown in figure 22. However, the PSAS does not always deliver a satisfactory performance since it is not possible to accurately predict the pile settlements. Currently, no simple and reliable design procedure for PSAS is available, and details such as specified reinforcement requirements must be in accordance with the guidelines (LADOTD 2002). The drawback of the PSAS is the cost and the unpredictable performance, evidenced by the observed inconsistent performance in the field. The motivation of the study of ribbed approach slab is to find a feasible solution for a longer approach span.

Previous studies indicated that flat approach slabs may be used for some short span applications. A large span length would require a very thick slab, which is not economical. The proposed new construction method will allow approach slabs strong enough to lose a portion of their contact

supports without detrimental deflection, perhaps by increasing the flexural rigidity (EI) of the approach slabs. In such a case, ribbed approach slabs (similar to slab-on-beam bridge decks) are more economical and are thus proposed in the present study because they provide advantages over both the flat approach slab and PSAS for some span ranges.

This study presents strategies and results from a 3-D finite element analysis. The objective is to systematically analyze the structural performance of ribbed approach slab with span lengths of 60 ft. and 80 ft. as examples and to understand the interaction of ribbed approach slabs and embankment settlements. In this study, three different beam spacings were considered. The results obtained are very useful for a proper design which will help mitigate the slab rideability (and structural safety) problems.

Description of Finite Element Model

For demonstration purposes, a ribbed approach slab with 60 ft. in span length and beam spacing of 16 ft. (3 beams) is used, and the other dimensions are shown in figure 23 with a 4 ft. sleeper slab. For convenience, the beams are modeled as rectangular sections with the equivalent section properties of ASSHTO Type II and Type III beam for approach span length of 60 ft. and 80 ft., respectively. Once the internal forces are predicted, engineers can choose either prestressed girders or case-in-place beams. Both alternatives are provided later.

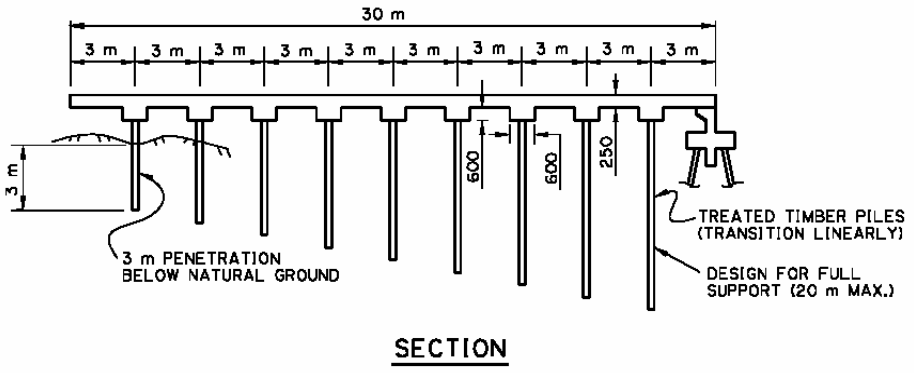

Figure 22
Typical pile-supported approach slab in louisiana

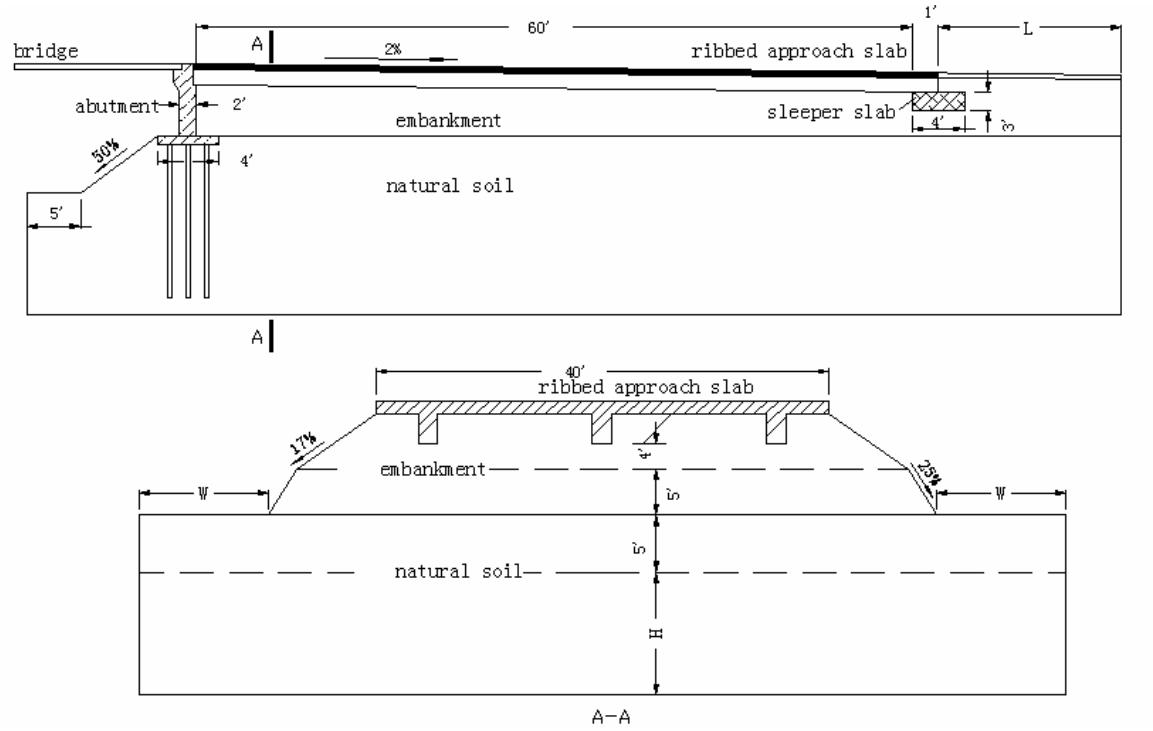

Figure 23
Sketch of bridge abutment

The sketch of abutment, embankment soil and subgraded natural soil, soil material properties, soil boundary conditions and the truck load on approach slab are all the same as those used in the flat approach slab model in figure 2.

In this study, 2, 3, and 4 beam alternatives were studied for a given approach slab width of 40 ft., which correspond to beam spacings of 32, 16 and 12 ft., respectively. For a ribbed slab with beam spaced at 32, 16, and 12 ft., the slabs with thickness of 14, 12 and 12 in. were used, respectively.

To design these ribbed beams, the truck loads were shifted transversally on the slab to maximize the load effects of the interior and exterior beams separately, and the corresponding reactions of all the beams were also predicted. Only the maximum deflection is presented in this report.

Predicted Results

Figures 24 to 27 show the increase of the magnitude of the beam's maximum deflections and internal moments of interior beams with the increase of the embankment differential settlements. If the differential settlement of an approach slab with a 60-ft.-long span is over 3 in., almost no change occurs in the approach slab's deflections and internal moments. This indicates that the settlement no longer affects the performance of the slab since the approach slab almost completely loses its contact with the soil, except at the end near the sleeper slab, and thus becomes a simply-supported beam.

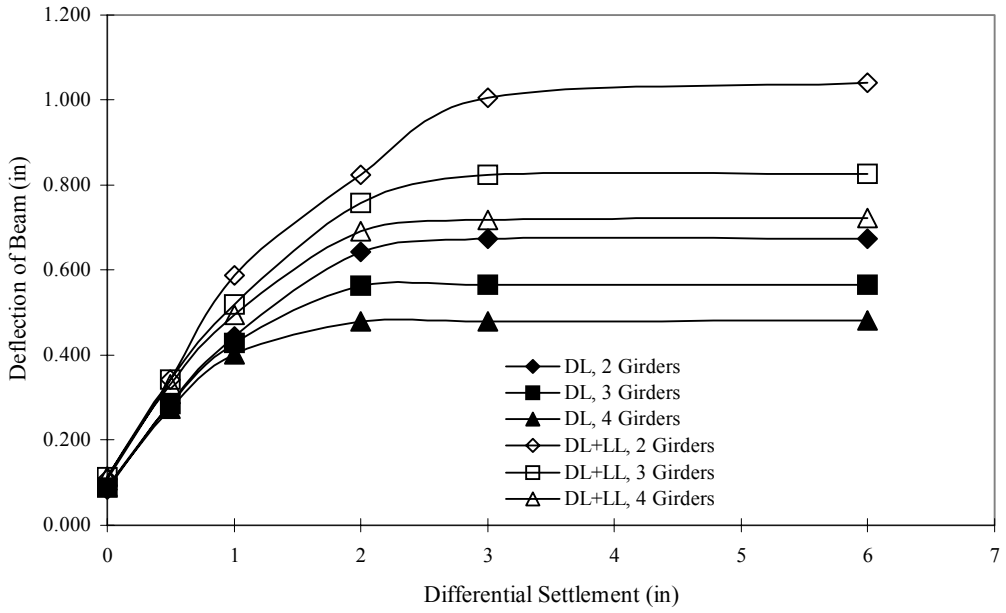

Figure 24
Deflection of beam versus differential settlement (60')

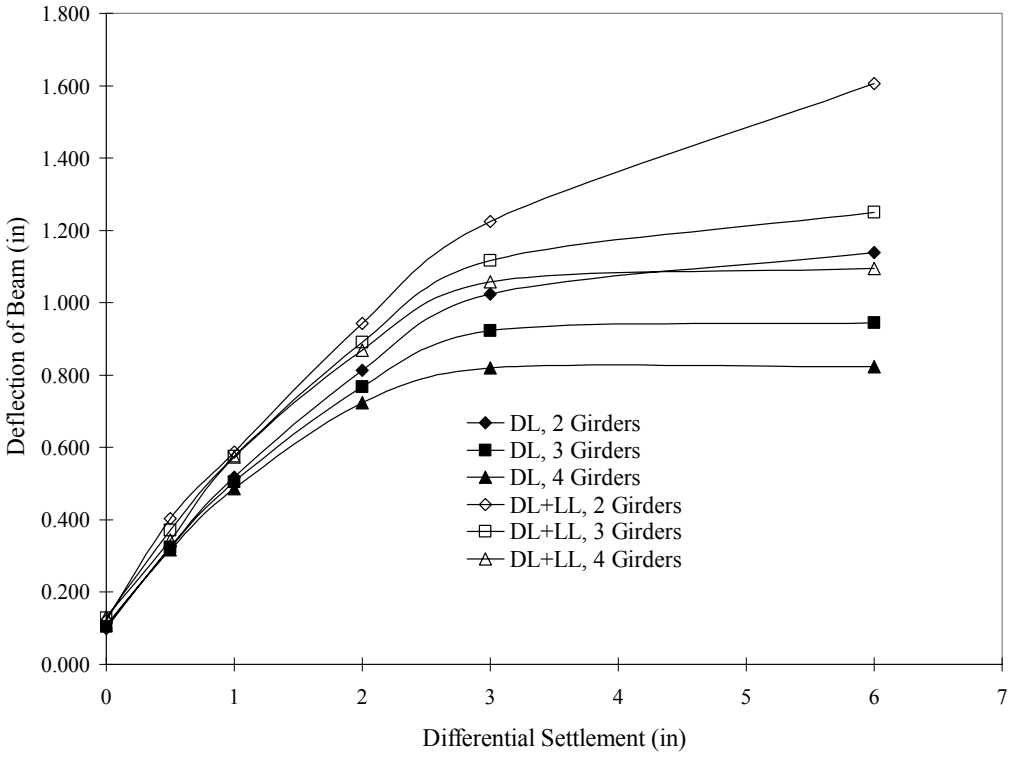

Figure 25
Deflection of beam versus differential settlement (80')

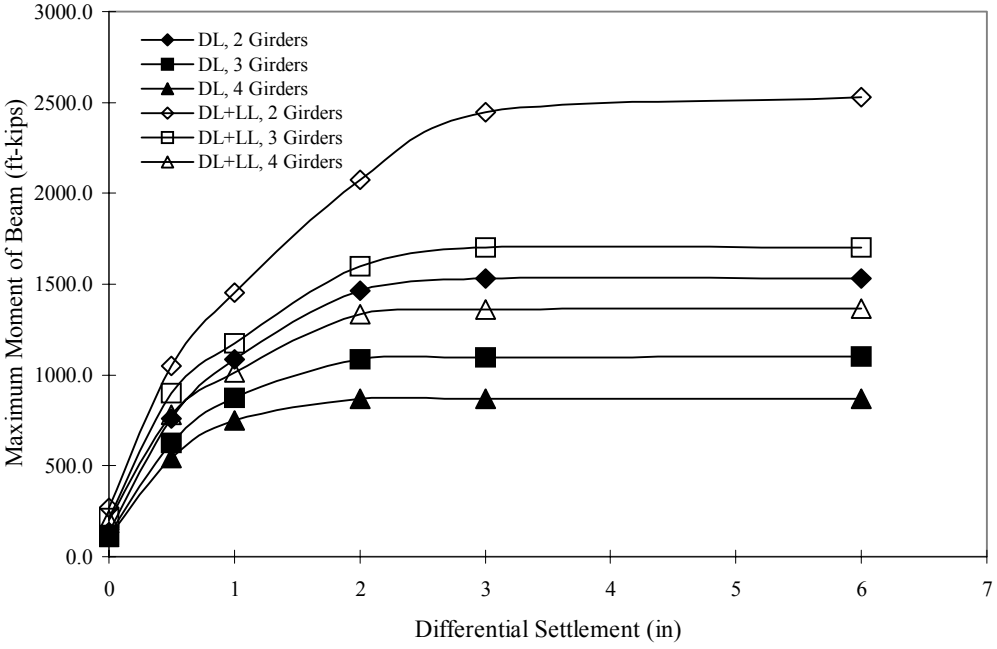

Figure 26
Maximum moment of interior beam versus differential settlement (60')

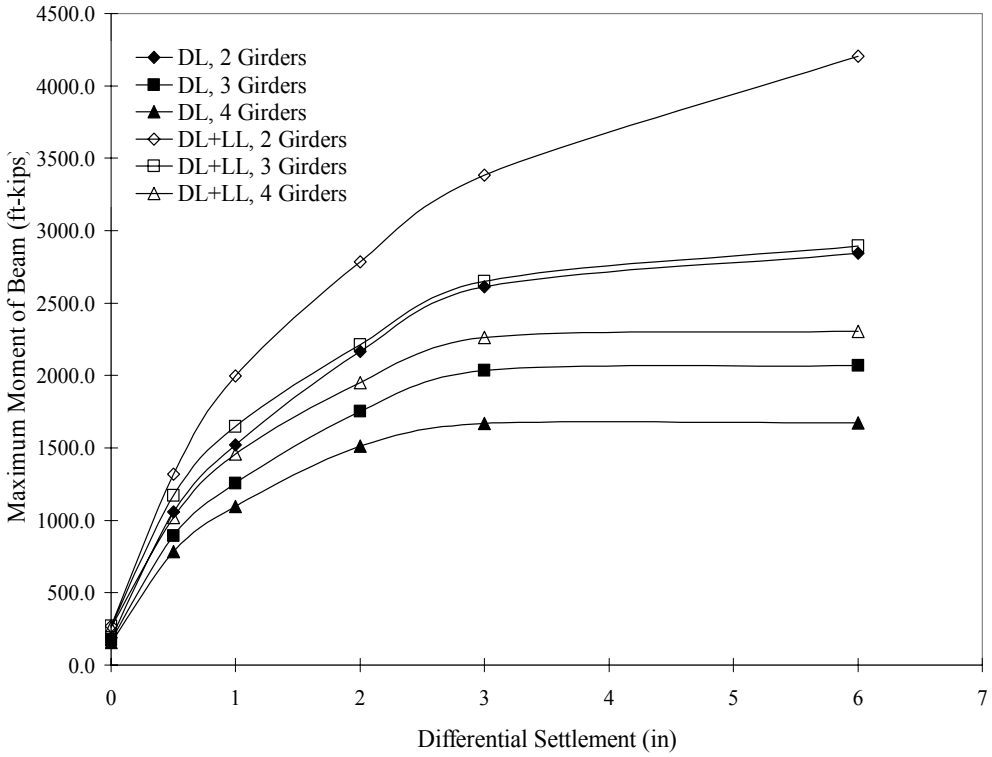

Figure 27
Maximum moment of interior beam versus differential settlement (80')

Similarly, as shown in figures 28 and 29, the total reaction force of beams at the sleeper slab end keeps increasing with the increase of the differential settlements. Since the slab loses more support from soil as the settlement increases, a larger portion of the slab self-weight and truck loads are passed to the sleeper slab instead of directly to the soil under the ribbed slab. 3-D contour plots of finite element results in figures 30 and 31 show how the settlement change affects the ribbed slab stress distributions.

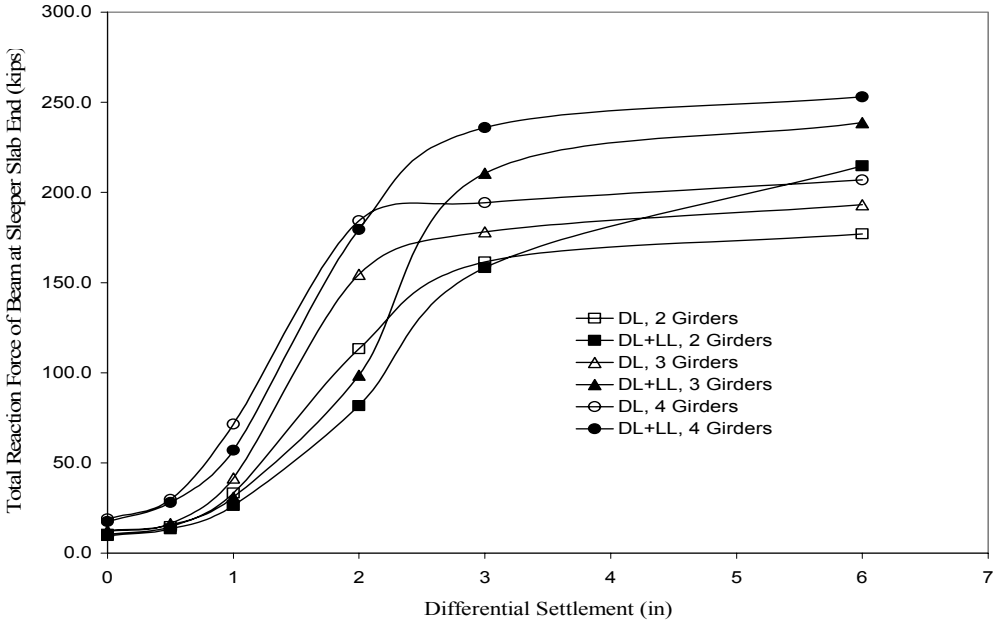

Figure 28

Total reaction force of beams at sleeper slab end versus differential settlement (60')

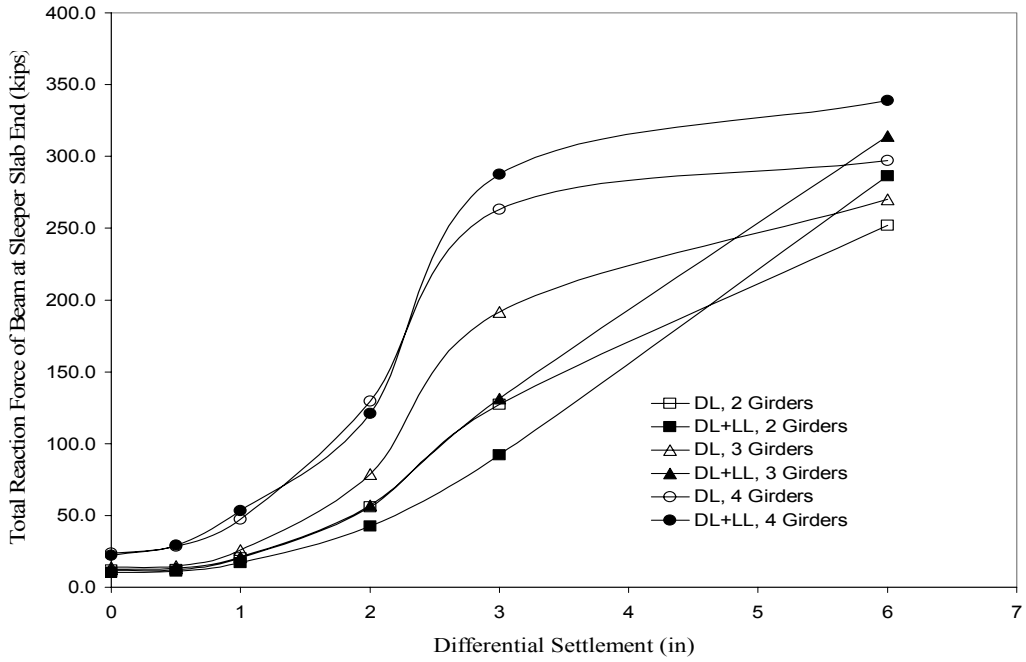

Figure 29

Total reaction force of beams at sleeper slab end versus differential settlement (80')

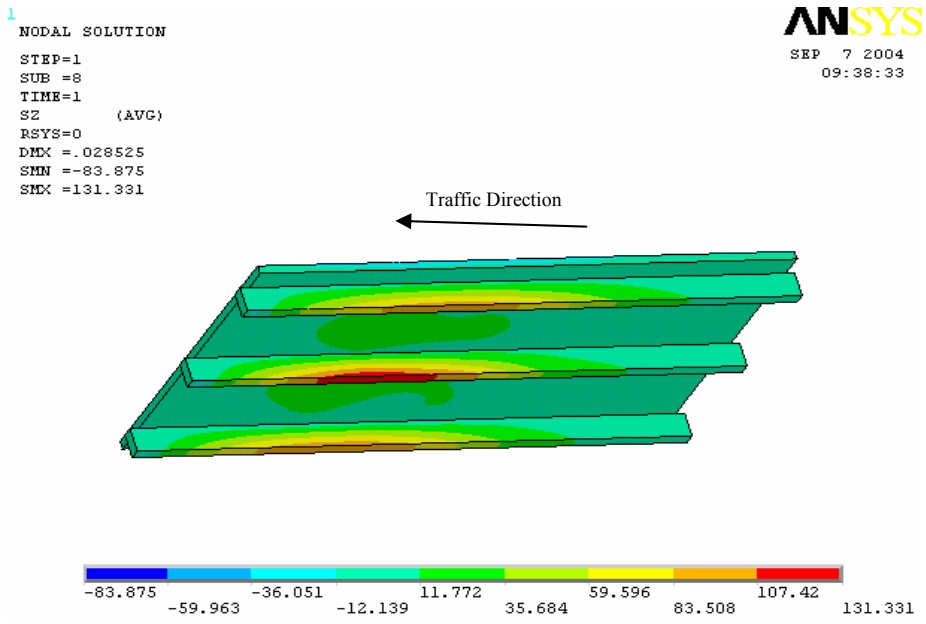

(a) Settlement = 0.5 in.

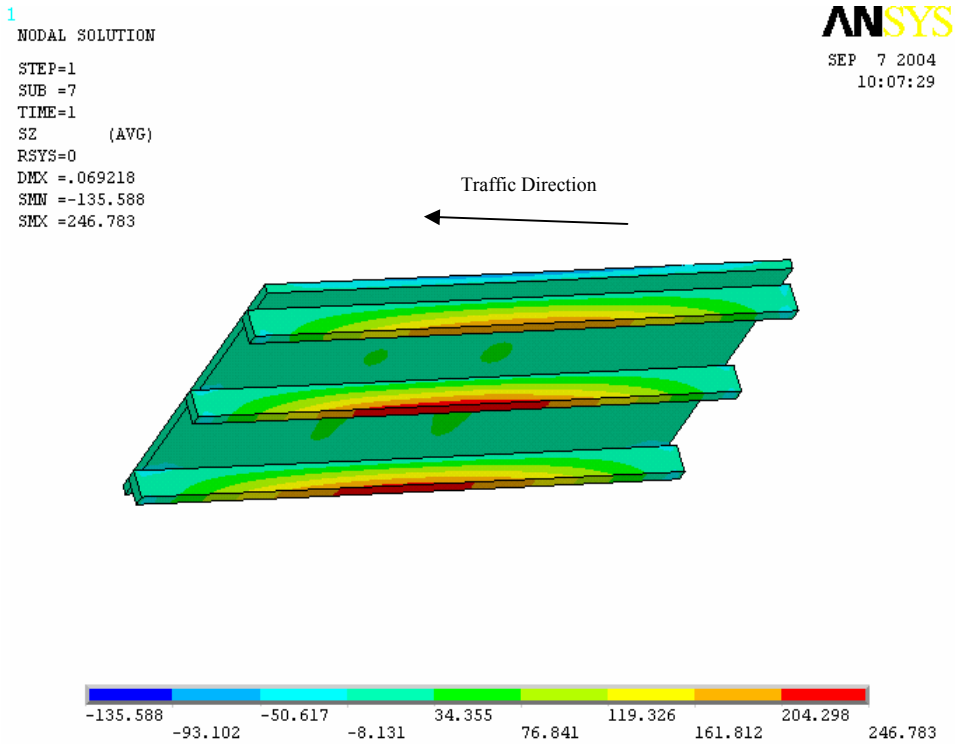

(b) Settlement = 6 in.

Figure 30
Longitudinal stress distribution in slab (ksf) (60 ft.)

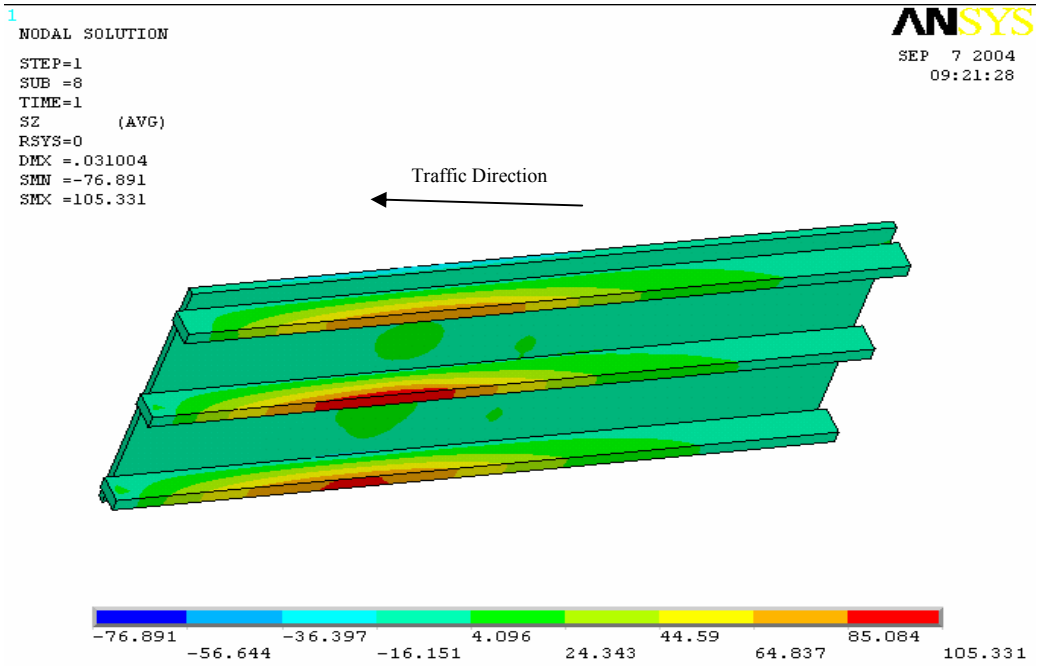

(a) Settlement = 0.5 in.

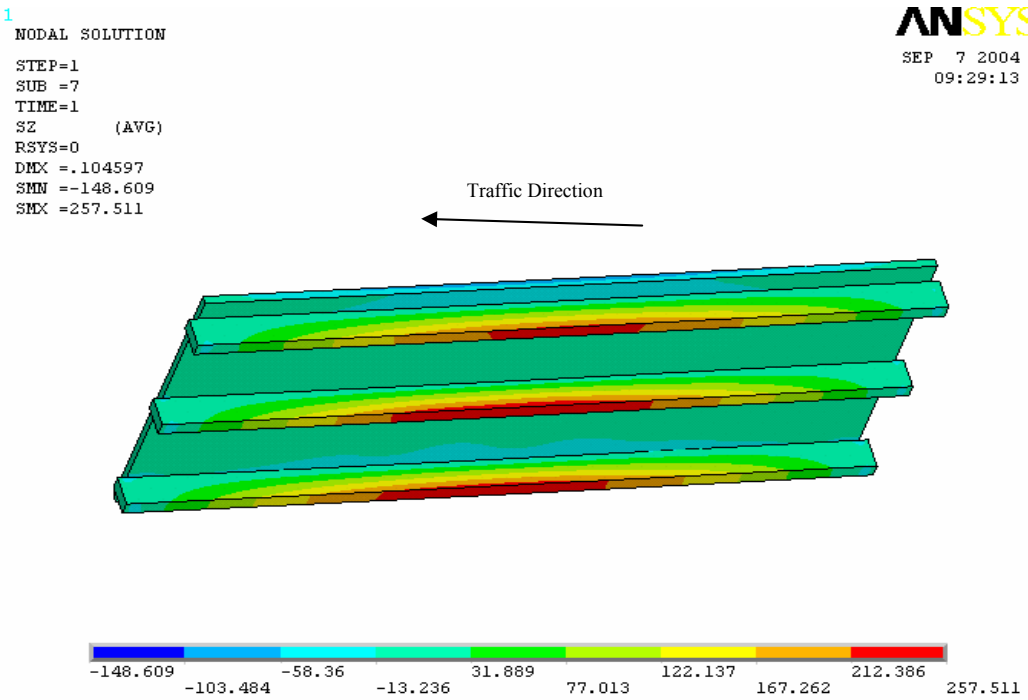

(b) Settlement = 6 in.

Figure 31
Longitudinal stress distribution in slab (ksf) (80 ft.)

Tables 6 to 13 show that the mid-span deflections and internal moments of beams with closer spacing are smaller than those of beams with larger spacing, which means using smaller beam spacing can control the mid span deflection and therefore control the change of the slope angle (θ1 in figure 1). However, tables 8 to 13 and figures 28 and 29 also show that for a given settlement, as beam spacing decreases, the total reaction force (corresponding to the maximum internal moment) of beams at the sleeper slab end increases, which means a higher percentage of the forces is transferred to the sleeper slab. Correspondingly, as shown in tables 6 and 7, the smaller the beam spacing, the more deformation (settlement) of the beam end near the sleeper slab (see Δ_1 in figure1). This is because the higher stiffness of the beam with a smaller spacing makes the beam lose more contact with the soil. It therefore transfers more load to the end near the sleeper slab for the same embankment settlement. Therefore, while a more rigid approach slab will decrease the change of slope angle (θ_1 in figure 1) and mid-span deflection(Δ_2 in figure 1), it may also increase the reaction force beneath the contact area of the sleeper slab, thereby increasing the faulting deflection (Δ_1 in figure 1). In such cases, a spread footing may be necessary to distribute this force. In these tables, both the maximum reaction of one control beam and the corresponding reactions of the rest beams are given. The "total" deflection in the tables refers to the load induced deformation (Δ_2 in figure1) that consists of the slab bending and the support settlement.

Meanwhile, tables 8 to 13 show that in some cases when the settlement is small, the reaction force of the beam at the sleeper slab end due to self-weight of the ribbed slab is surprisingly larger than the reaction force due to the self-weight and truck load together. The reason is that the beam has more deflection due to total load than due to self-weight. When settlement is small, beams subjected to the total load have more contact support from soil than those subjected to self-weight only, thus may have smaller reaction forces at the beam ends. The interaction of the ribbed slab and the soil is affected by the magnitude of the external load as well as the embankment settlement and the stiffness of the structure.

Table 6

Deflection of beam (60')

Differential Settlement (in)	Beam Spaced at 32 ft.				Beam Spaced at 16 ft.				Beam Spaced at 12 ft.			
	DL		DL+LL		DL		DL+LL		DL		DL+LL	
	Total Deflection (in)		Total Deflection (in)		Total Deflection (in)		Total Deflection (in)		Total Deflection (in)		Total Deflection (in)	
	at Mid-span	at End near Sleeper Slab	at Mid-span	At End near Sleeper Slab	At Mid-span	at End near Sleeper Slab	at Mid-span	at End near Sleeper Slab	at Mid-span	at End near Sleeper Slab	at Mid-span	at End near Sleeper Slab
0	0.072	0.084	0.105	0.094	0.074	0.088	0.109	0.099	0.074	0.090	0.111	0.102
0.5	0.288	0.096	0.343	0.101	0.285	0.098	0.342	0.109	0.274	0.101	0.331	0.112
1	0.445	0.099	0.587	0.108	0.428	0.107	0.519	0.118	0.403	0.111	0.495	0.122
2	0.643	0.113	0.824	0.121	0.562	0.123	0.759	0.136	0.480	0.123	0.692	0.141
3	0.674	0.118	1.005	0.137	0.566	0.125	0.824	0.147	0.481	0.124	0.718	0.147
6	0.675	0.119	1.041	0.145	0.566	0.126	0.826	0.150	0.481	0.126	0.723	0.149

Table 7

Deflection of beam (80')

Differential Settlement (in)	Beam Spaced at 32 ft.				Beam Spaced at 16 ft.				Beam Spaced at 12 ft.			
	DL		DL+LL		DL		DL+LL		DL		DL+LL	
	Total Deflection (in)		Total Deflection (in)		Total Deflection (in)		Total Deflection (in)		Total Deflection (in)		Total Deflection (in)	
	at Mid-span	at End near Sleeper Slab	at Mid-span	at End near Sleeper Slab	At Mid-span	at End near Sleeper Slab	at Mid-span	at End near Sleeper Slab	at Mid-span	at End near Sleeper Slab	at Mid-span	at End near Sleeper Slab
0	0.099	0.106	0.121	0.112	0.105	0.105	0.128	0.118	0.109	0.109	0.131	0.115
0.5	0.326	0.113	0.404	0.119	0.324	0.114	0.372	0.120	0.318	0.119	0.344	0.143
1	0.518	0.120	0.588	0.125	0.504	0.124	0.575	0.130	0.486	0.131	0.574	0.166
2	0.813	0.133	0.943	0.138	0.768	0.144	0.891	0.149	0.724	0.153	0.869	0.190
3	1.024	0.146	1.225	0.151	0.923	0.162	1.118	0.174	0.820	0.168	1.058	0.212
6	1.138	0.159	1.607	0.184	0.944	0.169	1.249	0.191	0.823	0.170	1.094	0.215

Table 8

Internal force of beam spaced at 32 ft. (60', with two beams only)

Differential Settlement (in)	Moment (kip-ft.)		Reaction Force at Sleeper Slab End (kips)			
	DL	DL+LL	Beam 1		Beam 2	
			DL	DL+LL	DL	DL+LL
0	135.8	270.2	5.0	4.6	5.3	5.1
0.5	757.9	1048.2	7.4	5.9	7.2	7.5
1	1085.1	1452.3	16.5	10.5	16.8	15.8
2	1466.3	2074.8	56.5	31.7	56.9	50.1
3	1533.6	2445.8	80.7	75.2	80.7	83.0
6	1532.9	2530.4	88.5	119.3	88.6	95.4

Table 9

Internal force of beam spaced at 32 ft. (80', with two beams only)

Differential Settlement (in)	Moment (kip-ft)		Reaction Force at Sleeper Slab End (kips)			
	DL	DL+LL	Beam 1		Beam 2	
			DL	DL+LL	DL	DL+LL
0	190.2	269.1	5.7	4.4	6.1	5.9
0.5	1056.5	1319.3	5.8	4.7	6.4	6.3
1	1520.0	1998.2	9.9	7.1	10.2	9.8
2	2165.9	2787.0	27.9	17.0	28.2	25.5
3	2613.0	3384.2	62.9	36.6	64.5	55.7
6	2845.9	4203.3	125.9	152.2	126.2	134.2

Table 10

Internal force of beam spaced at 16 ft. (60', with three beams)

Differential Settlement (in)	Exterior Beam								Interior Beam							
	Moment (kip-ft.)		Reaction Force at Sleeper Slab End (kips)						Moment (kip-ft.)		Reaction Force at Sleeper Slab End (kips)					
			Beam 1		Beam 2		Beam 3				Beam 1		Beam 2		Beam 3	
	DL	DL+LL	DL	DL+LL	DL	DL+LL	DL	DL+LL	DL	DL+LL	DL	DL+LL	DL	DL+LL	DL	DL+LL
0	92.9	171.6	3.4	3.3	5.1	5.5	3.7	3.8	121.5	211.5	3.4	3.3	5.1	5.7	3.7	3.5
0.5	540.2	822.1	5.0	3.8	6.6	6.4	4.8	4.9	627.9	898.3	5.0	4.7	6.6	5.9	4.8	4.9
1	763.2	1090.0	14.0	6.7	13.4	10.2	14.2	14.0	874.2	1174.4	14.0	10.4	13.4	8.3	14.2	12.3
2	964.5	1505.0	51.3	26.2	51.6	38.5	51.6	51.0	1086.4	1596.2	51.3	38.9	51.6	29.7	51.6	30.1
3	968.6	1543.8	58.4	73.4	61.2	69.9	58.6	61.2	1098.3	1700.2	58.4	70.5	61.2	72.8	58.6	67.3
6	968.2	1550.6	62.9	90.2	67.4	79.9	62.9	66.6	1099.2	1702.2	62.9	79.1	67.4	85.4	62.9	74.2

Differential Settlement (in)	Exterior Beam								Interior Beam							
	Moment (kip-ft.)		Reaction Force at Sleeper Slab End (kips)						Moment (kip-ft.)		Reaction Force at Sleeper Slab End (kips)					
			Beam 1		Beam 2		Beam 3				Beam 1		Beam 2		Beam 3	
	DL	DL+LL	DL	DL+LL	DL	DL+LL	DL	DL+LL	DL	DL+LL	DL	DL+LL	DL	DL+LL	DL	DL+LL
0	139.3	209.1	3.9	2.7	6.3	6.0	3.9	3.9	172.6	271.0	3.9	3.4	6.3	5.4	3.9	3.7
0.5	779.5	1054.9	4.0	2.7	7.0	6.4	4.0	3.9	894.7	1171.2	4.0	3.6	7.0	5.7	4.0	3.9
1	1000.2	1509.8	7.8	4.5	10.3	8.7	7.8	7.7	1256.9	1645.7	7.8	6.5	10.3	7.4	7.8	7.4
2	1565.2	2085.5	26.6	13.3	25.6	19.1	26.6	25.3	1751.1	2213.9	26.6	19.2	25.6	15.5	26.6	22.4
3	1828.5	2503.8	64.3	32.4	62.0	43.0	65.5	60.0	2034.5	2651.4	64.3	44.3	62.0	35.3	65.5	52.0
6	1862.4	2736.0	88.9	110.4	92.1	102.8	89.4	93.8	2069.4	2893.4	88.9	105.9	92.1	106.1	89.4	102.1

Table 11

Internal force of beam spaced at 16 ft. (80', with three beams)

Table 12

Internal force of beam spaced at 12 ft. (60', with four beams)

Differential Settlement (in)	Exterior Beam										Interior Beam									
	Moment (kip-ft.)		Reaction Force at Sleeper Slab End (kips)								Moment (kip-ft.)		Reaction Force at Sleeper Slab End (kips)							
			Beam 1		Beam 2		Beam 3		Beam 4				Beam 1		Beam 2		Beam 3		Beam 4	
	DL	DL+ LL	DL	DL+ LL	DL	DL+ LL	DL	DL+ LL	DL	DL+ LL	DL	DL+ LL	DL	DL+ LL	DL	DL+ LL	DL	DL+ LL	DL	DL+ LL
0	80.3	150.0	4.9	5.3	4.6	4.8	4.6	5.0	4.8	5.1	110.5	203.0	4.9	4.2	4.6	4.0	4.6	4.2	4.8	5.0
0.5	450.3	665.6	8.5	7.3	6.5	5.6	6.4	6.7	8.3	8.4	543.4	778.7	8.5	7.3	6.5	5.6	6.4	6.7	8.3	8.4
1	630.6	882.2	20.7	13.2	14.9	9.4	15.0	13.4	20.8	20.3	750.3	1013.8	20.7	14.2	14.9	9.1	15.0	12.7	20.8	20.0
2	734.1	1216.4	46.8	43.2	45.7	39.6	45.4	47.5	46.5	48.1	867.4	1336.0	46.8	45.4	45.7	38.4	45.4	46.7	46.5	49.0
3	734.6	1259.3	48.3	69.4	49.1	60.2	49.1	56.1	48.0	49.4	867.8	1359.5	48.3	67.2	49.1	60.7	49.1	57.3	48.0	50.7
6	734.8	1262.7	50.1	73.4	53.5	66.3	53.6	61.2	49.8	51.6	867.9	1367.9	50.1	70.9	53.5	66.9	53.6	62.4	49.8	52.8

Table 13

Internal force of beam spaced at 12 ft. (80', with four beams)

Differential Settlement (in)	Exterior Beam										Interior Beam									
	Moment (kip-ft.)		Reaction Force at Sleeper Slab End (kips)								Moment (kip-ft.)		Reaction Force at Sleeper Slab End (kips)							
			Beam 1		Beam 2		Beam 3		Beam 4				Beam 1		Beam 2		Beam 3		Beam 4	
	DL	DL+ LL	DL	DL+ LL	DL	DL+ LL	DL	DL+ LL	DL	DL+ LL	DL	DL+ LL	DL	DL+ LL	DL	DL+ LL	DL	DL+ LL	DL	DL+ LL
0	118.4	195.4	5.9	5.3	6.2	5.2	5.6	5.6	6.0	6.0	155.3	259.3	5.9	5.5	6.2	5.2	5.6	5.5	6.0	6.0
0.5	649.6	871.6	7.4	6.3	6.6	5.2	6.9	6.9	7.8	7.7	782.5	1021.6	7.4	8.0	6.6	6.4	6.9	7.2	7.8	7.5
1	921.8	1238.6	13.2	10.0	10.3	7.5	10.2	9.9	13.5	13.3	1097.0	1459.7	13.2	15.4	10.3	8.3	10.2	11.2	13.5	18.4
2	1285.3	1700.5	37.2	24.1	27.4	17.1	27.7	24.2	37.2	35.5	1513.4	1950.9	37.2	32.9	27.4	19.9	27.7	27.2	37.2	40.8
3	1423.9	2003.8	68.4	52.5	63.6	45.3	62.9	57.3	68.3	68.3	1669.1	2263.8	68.4	72.6	63.6	66.4	62.9	71.6	68.3	77.1
6	1427.2	2075.5	73.9	92.9	74.3	84.2	74.0	81.9	74.7	78.0	1672.6	2306.7	73.9	91.7	74.3	84.7	74.0	83.0	74.7	79.7

Effect of Settlement on Beam Design

Since the ribbed approach slab has partial contact supports from the embankment soil for a given embankment settlement, it is necessary to design the slab in order to provide enough strength for the given predicted settlement. When the ribbed approach slab is subjected to bending, the stresses that are induced by the concentrated loads are not uniformly distributed over the whole width of the slab. If the spacing of the beams is large, only part of the slab is effective in resisting a given bending load. It is necessary, for design purpose, to consider only an effective width as the top flange of the beam, as was conducted in flat approach slab design.

For the simply supported ribbed slab, the case of two trucks applied at the mid-span was chosen as the basic loading type and a uniformly distributed dead load was considered. By moving the trucks along the transverse direction of the slab, the critical scenario was observed for exterior and interior beams. The effective width, w_e, is defined in equation (2).

For a ribbed approach slab with a span length of 60 ft. a width of 40 ft. and a beam spacing of 32, 16 and 12 ft., the effective width w_e for both exterior beam and interior beam was calculated by varying the differential settlement from 0 to 6 in., and was plotted in figures 32 to 34. To avoid stress concentration caused by point loads that represent truck wheel loads, the effective width obtained in this paper is the average effective width within 2 ft. range of the point load along the longitudinal direction. As expected, the dead load is much more uniformly distributed across the bridge width and thus, the effective width is larger than that of the live load. The effective width for exterior and interior beams was also determined per AASHTO code (2002) and shown in figures 32 to 34. It is noted that these AASHTO calculations are based on a simply supported beam (partial contact case is not available in the code) that corresponds to the case with a very large differential settlement of embankment.

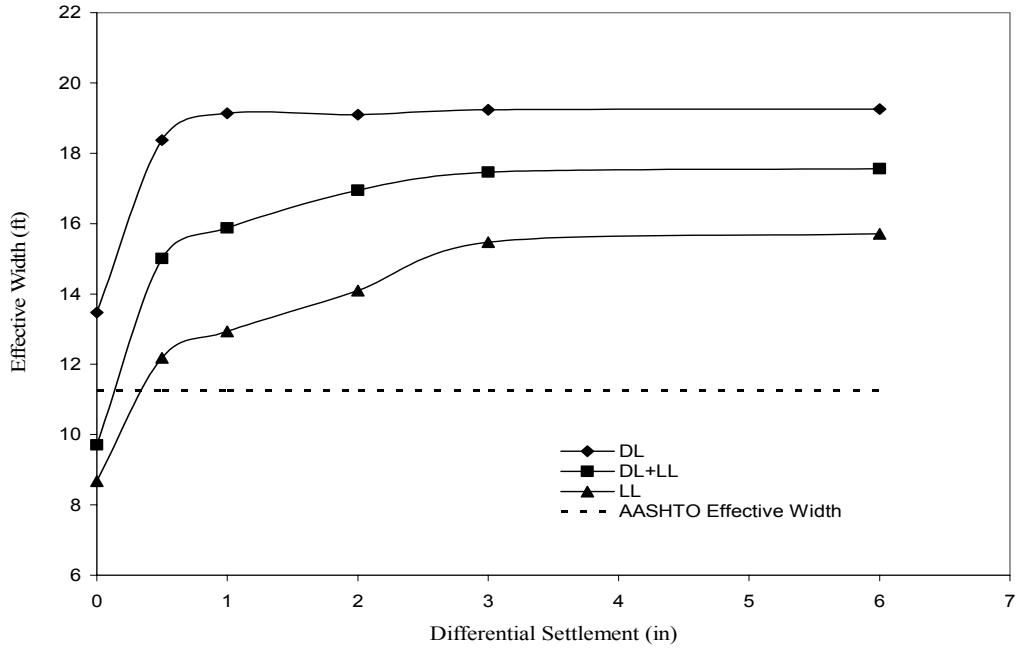

Figure 32
Effective width of beam spaced at 32 ft. (60')

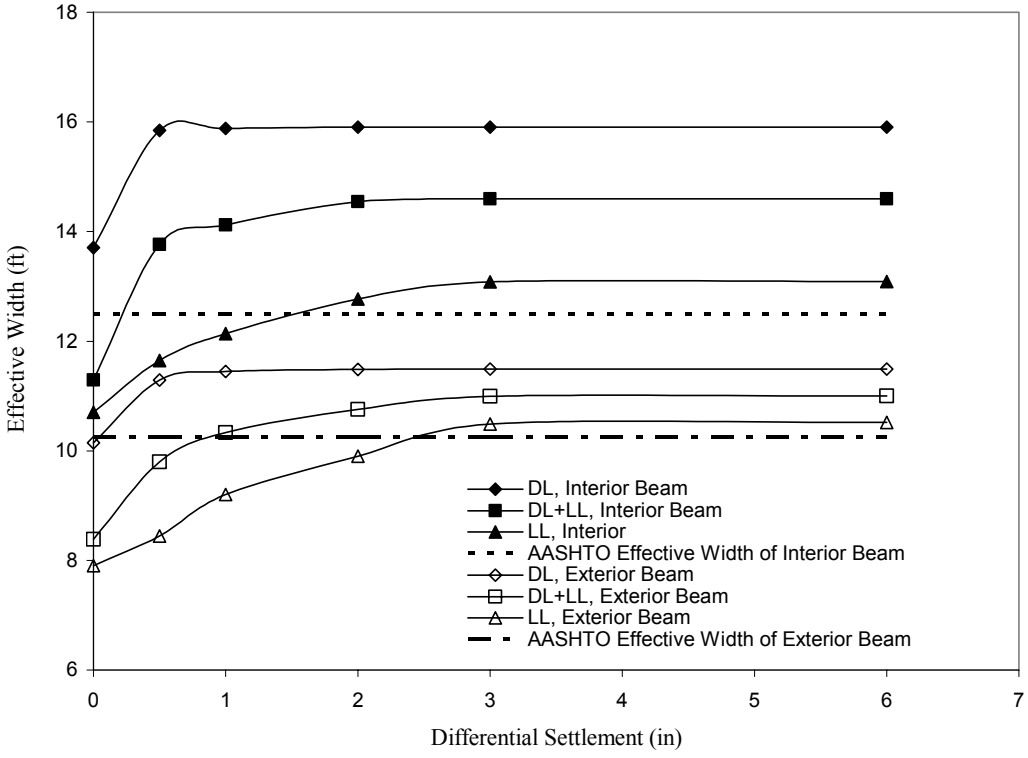

Figure 33
Effective width of beam spaced at 16 ft. (60')

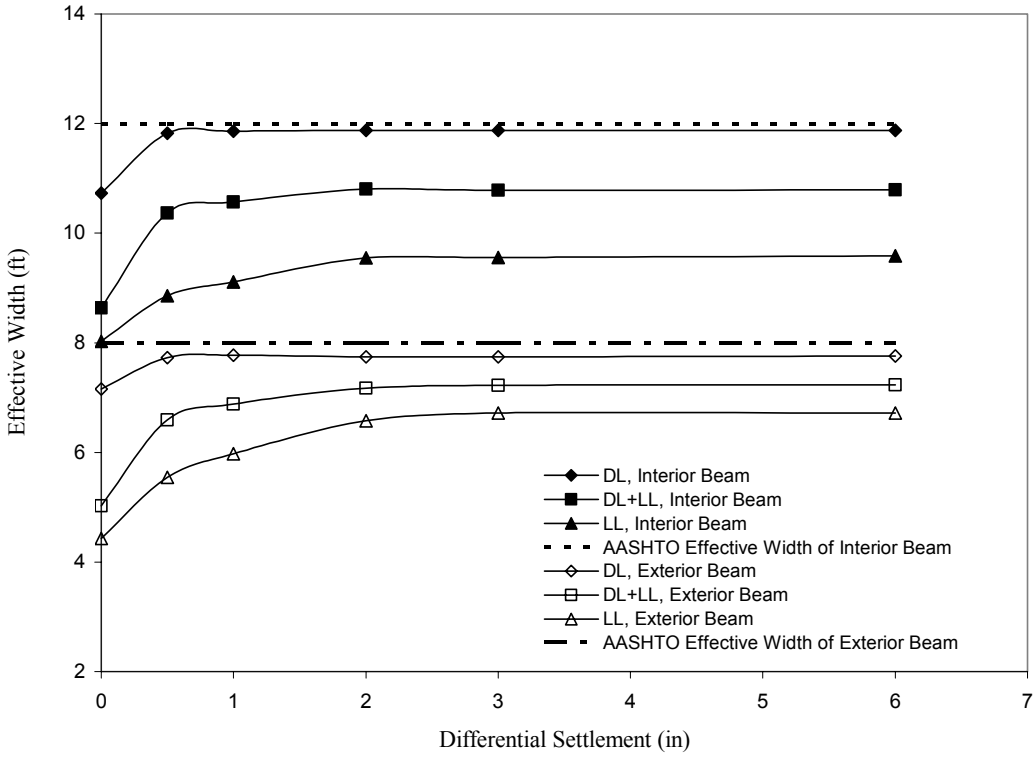

Figure 34
Effective width of beam spaced at 12 ft. (60')

As shown in figures 32 and 33, if the differential settlement is small for beams with a span length of 60 ft., spaced at 32 and 16 ft., the predicted effective width for live loads is smaller than that specified in the codes, implying that using the code effective width is not conservative for designing partial contact slabs. This is because the partial contact of the beam and soil decreases the effective span length of the beam. However, small settlement is not the critical condition. For larger settlement, the code effective width is more conservative.

For beams spaced at 12 ft., as shown in figures 34, the predicted effective width is smaller than the code effective width for both the exterior beams and the interior beams, namely 8 ft. and 12 ft. respectively. In the code specifications (AASHTO 2002), the effective width is controlled by the span length, the slab thickness, and the beam spacing. In the case of 12 ft. beam spacing, the slab effective width, controlled by the beam spacing, is the same as the beam spacing. This means that in this case, the whole slab width is effective, which assumes

that the stress distribution in the slab is perfectly uniform in the code. Since the predicted slab effective width from the finite element analysis is obtained by using equation 2 and the stress distribution cannot be perfectly uniform, the predicted values must be smaller than those of the code specifications in this case.

DISCUSSION OF RESULTS

Current LADOTD Approach Slab

Results in the previous section indicated that LADOTD's current slab design (with a span length of 40 ft.) is sufficient for cases when the embankment settlement is very small. However, this design's ultimate strength is not adequate for a differential settlement greater than 0.6 in., meaning that either more reinforcement, thicker slab section, and/or control of settlement is needed to satisfy the AASHTO structural design requirements. Even if the slab cannot meet the design requirements, the slab will not necessarily fail since load factors are considered in the design codes. However, an underdesigned slab does indicate a potential failure or underperformance, such as breaking, cracking, and deterioration, which have all been observed in the field.

Using the developed procedure shown in the calculation example (see Appendix A), the deflection and rotation angle can be predicted for the current LADOTD concrete approach slab (with a span length of 20 and 40 ft., and thickness of 12 in.) with bottom reinforcement #6@6". The predicted total instantaneous deformation for the 20 ft. approach slab versus different differential settlements is shown in figures 35 and 36 by using both effective and total width methods. Similarly, figures 37 and 38 show the total instantaneous deformation for the 40 ft. approach slab versus different differential settlements. Using the effective width of slab is more conservative than using the total slab width in calculating the deformation of the slab, though both methods are allowed by AASHTO (2002).

In LADOTD's current approach slab design, the reinforcement ratio ρ is identical for slabs with a span length of 20 ft. and 40 ft. For the 20 ft. long approach slab, the required reinforcement, predicted using the established analytical procedure (equations), is shown in table 14. However, for the slab with a length of 40 ft., the reinforcement was not predicted here again, since the reinforcement was predicted directly earlier with finite element modeling as shown in table 5.

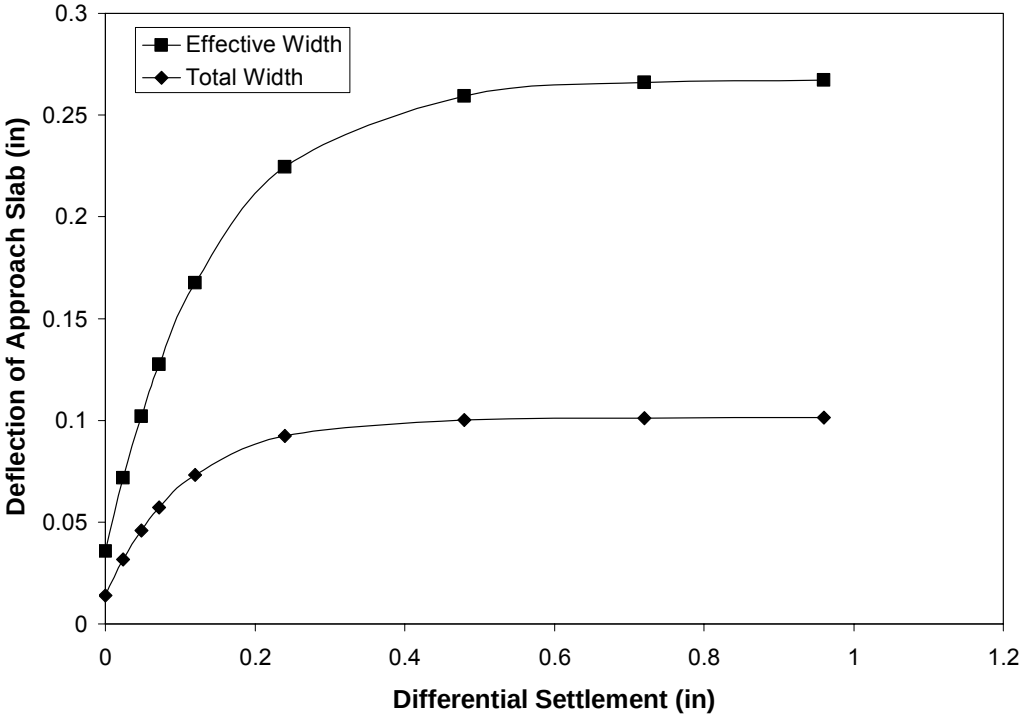

Figure 35
Deflection of 20-ft.-long approach slab versus differential settlement

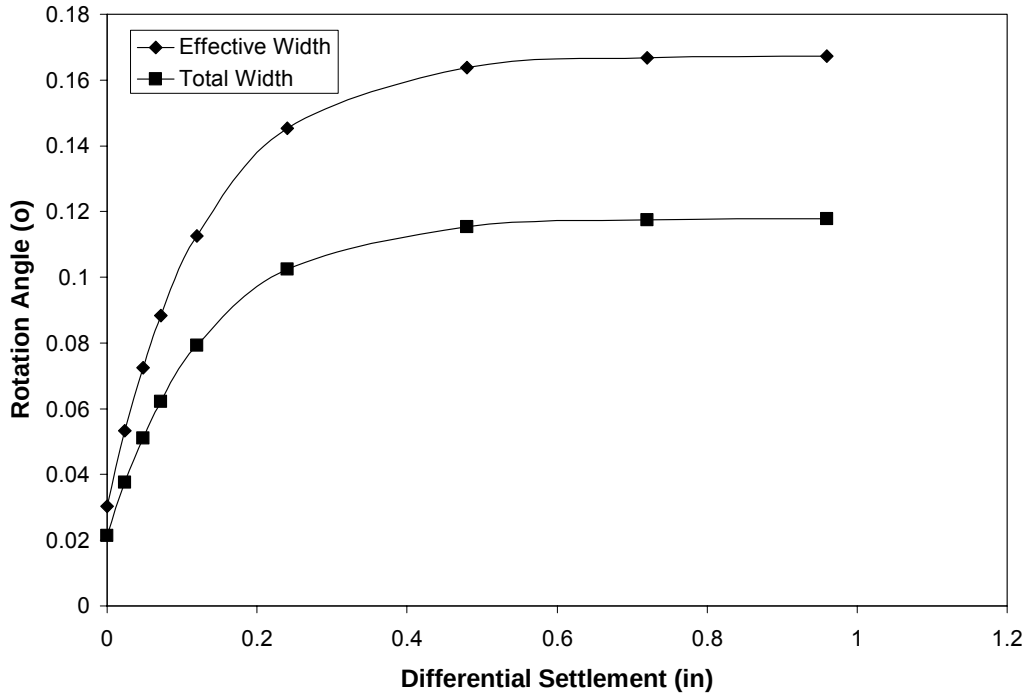

Figure 36
Rotation angle of 20-ft.-long approach slab versus differential settlement

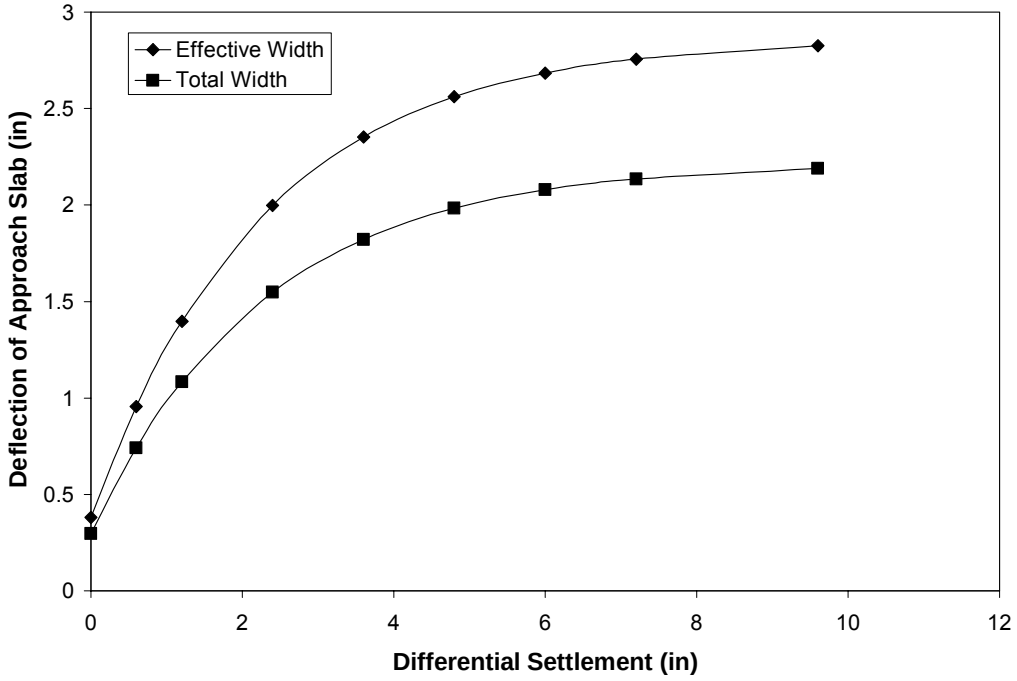

Figure 37
Deflection of 40-ft.-long approach slab versus differential settlement

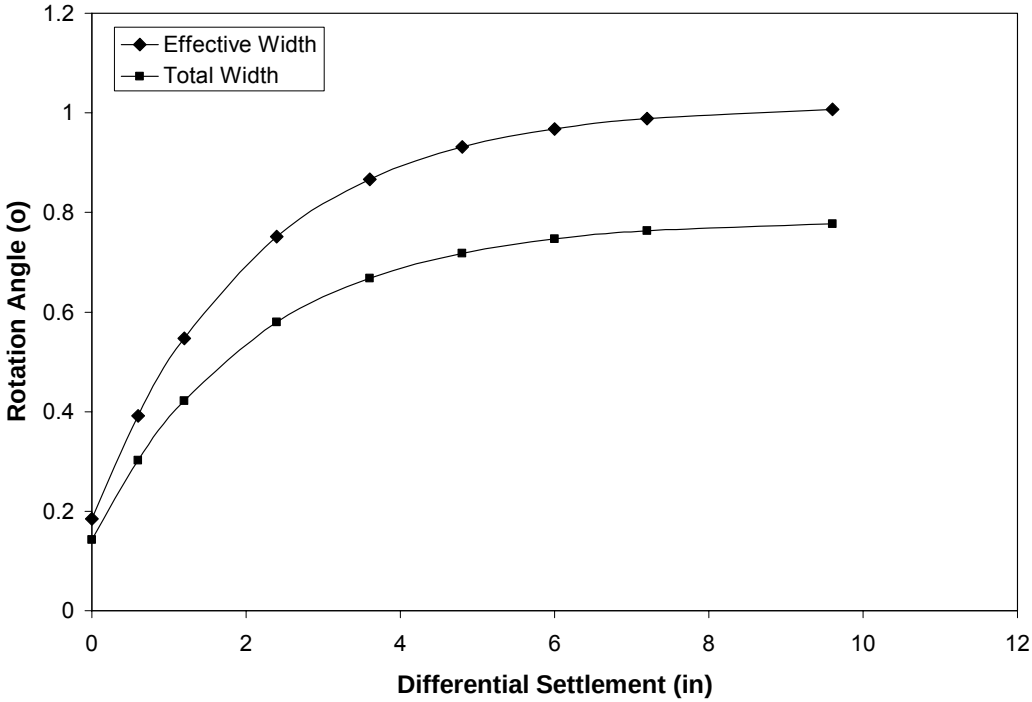

Figure 38
Rotation angle of 40-ft.-long approach slab versus differential settlement

Table 14
Reinforcement for slab under different settlement
(Span length of 20 ft, f'_c = 4000 psi and f_y = 60,000 psi)

Settlement (in)	M (kip-ft.)			ρ (required)	ρ max (allowed)	As ($in.^2/ft.$)	Reinforcement
	DL	LL	1.3DL +2.17(LL+IM)				
0.00	11.0	39.6	95.1	0.00172	0.0214	0.21	#4@12.0”
0.02	23.4	68.0	156.2	0.00286	0.0214	0.34	#4@ 7.0”
0.06	41.2	112.5	254.6	0.00474	0.0214	0.57	#4@ 4.0”
0.10	52.4	144.5	327.8	0.00618	0.0214	0.74	#5@ 5.0”
0.12	56.4	156.9	356.9	0.00677	0.0214	0.81	#5@ 4.5”
0.24	67.9	200.6	462.7	0.00895	0.0214	1.07	#6@5.0”
0.48	71.6	223.0	520.2	0.01019	0.0214	1.22	#7@6.0”
0.60	71.8	225.3	526.3	0.01032	0.0214	1.24	#8@7.5”
1.20	71.8	226.6	529.9	0.01040	0.0214	1.25	#8@7.5”
7.20	71.8	226.6	529.9	0.01040	0.0214	1.25	#8@7.5”

Table 14 shows that the current LaDOTD slab reinforcement 0.88 $in.^2/ft.$ is also not adequate for a 20 ft. slab if a differential settlement of more than 0.24 in. is considered. However, when the settlement increases beyond 0.48 in., no increase of reinforcement is required since the slab has become a two-end supported beam. Therefore, from the strength point of view, by increasing the reinforcement from #6@6” to #7@6”, the 12” thickness is still good for a 20 ft. slab, no matter how large the settlement is. In contrast, for the 40 ft. slab as shown in table 5, the required reinforcement continues to increase as the differential settlement increases. Eventually the maximum reinforcement ratio would be exceeded, and a thicker slab would be required.

For the same settlement of 0.6 in., the 20 ft. slab requires slightly more reinforcement than the 40 ft. slab does (1.24 $in.^2/ft.$ in table 14 versus 1.14 $in.^2/ft.$ in table 5). There are two reasons for this difference. First, the 40 ft. slab is designed directly with the finite element prediction as shown in table 5 while the 20 ft. slab is based on the established analytical procedure that has lost some accuracy. Second, for the given settlement, the 20 ft. slab has lost all contact with the soil except at the two ends, while the 40 ft. slab still has soil support, which reduces the internal moment.

Proposed Approach Slab

Flat Approach Slab

This research shows how the finite element procedure can be used to help design approach slabs for a given embankment settlement. Parametric studies were conducted to develop a simpler design procedure so that engineers do not need to use finite element analysis in a routine design. Instead, coefficients are multiplied to a simple beam response to consider the interaction of the embankment soil and the slab under a given settlement.

Table 15
Reinforcement ratio of slab under different settlement
(f'_c = 4000 psi and f_y = 60,000 psi)

Differential settlement (in)	40-ft. Slab			60-ft. Slab		
	ρ for thickness of 12 in. (1)	ρ for thickness of 18 in.	ρ for thickness of 24 in.	ρ for thickness of 21 in.	ρ for thickness of 27 in.	ρ for thickness of 36 in.
0	0.0061	0.0024	0.0014	0.0034	0.0022	0.0014
0.6	0.0137	0.0077	0.0056	0.0056	0.0043	0.0034
1.2	0.0207	0.0110	0.0072	0.0077	0.0061	0.0049
2.4	NA(2)	0.0138	0.0079	0.0112	0.0087	0.0066
3.6	NA	0.0147	0.0079	0.0140	0.0104	0.0072
4.8	NA	0.0149	0.0079	0.0162	0.0115	0.0075
6	NA	0.0149	0.0079	0.0178	0.0121	0.0075
7.2	NA	0.0150	0.0079	0.0191	0.0124	0.0076

Note: (1) The value ρ in this table is different from the ρ in table 5. The moment used to design reinforcement in this table is from equations (3) and (4), while moment used in table 5 is from finite element results.

(2) The required reinforcement ratio ρ exceeds the allowed maximum reinforcement of flexure, i.e., $\rho > \rho_{max} = 0.75\rho_b$, meaning that section dimension needs to be increased.

While the current 20 ft. approach slab with a thickness of 12 in. will have adequate strength by increasing the reinforcement to #7@6" as discussed earlier, slabs with a length of 40 ft.

and 60 ft. are designed here for different slab thickness using the procedure developed earlier (i.e., hand calculation instead of finite element modeling). Table 15 shows the reinforcement ratio required by the AASHTO design code specifications (AASHTO 2002), and figures 39 to 42 show the relationship of the predicted total instantaneous elastic deflection and the maximum rotation angle of reinforced approach slab with different thicknesses and the differential settlement of the embankment soil.

For a slab with the same dimensions, more settlement causes a larger internal moment in the approach slab and thus requires more reinforcement. For the same slab length and embankment settlement, increase in the thickness of the slab reduces the deformation of the slab. By comparing the deflection and rotation angle of the 40-ft. slab of LaDOTD's current design (12 in. thickness) with the proposed design (in figures 39 to 42), it is obvious that with the increase in slab thickness and reinforcement the slab deformation can be well controlled. Therefore, considering different levels of embankment settlements, an engineer can either use a thicker slab and/or more reinforcement to allow partial or full separation between the embankment and the slab.

In addition, the approach slabs were also designed following the AASHTO LRFD specifications, and the reinforcement is shown in table B5, in Appendix B. The LRFD code requires slightly more reinforcement and is therefore adapted in table 16 to satisfy both AASHTO Standard and LRFD specifications. Only four options that the writers believe more economical and also adequate in strength are kept in table 16 and will be recommended.

The designed slabs with reinforcement shown in table 16 were also rated against the three special trucks provided by LADOTD using both AASHTO Standard and LRFD codes. The results are shown in tables B18, B20, B22, and B24, in Appendix B. All the operation ratings are larger than 1.0. Therefore, the new designs are adequate for the special trucks.

Table 16
Reinforcement ratio of slab under different settlement (adopted new design)
(f'_c = 4000 psi and f_y = 60,000 psi)

Differential settlement (in)	40-ft. Slab		60-ft. Slab	
	ρ for thickness of 18 in.	ρ for thickness of 24 in.	ρ for thickness of 21 in.	ρ for thickness of 27 in.
0	0.0025 #7@16" (ρ = 0.0025)	0.0014 (ρ_{min}=0.0018) #6@11" (ρ = 0.0019)	0.0035 #6@7" (ρ = 0.0035)	0.0022 #6@8" (ρ = 0.0023)
0.6	0.0081 #8@6" (ρ = 0.0088)	0.0058 #8@6.5" (ρ = 0.0058)	0.0060 #8@7" (ρ = 0.0062)	0.0046 #8@7" (ρ = 0.0047)
1.2	0.0114 #9@5.5" (ρ = 0.0121)	0.0074 #10@8" (ρ = 0.0076)	0.0083 #9@6.5" (ρ = 0.0085)	0.0065 #9@6.5" (ρ = 0.0065)
2.4	0.0143 #10@6.0" (ρ = 0.0141)	0.0080 #10@8.5" (ρ = 0.0081)	0.0121 #10@5.5" (ρ = 0.0128)	0.0093 #10@5.5" (ρ = 0.0096)
3.6	0.0151 #10@5.5" (ρ = 0.0154)	0.0081 #10@8.5" (ρ = 0.0081)	0.0151 #10@4.5" (ρ = 0.0156)	0.0110 #10@4.5" (ρ = 0.0117)
4.8	0.0153 #10@5.5" (ρ = 0.0154)	0.0081 #10@8.5" (ρ = 0.0081)	0.0174 #10@4" (ρ = 0.0176)	0.0120 #10@4" (ρ = 0.0132)
6	0.0154 #10@5.5" (ρ = 0.0154)	0.0081 #10@8.5" (ρ = 0.0081)	0.0191 #10@3.5" (ρ = 0.0202)	0.0126 #10@4" (ρ = 0.0132)
7.2	0.0154 #10@5.5" (ρ = 0.0154)	0.0081 #10@8.5" (ρ = 0.0081)	0.0204 #10@3.5" (ρ = 0.0202)	0.0130 #10@4" (ρ = 0.0132)

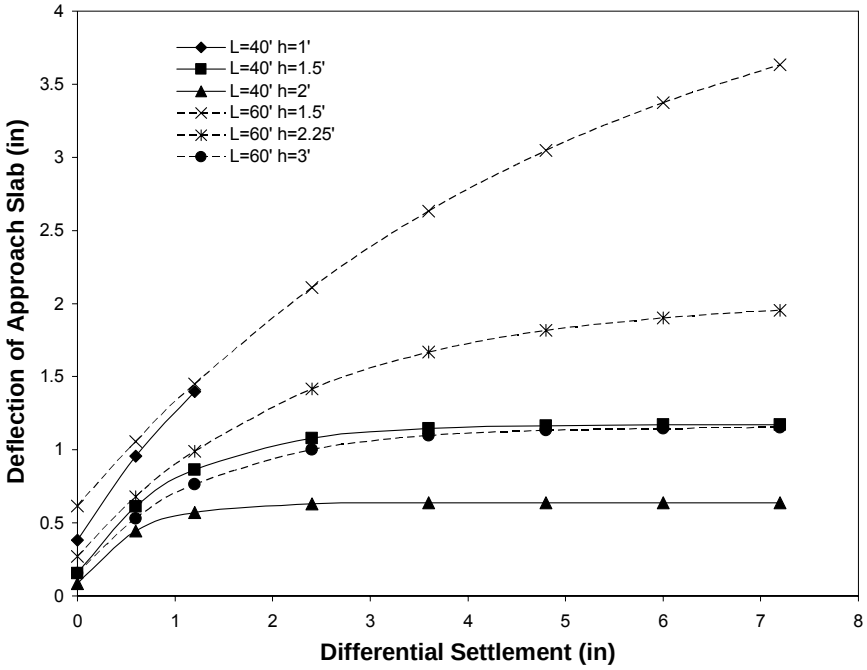

Figure 39
Deflection of approach slab versus differential settlement (effective sidth method)

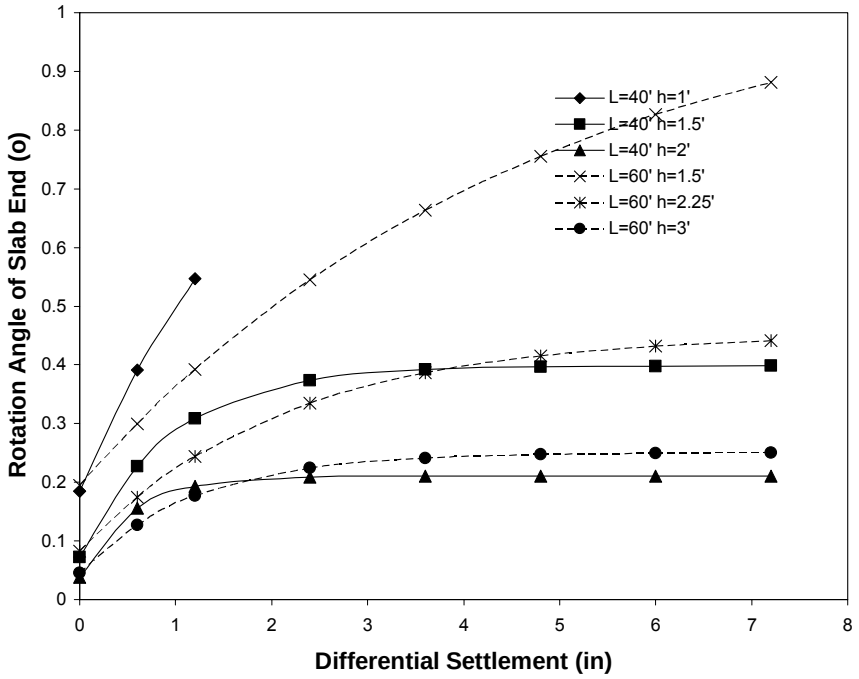

Figure 40
Rotation angle of approach slab versus differential settlement (effective wdth method)

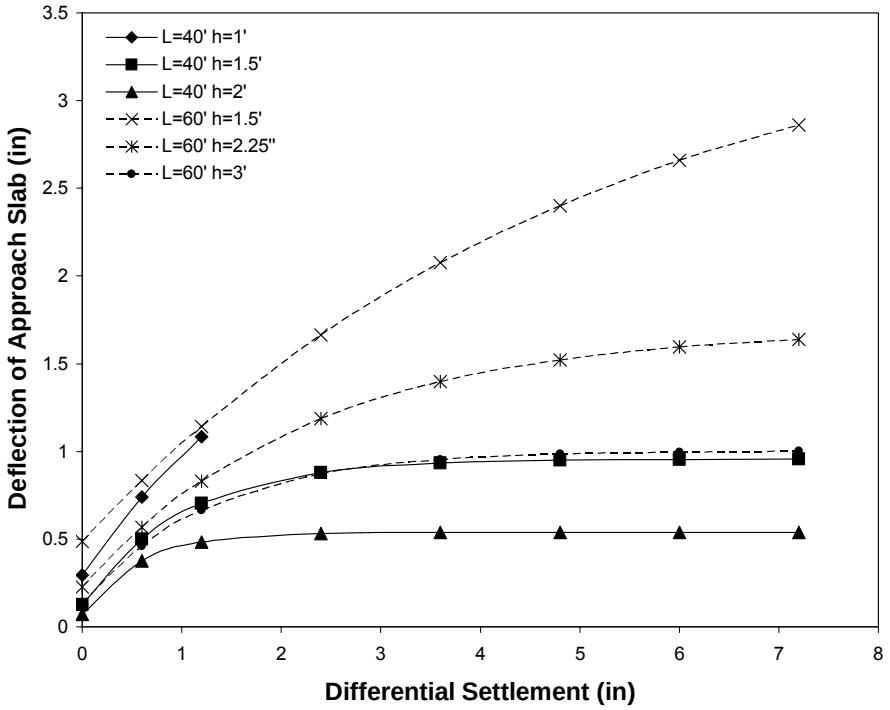

Figure 41
Deflection of approach slab versus differential settlement (total width method)

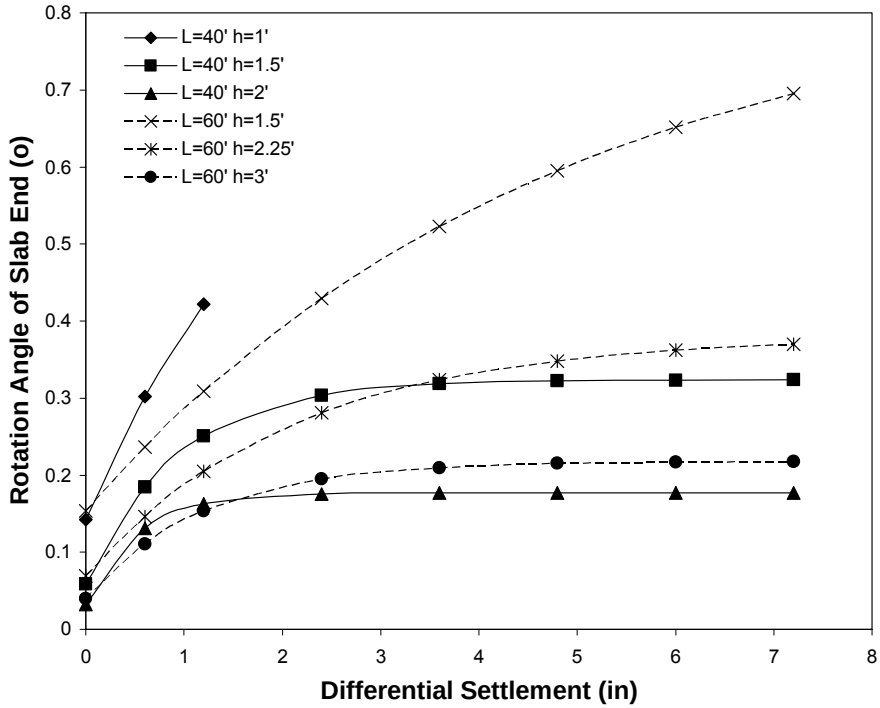

Figure 42
Rotation angle of approach slab versus differential settlement (total width method)

Ribbed Approach Slab (Prestressed Girders)

After the maximum internal moments of the exterior and interior beams were obtained, checking the strength of the beam of the ribbed slab was conducted according to the AASHTO Standard Specifications (AASHTO 2002), with load factors of 1.3 for dead load, and 2.17 for live load. Since the beam used in the finite element analysis has the same section properties as AASHTO Type II and Type III sections for the beam span of 60 and 80 ft., respectively, the AASHTO girders are used in the strength checking. For the extreme case when the ribbed slab loses contact with the soil, regular reinforced concrete beams may not provide the required stiffness, and prestressed concrete beams will be necessary.

Table 17
Design of prestressed beam (60'), AASHTO Type II Girder
(f_c'= 6500 psi, f_s = 270 ksi)

Differential Settlement (in)	Beam Spaced at 32 ft.			Interior Beam Spaced at 16 ft.			Interior Beam Spaced at 12 ft.		
	Moment (kip-ft.)		# of Strands(1)	Moment (kip-ft.)		# of Strands	Moment (kip-ft.)		# of Strands
	DL	LL		DL	LL		DL	LL	
0	135.8	134.4	4	121.5	89.9	3	110.5	92.5	3
0.5	757.9	290.3	12	627.9	270.4	11	543.4	235.3	9
1	1085.1	367.3	16	874.2	300.3	14	750.3	263.5	12
2	1466.3	608.5	26	1086.4	509.8	20	867.4	468.6	18
3	1533.6	912.2	30	1098.3	601.9	20	867.8	491.7	18
6	1532.9	997.5	NA	1099.2	603.0	20	867.9	500.0	18

Note: (1) The diameter of strands is 0.5 in.

Table 18
Design of prestressed beam (80'), Type III Girder
(f_c'= 6500 psi, f_s = 270 ksi)

Differential Settlement (in)	Beam Spaced at 32 ft.			Interior Beam Spaced at 16 ft.			Interior Beam Spaced at 12 ft.		
	Moment (kip-ft.)		# of Strands(1)	Moment (kip-ft.)		# of Strands	Moment (kip-ft.)		# of Strands
	DL	LL		DL	LL		DL	LL	
0	190.2	78.94	3	172.6	98.4	3	155.3	104.0	3
0.5	1056.5	262.7	12	894.7	276.5	12	782.5	239.1	10
1	1520.0	478.3	18	1256.9	388.8	16	1097.0	362.7	14
2	2165.9	621.1	26	1751.1	462.8	22	1513.4	437.5	20
3	2613.0	771.3	34	2034.5	616.9	26	1669.1	594.7	24
6	2845.9	1357.4	46	2096.4	824.0	30	1672.6	634.1	24

Note: (1) The diameter of strands is 0.5 in.

The results of the prestressed reinforcement design considering the effects of different differential settlements are shown in tables 17 to 18. Since the required reinforcement in the exterior beam is less than that in interior beam, the exterior beam should be designed the same as the interior beam according to the AASHTO code.

When the embankment settlement increases, more prestressing strands are required. If the settlement exceeds 3 in. for a ribbed slab with a length of 60 ft. and a beam spacing of 32 ft., the required prestressing strands will exceed the allowed maximum value (i.e., we cannot reasonably design the section). In this case, either the beam spacing should be reduced or the soil should be improved to control the settlement within the allowable limit. Table 17 also indicates that ribbed slabs with beams spaced at 16 and 12 ft. can provide enough strength if the given settlement exceeds 3 in.

Ribbed Approach Slab (Cast-in-Place Reinforced Concrete Beams)

Since the precast prestressed concrete girders may not be convenient for construction, a strength design using cast-in-place reinforced concrete beams was also conducted according to the AASHTO Standard Specifications (AASHTO 2002), with load factors of 1.3 for dead load, and 2.17 for live load. The results of the reinforcement design of the beams are listed in tables 19 and 20. The dimensions of these beam sections are shown in figure 43.

Table 19
Design of reinforced beam (60')
(f_c'= 4000 psi, f_s = 60,000 psi)

Differential Settlement (in)	Beam Spaced at 32 ft.			Interior Beam Spaced at 16 ft.			Interior Beam Spaced at 12 ft.		
	Moment (kip-ft.)		# of #10 Bars	Moment (kip-ft.)		# of #10 Bars	Moment (kip-ft.)		# of #10 Bars
	DL	LL(HS20)		DL	LL(HS20)		DL	LL(HS20)	
0	135.8	134.4	3	121.5	89.9	2	110.5	92.5	2
0.5	757.9	290.3	7	627.9	270.4	7	543.4	235.3	6
1	1085.1	367.3	10	874.2	300.3	8	750.3	263.5	7
2	1466.3	608.5	15	1086.4	509.8	12	867.4	468.6	10
3	1533.6	912.2	19	1098.3	601.9	15	867.8	491.7	13
6	1532.9	997.5	21	1099.2	603.0	15	867.9	500.0	13

Table 20
Design of reinforced beam (80')
(f_c'= 4000 psi, f_s = 60,000 psi)

Differential Settlement (in)	Beam Spaced at 32 ft.			Interior Beam Spaced at 16 ft.			Interior Beam Spaced at 12 ft.		
	Moment (kip-ft.)		# of #11 Bar	Moment (kip-ft.)		# of #11 Bar	Moment (kip-ft.)		# of #11 Bar
	DL	LL(HS20)		DL	LL(HS20)		DL	LL(HS20)	
0	190.2	78.94	3	172.6	98.4	2	155.3	104.0	2
0.5	1056.5	262.7	6	894.7	276.5	6	782.5	239.1	5
1	1520.0	478.3	9	1256.9	388.8	8	1097.0	362.7	7
2	2165.9	621.1	13	1751.1	462.8	10	1513.4	437.5	9
3	2613.0	771.3	16	2034.5	616.9	13	1669.1	594.7	11
6	2845.9	1357.4	24	2096.4	824.0	17	1672.6	634.1	13

In addition, the ribbed approach slabs were also designed following the AASHTO LRFD specifications, and the reinforcement is shown in tables B14 and B15, in Appendix B. The two codes require close reinforcement, so the more critical one is adopted in table 21 to satisfy both AASHTO Standard and LRFD specifications and also to meet the requirement that the operating rating factor is larger than 1.0 (discussed later). Only four options that the writers believe more economical and also adequate in strength are kept in table 21 and will be recommended.

The designed ribbed slabs with reinforcement shown in table 21 were also rated against the three special trucks provided by LADOTD using both AASHTO Standard and LRFD codes. The results are shown in tables B19, B21, B23, and B25, in Appendix B. To ensure all the operation ratings are larger than 1.0, the reinforcement in table 21 was raised in some cases so that the new designs are adequate for the special trucks. The two-beam option (with a spacing of 32 ft.) is not recommended since it did not pass the rating. Therefore, this option is not included in the rating table in Appendix B. Figure 43 shows the final recommended reinforcement arrangement for girders with a span length of 60 ft. and 80 ft. and spacing of 16 and 12 ft.

Table 21
Design of reinforced beam (adopted new design)
(f_c'= 4000 psi, f_s = 60,000 psi)

Differential Settlement (in)	60-ft. Span		80-ft. Span	
	Interior Beam Spaced at 16 ft.	Interior Beam Spaced at 12 ft.	Interior Beam Spaced at 16 ft.	Interior Beam Spaced at 12 ft.
	# of #10 Bars	# of #10 Bars	# of #11 Bars	# of #11 Bars
0	2	2	2	2
0.5	7	6	6	5
1	8	7	8	7
2	12	10	10	9
3	15	13	13	11
6	15	13	17	13

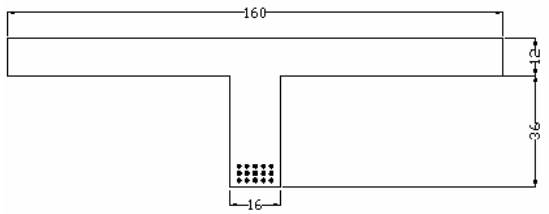

(a) L=60 ft., Spacing=16 ft.

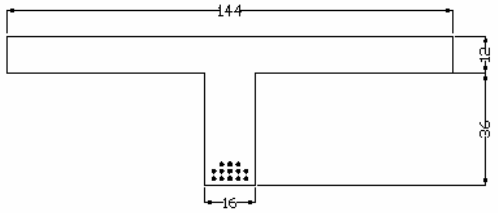

(b) L=60 ft., Spacing=12 ft.

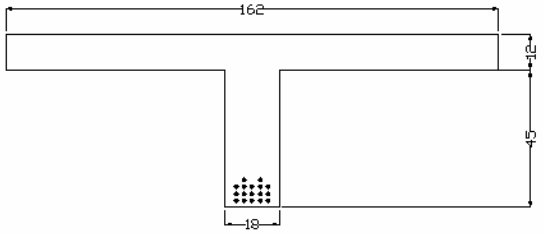

(c) L=80 ft., Spacing=16 ft.

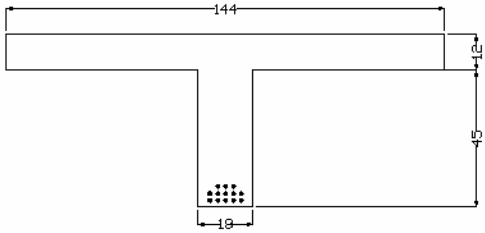

(d) L=80 ft., Spacing=12 ft.

Figure 43
Proposed beam size and reinforcement for 60 and 80 ft. approach slab

Instrumentation Plan

A preliminary instrumentation plan was developed to monitor the approach slab performance and also confirm some observations made in the present study. Since the numerical study was based on assumed settlements and known design highway loads as well as many other assumptions targeted at general conditions, a more detailed analysis for the specific field condition is needed for a direct comparison between field measurements and numerical predictions. A more detailed instrumentation plan is also needed for any specific bridge site conditions. The monitoring program can be incorporated into LADOTD's testing plan when LADOTD builds test sections of concrete approach slabs. The monitoring should not be limited to only approach slabs, in other words, monitoring should be considered together also for the performance of the abutment system.

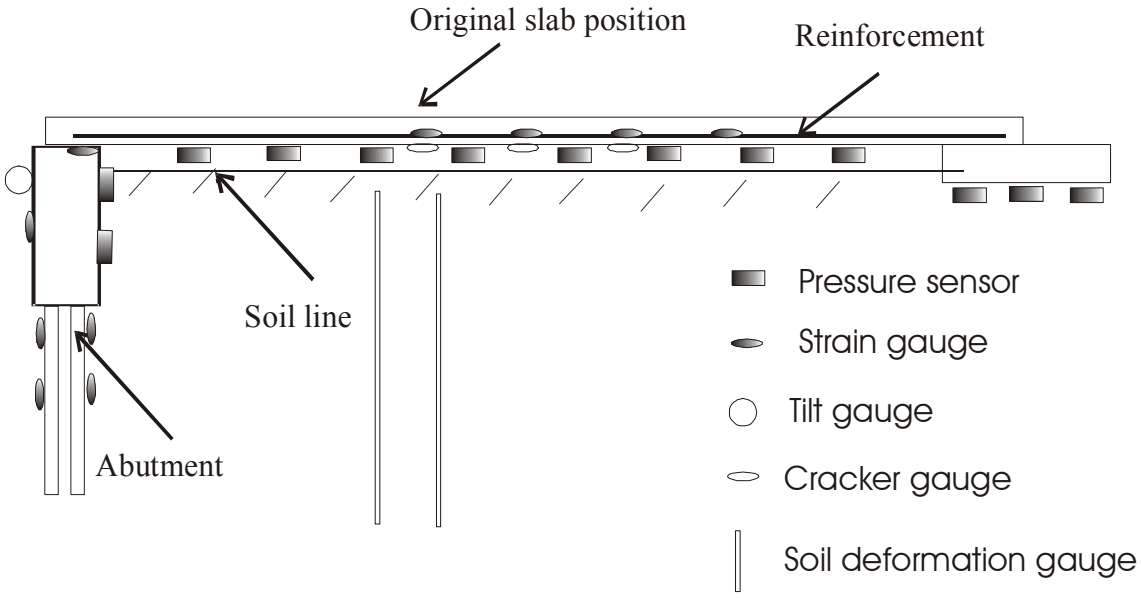

Figure 44
Preliminary plan of instrumentation

The instrumentation shown in figure 44 consists of two main parts. The first part's main function is structural performance monitoring, including the slab and abutment deformation and strength. The authors propose that strain gauges be imbedded in the concrete to measure

the reinforcement strain and that crack gauges be installed to measure concrete cracking. Tilt gauges can be installed to monitor the abutment rotation under earth pressure.

The main function of the second part is soil measuring, including contact stress and deformation. The pressure cells can be installed along the interface of soil and approach slab, and the interface of soil and abutment structures. Deflection gauges can likely be embedded in the soils to measure soil settlement. CTL has developed a multi-depth deflectometer (SnapMDD). This gauge can measure the load-bearing performance of multi-layer strata and pavements that used to be tricky, cumbersome, and costly. Data from these gauges can also be remotely acquired.

Surveys can be used to measure the deformation of the slabs, relative to their original configurations. Surface profilers can also be used to measure the roughness of the slab surface and the bumps near the approach slab ends.

Considering the special requirement of long-term performance monitoring of soil and slab/abutment structures, the gauges must be durable, stable, and rugged. An alternative to traditional soil/geotechnical instrumentation gauges is fiber optic sensors (FOSs). FOSs have become increasingly popular in long-term monitoring of structures, especially in harsh environments. The FOSs' major unique benefits related to this project are summarized below:

- Corrosion-resistance and long-term stability, which make it very useful for both surface mounting and embedment in the concrete structure and soil.
- Distributed sensing capability and multiplexing capabilities, which make it possible to monitor large areas with a sensor network by using multi-gauges along a single optic fiber.
- Small size and light weight with little disturbance to the structure and soil
- Absolute readings, instead of relative readings, which make it capable of intermittent readings with reconnection between readings, thus being convenient for long-term monitoring.
- Immunity to electromagnetic/radio frequency interference

- Large selection of gauge length possibilities, which make it possible to measure from small to large scale deformations.

Due to the nature of the proposed project, an FOS system should be explored for this application, either independently or combined with the traditional system so that the results of these two systems can be compared. By using the measured deformation and settlement of the soil, the approach slab performance can be correlated with the numerical predictions.

CONCLUSIONS

The analysis of interaction between the slab and the supporting embankment using 3-D finite element modeling has demonstrated the effects of differential settlement on the stress distribution of the embankment soil, the deformation of approach slab, and the approach slab design. With the increase of the differential settlement, the contact area between the embankment soil and the slab decreases. As a result, a greater portion of the slab load is transferred to the sleeper slab; the affected (high stress) area in the soil moves towards the sleeper slab end; and the contact stresses in the soil increase (figures 11 to 14). The magnitude of the slab's deformations and internal forces increase correspondingly. When the settlement increases to some large value, it no longer affects the performance of slab since the approach slab almost completely loses its contact with the soil and the slab becomes a simple beam.

The parametric study provided results of the approach slab for different settlements and slab parameters (figures 16 to 18). Based on the results, correlation among the slab parameters (including length and flexural rigidity), deflection of the approach slab, internal moment of the slab, and the differential settlement between the abutment end and the pavement end of the approach slab was established by regression analysis. Equations 3 to 11 make it convenient to design approach slabs considering different levels of embankment settlements. An example showing the calculation procedure and how to use the equations is provided in Appendix A.

Evaluation of the current LADOTD approach slab design was conducted. It seems that the current approach slabs are underdesigned if embankment settlement is considered. For approach slabs with a span length of 20 ft., the reinforcement should be raised to #7@6". However, for span length of 40 ft., the slab thickness has to be increased to accommodate the settlements. Sample new designs have been provided by increasing the slab thickness and reinforcement ratio for the approach slab length of 40 ft. and 60 ft. The developed procedure can be used in designing the approach slab to meet the established deformation requirements.

For longer approach spans, a stiffer approach slab, namely the ribbed slab, was proposed and analyzed. This option can reduce the slab thickness compared with the flat approach slabs. The effect of the embankment settlement on the structural performance of the ribbed approach slab was investigated. Deflections and internal moments of the beam and reaction forces of the beam at the sleeper slab end corresponding to the maximum moment were predicted (tables 8 to 13); they increase with the increase of the embankment settlement. Since the beams with different spacings were also investigated, with a given settlement and deflection limit, proper beam spacing can be determined. Preliminary results indicated that for an approach slab of 60 ft. span length, the AASHTO Type II beam spaced at 32 ft. is good for cases with an embankment settlement less than 3 in. For larger settlements, beam spacing of 16 ft. and 12 ft. is adequate. Considering the construction issues using precast prestressed beams, cast-in-place reinforced concrete ribbed beams were also designed.

Both the flat and ribbed slabs were designed according to both AASHTO Standard and AASHTO LRFD specifications and also rated in terms of both codes for the special trucks provided by LADOTD. Based this information, slab designs were finalized and recommended (tables 16 and 21).

The failure mechanisms near the interface of the abutment and approach slab were investigated. Under a large differential embankment settlement (e.g., 6 in. for a 40 ft. slab), the bolts and dowel rebars may be overstressed, the concrete near the bearing may be crushed, and the abutment may be cracked.

All results were obtained by using the soil with material properties listed in table 4. If material properties are significantly different, then these conclusions may not be valid.

RECOMMENDATIONS

From the previous analysis and results, the following recommendations can be made. The recommendations are based on strength requirements only. The deformation requirements that may be imposed based on the comfort analysis may change the recommendations. A comfort analysis of driving on the approach slab and deformation control is under investigation by other research teams supported by the Louisiana LQI program.

Recommendation for Implementation

For flat approach slabs with a span length of 20 ft., the major reinforcement (bottom layer in the span direction) should be changed to #7@6".

For flat approach slabs with a span length of 40 ft. and 60 ft., the major reinforcement (bottom layer in the span direction) should follow table 16.

For ribbed approach slabs with a span length of 60 ft. and 80 ft, the reinforcement of the beam should follow table 21.

The connection detail between the approach slab and the abutment should be changed if a large embankment differential settlement (e.g., more than 6 in.) is expected in order to avoid damage near the connection area. The authors recommend removing or loosening those anchoring bolts after construction and changing the layout of the dowel rebar. However, the decision to remove the anchoring bolts should also be based on the deformation requirement of the joint, but that information is not currently available.

Recommendation for Future Research

Unless very minimal settlement is allowed in the embankment (both geotechnical and construction related), a bump will always be present at the bridge approach slab. Regardless of the efforts made to improve the structural rigidity and long-term performance of the approach slab, the magnitude of the bump will be a function of the total settlement. A more rigid approach slab will reduce the change of slope angle (θ_1 in figure 1), but it may also

increase the local soil pressure beneath the contact area (sleeper slab), thereby increasing the faulting deflection (Δ_1 in figure 1). Therefore, a balanced/optimal approach slab design is desirable and will require a team work between structural and geotechnical engineers to implement the developed procedure. Therefore, further revision of the present study may be needed after the geotechnical design of the sleeper slab.

This research is based on a given differential settlement. Therefore, a more accurate settlement prediction procedure based on field data is necessary. Field instrumentation will help improve the prediction accuracy in terms of settlements and soil stress. Without a known settlement, the developed procedure in this study cannot be fully implemented, though the approach slab can be conservatively designed as a simple beam.

Since the "bump" is a subjective description, a further study may focus on establishing an acceptance guideline for "bumps", i.e., the criteria for acceptable slope change and faulting of approach span. Without this information, the approach design can only be based on strength requirement as the present study does, though deformation has been predicted. A dynamic approach slab analysis simulating the truck system and driver response will help develop such a guideline.

This study shows that the interaction of the slab and the soil is affected by the magnitude of the external load, the embankment settlement, and the stiffness of the structure. The current impact load factor specified by AASHTO LRFD code (AASHTO 2004) is 33 percent for truck load in bridge design. However, the truck impact load (bump load) on approach slabs is caused by faulting and slope changing at slab ends as well as irregularities (or roughness) of the approach slab. The impact load on the approach slab and the response of heavy vehicles may be different from those on bridges and deserve further dynamic study.

Since the numerical prediction has shown the reinforcement of the approach slab specified in the current Bridge Design Manual (LADOTD 2002) for a 40 ft. span length is not adequate, the current LADOTD design specifications related to the approach slab should be reexamined.

REFERENCES

1. AASHTO, “Standard specifications for highway bridges.” American Association of State Highway and Transportation Officials, Washington, D.C., 2002.
2. AASHTO, *LRFD Bridge Design Specifications.* American Association of State Highway and Transportation Officials, Washington, D.C., 2004.
3. Zhang, Z. “Preservation of Bridge Approach Rideability.” Louisiana Quality Initiative, Louisiana Transportation Research Center/Louisiana Department of Transportation and Development, 2002.
4. Stewart, C.F. “Highway Structure Approaches.” California Department of Transportation, Sacramento, 1985.
5. Kramer, S.L., & Sajer, P. “Bridge Approach Slab Effectiveness.” Washington State Transportation Center, Seattle, 1991.
6. Mahmood, I.U. “Evaluation of Causes of Bridge Approach Settlement and Development of Settlement Prediction Models.” Ph.D. Thesis, University of Oklahoma, Norman, 1990.
7. Wahls, H. E. “Design and Construction of Bridge Approaches.” NCHRP Synthesis 159, Transportation Research Board, National Research Council, Washington, D.C., 1990.
8. Chini, S.A., Wolde-Tinsae, A.M., & Aggour, M.S. “Drainage and Backfill Provisions for Approaches to Bridges.” University of Maryland, College Park., 1992.
9. Briaud, J. L., James, R. W., and Hoffman, S. B. “Settlement of Bridge Approaches (the Bump at the End of the Bridge).” NCHRP Synthesis 234, Transportation Research Board, National Research Council, Washington, D.C.,1997.
10. Hoppe, E.J., & Gomez, J.P. “Field Study of an Integral Backwall Bridge.” Virginia Transportation Research Council, Charlottesville, 1997.
11. Hoppe, E. J. “Guidelines for the use, design, and construction of bridge approach slabs,” Virginia Transportation Research Council, Final Report VTRC 00-R4., 1999.
12. Stark, T.D., Olson, S.M., & Long, J.H. “Differential Movement at the Embankment/Structure Interface: Mitigation and Rehabilitation. (Report No. IAB-H1, FY 93).” Illinois Department of Transportation, Springfield, 1995.
13. Tadros, M.K., & Benak, J.V. “Bridge Abutment and Approach Slab Settlement

(Phase1).” University of Nebraska, Lincoln, 1989.

14. Ha, H., Seo, J. B., Briaud, J.L. “Investigation of Settlement at Bridge Approach Slab Expansion Joint: Survey and Site investigations,” Report No. 4147-1 to the Texas Department of Transportation, published by the Texas Transportation Institute, Texas A&M University System, 2002.
15. Ha, H., Seo, J. B., Briaud, J.L. “Investigation of Settlement at Bridge Approach Slab Expansion Joint: Numerical Simulations and Model Tests,” Report No. 4147-2 to the Texas Department of Transportation, published by the Texas Transportation Institute, Texas A&M University System, 2002.
16. White, D., Sritharan, S., Suleiman,M., Mekkawy, M., and Chetlur, S. “Identification of the Best Practices for Design, Construction, and Repair of Bridge Approaches,” January 2005, Report of Iowa DOT Project TR-481, CTRE Project 02-118.
17. Nassif, H., Vittlo, N., and Amra, T. A., “Analysis and Design of Bridge Approach and Transition Slabs in New Jersey,” TRB, 2003.
18. Briaud, J. L., Maher S. F., and James R. W. “Bump at the end of the bridge,” *Civil Engineering*, 68-69, May 1997.
19. Long, J.H., Olson, S.M, & Stark, T.D. “Differential Movement at Embankment/Bridge Structure Interface in Illinois.” Transportation Research Board, Washington, D.C., 1998.
20. Dobry, R., Ng, T.T., Petrakis, E. and Seridi, A. “General Model for Contact Law between Rough Spheres,” *J. of EM Div. ASCE*, Vol. 117, No. 6, 1991, June, pp. 1365-1381.
21. Louisiana Department of Transportation and Development (LaDOTD 2002) “Bridge Design Metric Manual.”
22. Budhu, M., *Soil Mechanics and Foundations*, Publisher: John Wiley & Sons; November 1999.
23. Kulhawy, F.H. Manual on Estimating Soil Properties for Foundation Design. EPRI, 1990.
24. Monley, G. J., and Wu, J. T. H. “Tensile reinforcement effects on bridge-approach settlement,” *J. of Geotechnical Engineering*, ASCE, 119 (4) 749-762, 1993.
25. Zaman, M., Gopalasingam, A. and Laguros, J. G. “Consolidation settlement of bridge

approach foundation." *J. of Geotechnical Engineering*, 117(2) 219-239, 1991.

26. Huang, B.S. and Mohammad, L.N. "3-D Numerical Simulation of Asphalt Pavement at Louisiana Accelerated Loading Facility" TRB, 2001.
27. McGrath, T.J., Moore, I.D., Selig, E.T., Webb, M.C., and Taleb, B. "Recommended Specifications for Large-Span Culverts." NCHRP Report 473, Transportation Research Board, National Research Council, Washington, D.C., 2002.
28. AASHTO, "Manual for Condition Evaluation of Bridges." American Association of State Highway and Transportation Officials, Washington, D.C., 1994.
29. AASHTO, "Guide Manual for Condition Evaluation and Load and Resistance Factor Rating (LRFR) of Highway Bridges," American Association of State Highway and Transportation Officials, Washington, D.C., 2003.
30. Bazant, Z.P. and Kim, J.K. "Creep of Anisotropic Clay: Microplane Model," *J. of GE*, Vol. 112, No. 4, 1986, pp. 458-475.
31. Biot, M.A. "Theory of Elasticity and Consolidation for a Porous Anisotropic Solid," *J. of Appl. Phys*. Vol. 26, 1955,pp. 182-185.
32. Cheney, R.S., & Chassie, R.G. "Soils and Foundations Workshop Manual." Federal Highway Administration, Washington, DC., 1993.
33. Creimann, L. F., Yang, P. and Wold-Tinsae, M. M. "Nonlinear analysis of integral abutment bridges", *J. of Structural Engineering*, ASCE, 112 (10) 2263-2280, 1986.
34. Dixon, K.K., Hummer, J.E, & Lorscheider, A.R. "Capacity for North Carolina Freeway Work Zones." Transportation Research Record No. 1529. Transportation Research Board, Washington, DC., 1996.
35. Ioannides, A. M. and Korovesis, G. T. "Analysis and design of doweled slab-on-grade pavement systems," *J. of Transportation Engineering*, ASCE, 118(6), 745-768., 1992.
36. . Kiousis, P.D. and Voyiadjis, G.Z. "Lagrangian Continuum Theory for Saturated Porous Media," *Journal of EM, ASCE*. Vol. 111, No. 10, 1985, pp. 1277-1288.
37. Lee, E.H. "Interaction between Physical Mechanism and Structure of Continuum Theories," *Large Deformations of Soils: Physical Basis and Mathematical Modelling*, edited by J. Gittus, J. Zarka, and S. Nemat-Nasser, Elsvier, pp. 143-161, 1993.
38. Monahan, E.J. *Construction of Fills*. John Wiley & Sons, Bloomfield, New Jersey,

1994.

39. Prevost, J.H. "Mechanics of continuous porous media," *Int. J. of Eng. Sci*. Vol. 18, 1980, pp. 787-800.
40. Voyiadjis, G.Z. and Abu-Farsakh, Y. M. "Coupled theory of mixtures for clayey soils," *Computer and Geotechnics*, Vo. 20, No. 3-4, 1997, pp. 195-222.
41. Wong, H. K. W. and Small, J. C. "Effect of orientation of approach slabs on pavement deformation," *J. of Transportation Engineering*, ASCE, 120 (4) 590-602, 1994.
42. Wu, J. T. H. and Helway, M. B. "Alleviating bridge approach settlement with geosynthetic reinforcement." Proc. 4th Int. Conf. on Geotexiles, Geomembranes and Related Products. The Hague, Netherlands, 107-111, 1990.

APPENDIX A

Collections of Soil Properties

Typical parameters of soil from related research reports were collected and compared in order to select the most appropriate material parameters of soil for this research.

- Parameters recommended in *Soil Mechanics and Foundations [22]*.

Typical recommended Values of E, G, and internal friction angle for different soils are shown in tables A1 and A2.

Table A1
Typical values of E and G *[22]*

Soil Type	E, ksi (MPa)	G, ksi (MPa)
Clay Soft	0.145-2.18 (*1-15*)	0.073-0.73 (*0.5-5*)
Clay Medium	2.18-4.36 (*15-30*)	0.73-2.18 (*5-15*)
Clay Stuff	4.36-14.5 (*30-100*)	2.18-5.81 (*15-40*)

Table A2
Ranges of friction angles for soils *[22]*

Soil Type	Φ_{cs} (^{o})	Φ_p (^{o})
Gravel	30-35	35-50
Mixture of gravel and sand with fine-grained soils	28-33	30-40
Sand	27-37	32-50
Silt or silty sand	24-32	27-35
Clays	15-30	20-30

Note: Φ_{cs} is critical state friction angle, and Φ_p is peak friction angle for dilating soil.

- Parameters recommended in *Manual on Estimating Soil Properties for Foundation Design [23]*.

Typical values of soil unit weight, internal friction angle and Poisson's ratio for different soils are shown in tables A3 to A5.

Table A3

Typical soil unit weights *[23]*

Soil Type	Approximate Particle size (mm)			Uniformity coefficient	Void Ratio		Normalized Unit weight			
							Dry, γ_{dry}/γ_w		Saturated, γ_{sat}/γ_w	
	D_{max}	D_{min}	D_{10}	D_{60}/D_{10}	e_{max}	e_{min}	min	Max	min	max
Silty or sandy clay	2.0	0.001	0.003	10 to 30	1.8	0.25	0.96	2.16	1.60	2.36
Gap-graded silty clay w. gravel or larger	250	0.001	-	25 to 1000	1.00	0.20	1.35	2.24	1.84	2.42
Well-graded gravel, asnad, silt, and clay	250	0.001	0.002	-	0.70	0.13	1.60	2.37	2.00	2.50
Clay (30 to 50 % < 2μ size)	0.05	0.5μ	0.001	-	2.40	0.50	0.80	1.79	1.51	2.13
Colloid clay (over 50% < 2μ size)	0.01	10μ	-	-	12.00	0.60	0.21	1.70	1.14	2.05
Organic silt	-	-	-	-	3.00	0.55	0.64	1.76	1.39	2.10
Organic clay (30 to 50% < 2μ size)	-	-	-	-	4.4	0.70	0.48	1.60	1.30	2.00

Note: γ_w= 62.4 lb/ft.^{3} =1gm/cm^3.

Table A4

Representative values of internal friction angle *[23]*

Soil Material	Φ (^{o})	
	Loose	Dense
Sand, round grains, uniform	27.5	34
Sand, angular grains, well-graded	33	45
Sandy gravels	35	50
Silty sand	27 to 35	30 to 34
Inorganic silt	27 to 33	30 to 35

Table A5

Typical ranges of drained poisson's ratio *[23]*

Soil	Drained Poisson's Ratio
Clay	0.2 to 0.4
Dense sand	0.3 to 0.4
Loose sand	0.1 to 0.3

- Parameters used in *Tensile reinforcement effects on bridge-approach settlement [24]*.

In this article, lateral and vertical movements were restrained at the abutment face to simulate the geogrid fixed to the rigid abutment wall, and mobilization of frictional resistance between the fill and the wall. Soil parameters used in finite element analysis are shown in table A6.

Table A6

Soil parameters used *[24]*

	Classifi-cation	γ, pcf (kN/m^3)	Φ (^{o})	C, psi (kPa)	υ
Approach fill					
1	GP	124.9 (*19.6*)	36	0.349 (*2.4*)	0.3
2	SP	119.8 (*18.8*)	32	0.349 (*2.4*)	0.3
Foundation					
3	CL	119.8 (*18.8*)	32	6.96 (*47.9*)	0.3
4	CL	114.7 (*18.0*)	30	3.47 (*23.9*)	0.3

- Parameters used in *Consolidation settlement of bridge approach foundation [25]*.

This article analyzed the consolidation-settlement characteristics at a bridge-approach site (Wewoka) in Oklahoma. The soil properties at this site, obtained from laboratory experiments, are shown in table A7.

Table A7

Soil parameters used *[25]*

Layer	E, psi (MPa)	γ, pcf (kN/m^3)	υ
1	700 (*4.820*)	65.0 (*10.2*)	0.4
2	835 (*5.750*)	60.0 (*9.4*)	0.4
3	970 (*6.680*)	65.0 (*10.2*)	0.4

- Soil parameters used in *3-D Numerical Simulation of Asphalt Pavement at Louisiana Accelerated Loading Facility [26]*

The Drucker Prager model was used for the compacted embankment soil and subgrade soil. Parameters for compacted embankment soil and subgrade soil used in finite element simulation are shown in table A8.

Values of Young's modulus used in this article are much larger than values used in other reference mentioned here. The difference may be induced by different soil types. In table A8, materials are compacted soil, which may has larger stiffness due to compact operation.

Table A8
Soil parameters used *[26]*

Material	Material Model	E, ksi (MPa)	υ	c, psi (kPa)	Internal friction angle
Compacted Soil	Drucker Prager	37.7 (*260*)	0.3	11.6 (*80*)	30^o
Subgrade Soil	Drucker Prager	21.7 (*150*)	0.45	7.2 (*50*)	20^o

- Soil parameters used to model the backfill and native soils in *Recommended Specifications for Large-Span Culverts [27]*.

Parameters estimated for each of the soil density conditions used to model the backfill and native soils in this article are presented in table A9. Values used in the Class A reductions are shown, as are values revised for the actual field densities. Revisions in this table included unit weights actually measured in the field as well as a slight reduction in Poisson's ratio. The strength and stiffness parameters increase monotonically with density, with the exception of the surface layer properties for the 96 percent density soil. These have parameters reduced somewhat so they better represent strength and stiffness close to the ground surface instead of at greater depths.

Table A9

Soil parameters used *[27]*

			E, psi (MPa)	υ	c, psi (kPa)	Φ (°)	γ, pcf (kN/m^3)
Native Soil			2900 (*20.0*)	0.28	0.0	43.0	*127.4* (*20.0*)
Percent of Maximum Standard Proctor	85%	Loose Class A Material	973 (*6.7*)	0.3	0.0	34.0	*127.4* (*20.0*)
	87%	Loose Material	1160 (*8.0*)	0.28	0.0	34.5	*111.5* (*17.5*)
	92%	Dense Material	2090 (*14.3*)	0.28	0.0	38.5	*117.9* (*18.5*)
	95%	Dense Class A Material	2900 (*20.0*)	0.3	0.0	43.0	*127.4* (*20.0*)
	96%	Surface Material	2470 (*17.0*)	0.28	0.0	41.5	*122.9* (*19.3*)

Calculation Example and Discussion

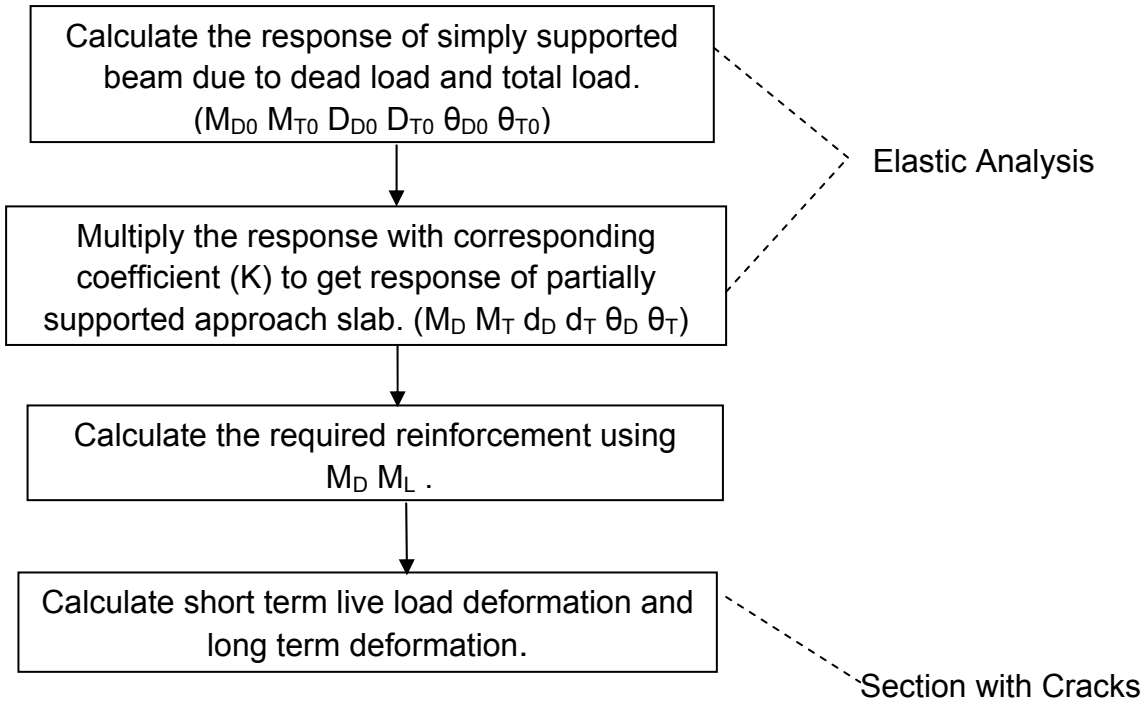

Figure A1
Flowchart of calculation procedure

Figure A1 shows a flowchart of the calculation procedure of approach slabs by using the equations developed earlier. The following sample calculation shows the calculation procedure developed in the present study to consider the interaction between the approach slab and embankment without conducting complicated finite element analysis. Engineers can use this procedure to calculate deformations and design approach slabs for a given differential settlement.

Given information: approach slab span length L = 40 ft., thickness h = 1 ft., differential settlement δ = 0.1 ft., slab width W = 40 ft., self-weight of concrete w_c=150.0 lb/ft.^{3}, f_c' = 5500 psi, $E_c = w_c^{1.5}33(f_c')^{0.5}$ = 4,496,061 psi, f_y = 60,000 psi, and $E_s = 2.9 \times 10^7$ psi.

Effective width of two lane loaded slab *[2]* is:

$$E = 84.0 + 1.44\sqrt{L_1 W_1} \le \frac{12.0W}{N_L}$$

where L_1 is the modified span length taken to be equal to the lesser of the actual span or 60.0 ft.; W_1 is the modified edge-to-edge width of bridge taken to be equal to the lesser of the actual width or 60.0 ft. for multilane loading, or 30 ft. for single-lane loading (ft.); W is the physical edge-to-edge width of bridge (ft.); N_L is the number of design lanes; and E is the equivalent width of longitudinal strips per lane.

$$E = 84.0 + 1.44\sqrt{(40)(40)} = 141.6\ in = 11.8\ ft$$

The uniform dead load is

W_D = 150x11.8x1 = 1711 lb/ft. = 1.770 kips/ft.

The moment of inertial of the slab is

$$I_g = \frac{Eh^3}{12} = \frac{11.8 \times 1^3}{12} = 0.9833\ ft^4 = 20390.4\ in^4$$

Elastic Analysis of Simple Beam

As described earlier, the internal force and deformation of partially supported slabs can be calculated by multiplying the corresponding values of a simple beam with the coefficients developed in the present study. To this end, the simple beam values are needed and are calculated below. *While the following hand calculations seem to be a lengthy process, any other methods, such as finite element modeling or structural analysis software can be easily used to predict these values of a simple beam under dead and live loads.*

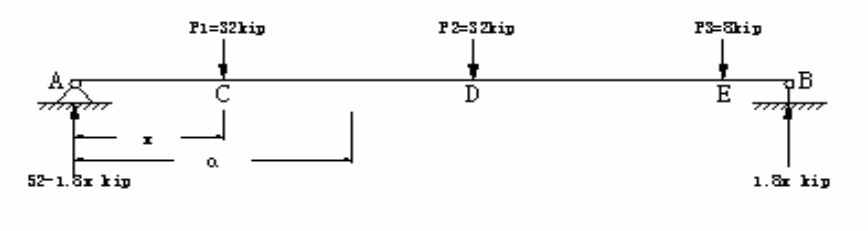

Figure A2
Beam with truck load

(a) Calculation of internal forces

The maximum moment of simple beam due to live load in figure A2 is determined as follows:

Moment at section C is

$$M_{L0} = (55.2 - 1.8x)x = -1.8(x - \frac{27.6}{1.8})^2 + 423.2 \le 423.2 \ \ ft - kips$$

Moment at section D is

$$M_{L0} = (55.2 - 1.8x)(x + 14) - (32)(14) = -1.8(x - \frac{15}{1.8})^2 + 449.8 \le 449.8 \ \ ft - kips$$

Moment at section E is

$$M_{L0} = (55.2 - 1.8x)(x + 28) - (32)(28) - (32)(14) = -1.8(x - \frac{2.4}{1.8})^2 + 204.8 \le 204.8 \ \ ft - kips$$

The maximum moment due to live load M_{L0} is 449.8 ft.-kips occurring at section D, when x = 15/1.8 = 8.33 ft. Correspondingly, the moment due to dead load at section D (a = 14'+8.33'= 22.33' see figure A2) is

$$: M_{D0} = 0.5 w_D a(L - a) = 0.5(1.770)(22.33)(40 - 22.33) = 349.32 \ \ ft - kips$$

Moment due to the dead load and live load at section D:

$$M_{T0} = M_{D0} + M_{L0} = 799.12 \ \ ft - kips$$

(b) Deformation, d and θ

Deformation of a simple beam due to dead load (figure A3) is calculated as

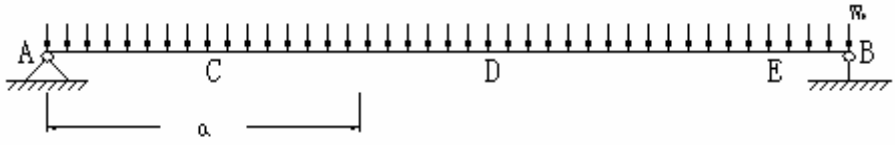

Figure A3
Beam with Dead Load

$$d_{D0}(a) = \frac{w_D}{24E_cI_g} a(L^3 - 2La^2 + a^3)$$

$$\theta_{D0} = \frac{w_D}{24E_cI_g} L^3$$

Deformation of a simple beam due to a single concentrated load (figure A4) is

Figure A4
Beam deformation due to one concentrated load

$$d_p(a) = \begin{cases} \dfrac{P(L-x)a}{6E_cI_gL}(L^2 - (L-x)^2 - a^2) & when \quad a < x \\ \dfrac{Px(L-a)}{6E_cI_gL}(L^2 - x^2 - (L-a)^2) & when \quad a > x \end{cases}$$

and rotations at A and B ends are

$$\theta_{p-A} = \frac{Px}{6E_cI_gL}(2L - x)(L - x)$$

$$\theta_{p-B} = \frac{Px}{6E_cI_gL}(L^2 - x^2)$$

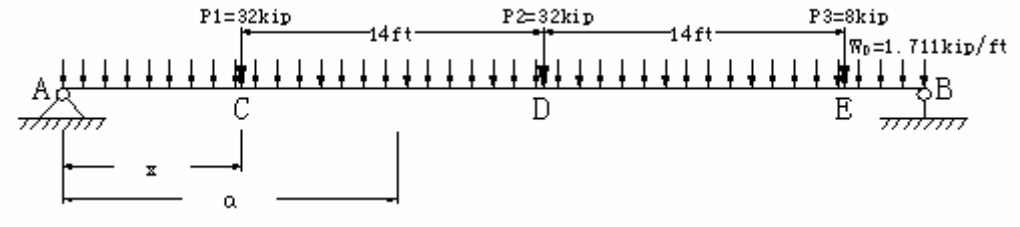

Figure A5
Beam due to total load

For a simple beam subjected to dead load and live load as shown in figure A5, the deflection of an arbitrary section with a distance of "a" away from support A is :

$$d_{T0}(a) = \frac{w_D}{24E_cI_g}a(L^3 - 2La^2 + a^3) + \frac{P_1(x_1)(L-a)}{6E_cI_gL}(L^2 - x^2 - (L-a)^2)$$
$$+ \frac{P_2(L-x_2)a}{6E_cI_gL}(L^2 - (L-x_2)^2 - a^2) + \frac{P_3(L-x_3)a}{6E_cI_gL}(L^2 - (L-x_3)^2 - a^2)$$
$$= \frac{1}{E_cI_g}(0.0713a^4 - 7.071a^3 - 133.28a^2 + 11421.94a - 3082.72)$$

where $d_{t0}(a)$ = total deflection at the section of "a"; $x_2 = x + 14'$; and $x_3 = x_2 + 14'$. To obtain the maximum deflection, let the first differentiation of d_{T0} with respect to "a" to be equal to zero, i.e.:

$$\frac{\partial(d_{T0}(a))}{\partial a} = \frac{1}{E_cI_g}(0.2853a^3 - 21.213a^2 - 266.56a + 11421.94) = 0$$

from which we have:

$$a = 20\ ft$$

$$d_{T0}(a) = 0.202\ ft$$

$$d_{D0}(a) = \frac{w_D}{24E_cI_g}a(L^3 - 2La^2 + a^3) = 0.0927\ ft$$

Similarly, we have the total rotation due to the dead and live loads as

$$\theta_{T0-A} = \frac{W_D}{24E_cI_g}L^3 + \frac{P_1}{6E_cI_g}(2L - x_1)(L - x_1) + \frac{P_2}{6E_cI_g}(2L - x_2)(L - x_2) + \frac{P_3}{6E_cI_g}(2L - x_3)(L - x_3) = 0.0164$$

$$\theta_{T0-B} = \frac{W_D}{24E_cI_g}L^3 + \frac{P_1}{6E_cI_g}(L^2 - x_1^2) + \frac{P_2}{6E_cI_g}(L^2 - x_2^2) + \frac{P_3}{6E_cI_g}(L^2 - x_3^2) = 0.0158$$

$\theta_{T0} = 0.0164$ (The maximum value occurs at end A)

and the rotation due to the dead load is

$$\theta_{D0} = \frac{w_D}{24E_c I_g} L^3 = 0.00741$$

In the above rotation angle calculation, x = 8.33 ft., L= 40 ft., x_1, x_2, and x_3 = 8.33, 22.33, and 36.33 ft., respectively.

Internal Force and Deformation of Partially Supported Beam (Uncracked)

The corresponding values of the partially supported beam considering the slab-soil interaction and differential settlements are calculated using the developed coefficients as

$$M_D = \left(0.9538 - 0.8080e^{-2.1938\times10^7(\frac{\delta h^2}{L^4})}\right) M_{D0} = \left(0.9538 - 0.8080e^{-2.1938\times10^7(\frac{0.1\times1^2}{40^4})}\right)(349.32) = 213.3\ kip - ft$$

$$M_T = \left(0.9629 - 0.7945e^{-1.5795\times10^7(\frac{\delta h^2}{L^4})}\right) M_{T0} = \left(0.9629 - 0.7945e^{-1.5795\times10^7(\frac{0.1\times1^2}{40^4})}\right)(799.12) = 426.8\ kip - ft$$

$$M_L = M_T - M_D = 426.8 - 213.3 = 213.5\ \ ft - kip$$

$$d_D = \left((3.0003 - 2.5895e^{-1.8194\times10^7(\frac{\delta h^2}{L^4})}) \times (\frac{h}{L})^{0.3}\right) d_{D0} = \left((3.0003 - 2.5895e^{-1.8194\times10^7(\frac{0.1\times1^2}{40^4})}) \times (\frac{1}{40})^{0.3}\right)(0.0927) = 0.0529\ ft$$

$$d_T = \left((2.9359 - 2.5443e^{-1.3475\times10^7(\frac{\delta h^2}{L^4})}) \times (\frac{h}{L})^{0.3}\right) d_{T0} = \left((2.9359 - 2.5443e^{-1.3475\times10^7(\frac{0.1\times1^2}{40^4})}) \times (\frac{1}{40})^{0.3}\right)(0.202) = 0.0958\ ft$$

$$\theta_D = \left((1.8378 - 1.4904e^{-2.0574\times10^7(\frac{\delta h^2}{L^4})}) \times (\frac{h}{L})^{0.2}\right) \theta_{D0} = \left((1.8378 - 1.4904e^{-2.0574\times10^7(\frac{0.1\times1^2}{40^4})}) \times (\frac{1}{40})^{0.2}\right)(0.00741) = 0.00415$$

$$\theta_T = \left((1.8547 - 1.5177e^{-1.4662\times10^7(\frac{\delta h^2}{L^4})}) \times (\frac{h}{L})^{0.2}\right) \theta_{T0} = \left((1.8547 - 1.5177e^{-1.4662\times10^7(\frac{0.1\times1^2}{40^4})}) \times (\frac{1}{40})^{0.2}\right)(0.0164) = 0.00785$$

where M_D, M_T, and M_L = maximum moment due to dead load, total load, and live load, respectively; and d_D, d_T, θ_D and θ_T = maximum deflection due to dead load, maximum deflection due to total load, maximum rotation due to dead load, and maximum rotation due to total load.

Once the internal moments are predicted, the approach slab can be designed. The following calculation of long-term deformation is meant to show the procedure only. The reader should be cautious in judging the applicability of the results.

Deformation of Partially Supported Beam (Considering the Effect of Cracking)

It should be noted that the finite element modeling predicted only the instantaneous elastic deformation in the present study. A time-dependent finite element analysis considering concrete cracking would be much more complicated and is beyond the scope of this study. Instead, the long term deformation of cracked section was hand-calculated by using the equivalent moment of inertia method that has been commonly used in practice. *However, this hand calculation cannot consider the interaction between the soil and the approach slab.* In reality, when the approach slab is trying to deform more due to time-dependent effects, the soil will provide a support unless the differential settlement is large where the soil and approach slab are not expected to be in contact. Therefore, the long-term deformation calculation shown in the following calculation procedure is an upper bound and may be significantly different from the true values.

To calculate the deflection of a cracked section, the reinforcement in the section is needed. Therefore, the reinforcement is first designed based on AASHTO standard specifications (AASHTO 2002):

$$M_u = 1.3M_D + 2.17(M_{L+IM}) = 879.7\ ft-kips$$

$$M_u = \phi M_n = \phi A_s f_y (d - \frac{a}{2}) = \phi b d^2 f_y \rho_s (1 - \frac{\rho_s f_y}{1.7 f_c'})$$

$$\rho_s = 0.0153 < \rho_{\max} = 0.75(\frac{0.85\beta_1 f_c'}{f_y})(\frac{87000}{87000 + f_y}) = 0.0268$$

$$A_s = \rho_s(b)(d) = (0.0166)(11.8)(12)(12-2) = 21.68 in^2$$

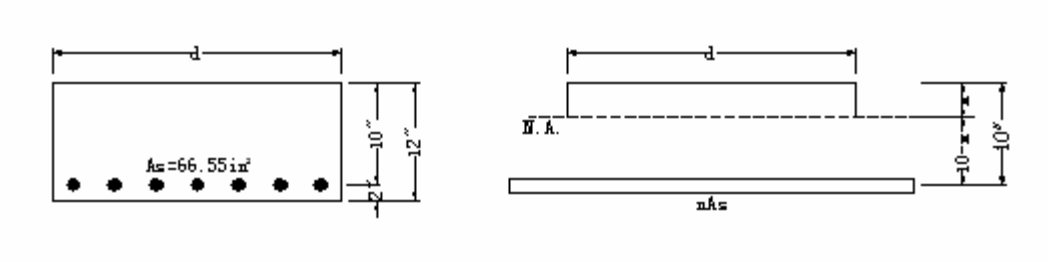

Figure A6
Transformed area of cracked section

Transformed moment of inertia of the cracked section in figure A6 is

$$I_{cr} = (\frac{1}{3})(11.8)(12)(x)^3 + nA_s(10-x)^2$$

Using the definition of neutral axle, x is obtained as

$$(11.8)(12)(x)(\frac{x}{2}) = nA_s(10-x)$$

$$n = \frac{E_s}{E_c} = \frac{2.9\times10^7}{4496061} = 6.45$$

$$x = 3.56in$$

$$I_{cr} = (\frac{1}{3})(11.8)(12)(3.56)^3 + (6.45)(21.68)(10-3.56)^2 = 7928.6\ in^4$$

Cracking moment is calculated as

$$f_t = 7.5\sqrt{5500} = 556.2 \quad psi$$

$$M_{cr} = \frac{f_r I_g}{0.5h} = 189.0\ kip - ft$$

(a) Short-term deformation

Short-term dead load deformation is calculated based on equivalent I_e as

$$I_e = (\frac{M_{cr}}{M_a})^3 I_g + \left[1-(\frac{M_{cr}}{M_a})^3\right] I_{cr} = (\frac{M_{cr}}{M_D})^3 I_g + \left[1-(\frac{M_{cr}}{M_D})^3\right] I_{cr} = (\frac{189.0}{213.3})^3(20390.4) + \left[1-(\frac{189.0}{213.3})^3\right](7928.6)$$
$$= 12947.3 in^4$$

Then the dead load deflection considering cracking is calculated by using the ratio of the moment of inertia as

$$d_D' = \frac{I_g}{I_e} d_D = \frac{20390.4}{12947.3}(0.0529) = 0.0833\ ft$$

$$\theta_D' = \frac{I_g}{I_e} \theta_D = \frac{20390.4}{12947.3}(0.00415) = 0.00653$$

Similarly, short-term dead load + live load deformation

$$I_e = (\frac{M_{cr}}{M_a})^3 I_g + \left[1 - (\frac{M_{cr}}{M_a})^3\right] I_{cr} = (\frac{M_{cr}}{M_D})^3 I_g + \left[1 - (\frac{M_{cr}}{M_D})^3\right] I_{cr} = (\frac{189.0}{426.8})^3 (20390.4) + \left[1 - (\frac{189.0}{426.8})^3\right](7928.6)$$
$$= 8554.9 in^4$$

$$d_T' = \frac{I_g}{I_e} d_T = \frac{20390.4}{8554.9}(0.0958) = 0.228\ ft$$

$$\theta_T' = \frac{I_g}{I_e} \theta_T = \frac{20390.4}{8554.9}(0.00785) = 0.0187$$

Short-term live load deformation

$$d_L^{'} = d_T' - d_D' = 0.145\ ft$$

$$\theta_L^{'} = \theta_T' - \theta_D' = 0.0122$$

(b) Long-term deformation

Considering time-dependent effects, the long term deformation factor for sustained load is

$$\lambda = \frac{\xi}{1 + 50\rho'} = 2$$

The final total deformation considering cracking and time-dependent effect = instantaneous deformation + long term deformation, i.e.,

$$d_{LT}^{'} = d_L^{'} + \lambda_\infty d_D^{'} = 3.74 in$$

$$\theta_{LT}^{'} = \theta_L^{'} + \lambda_\infty \theta_D^{'} = 1.45^o$$

The support for an approach slab from embankment soil is not considered in the long term deformation factor λ. Therefore, the long term deformation calculated above is conservative.

Analysis Based on Slab with Total Width (Alternative)

According to AASHTO code, when we calculate slab deformation, the total section instead of effective width can also be used, i.e., assuming the entire section deforms together. Therefore, an alternative calculation is provided here. The calculation procedure is the same as previous effective section method. The only difference is the width of slab that is assumed to take the truck load.

$E = 40\ ft$ (total slab width for two trucks)

W_D = 150x40x1 = 6000 lb/ft. = 6.0 kip/ft.

$$I_g = \frac{Eh^3}{12} = \frac{40 \times 1^3}{12} = 3.3333\, ft^4 = 69120\, in^4$$

(a) Internal force and Deformation of Simple Beam:

The maximum moment due to two truck live load is 899.6 ft.-kip, when x = 8.33 ft., at section D.

Moment due to the dead load at section D: $M_{D0} = 0.5(6.0)(22.33)(40 - 22.33) = 1183.7\ ft - kip$

Moment due to the dead load + live load: $M_{T0} = M_{D0} + M_{L0} = 2083.3\, ft - kip$

Deformation d and θ

$$d_{T0}(a) = \frac{1}{E_c I_g}(0.2417a^4 - 21.957a_3 - 266.58a^2 + 29165.238a - 6165.44)$$

$$d_{T0}(a)' = \frac{1}{E_c I_g}(0.9664a^3 - 65.871a^2 - 533.16a + 29165.238) = 0$$

$a = 19.944\ ft$

$d_{T0}(a) = 0.157\, ft$

$d_{D0}(a) = 0.0927\ ft$

$\theta_{T0} = 0.0127$

$$\theta_{D0}(a) = 0.00741$$

(b) Internal Force and Deformation of Partially Supported Beam (uncracked):

Internal force:

$$M_D = \left(0.9538 - 0.8080e^{-2.1938\times10^7(\frac{\delta h^2}{L^4})}\right)M_{D0} = \left(0.9538 - 0.8080e^{-2.1938\times10^7(\frac{0.1\times1^2}{40^4})}\right)(1183.7) = 723.1\ kip - ft$$

$$M_T = \left(0.9629 - 0.7945e^{-1.5795\times10^7(\frac{\delta h^2}{L^4})}\right)M_{T0} = \left(0.9629 - 0.7945e^{-1.5795\times10^7(\frac{0.1\times1^2}{40^4})}\right)(2083.3) = 1112.9\ kip - ft$$

Deformation:

$$d_D = \left((3.0003 - 2.5895e^{-1.8194\times10^7(\frac{\delta h^2}{L^4})})\times(\frac{h}{L})^{0.3}\right)d_{D0} = \left((3.0003 - 2.5895e^{-1.8194\times10^7(\frac{0.1\times1^2}{40^4})})\times(\frac{1}{40})^{0.3}\right)(0.0927) = 0.0529\ ft$$

$$d_T = \left((2.9359 - 2.5443e^{-1.3475\times10^7(\frac{\delta h^2}{L^4})})\times(\frac{h}{L})^{0.3}\right)d_{T0} = \left((2.9359 - 2.5443e^{-1.3475\times10^7(\frac{0.1\times1^2}{40^4})})\times(\frac{1}{40})^{0.3}\right)(0.157) = 0.0745\ ft$$

$$\theta_D = \left((1.8378 - 1.4904e^{-2.0574\times10^7(\frac{\delta h^2}{L^4})})\times(\frac{h}{L})^{0.2}\right)\theta_{D0} = \left((1.8378 - 1.4904e^{-2.0574\times10^7(\frac{0.1\times1^2}{40^4})})\times(\frac{1}{40})^{0.2}\right)(0.00741) = 0.00415$$

$$\theta_T = \left((1.8547 - 1.5177e^{-1.4662\times10^7(\frac{\delta h^2}{L^4})})\times(\frac{h}{L})^{0.2}\right)\theta_{T0} = \left((1.8547 - 1.5177e^{-1.4662\times10^7(\frac{0.1\times1^2}{40^4})})\times(\frac{1}{40})^{0.2}\right)(0.0127) = 0.00608$$

(c) Deformation of Partially Supported Beam (considering cracking):

According to the code, the effective width must be used in reinforcement design. Here, the reinforcement ratio obtained by using effective width should be used.

$$\rho_s = 0.0153 < \rho_{\max} = 0.0268$$

$$A_s = \rho_s(b)(d) = (0.0153)(40)(12)(12-2) = 73.48\,in^2$$

Transformed moment of inertia of the cracked section:

$$x = 3.56\,in$$

$$I_{cr} = (\frac{1}{3})(40)(12)(x)^3 + nA_s(10-x)^2 = (\frac{1}{3})(40)(12)(3.56)^3 + (6.45)(79.48)(10-3.56)^2 = 26876.5\ in^4$$

Cracking moment:

$$f_r = 7.5\sqrt{f_c'} = 556.2\ psi$$

$$M_{cr} = \frac{f_r I_g}{0.5h} = \frac{(556.2)(69120)}{(0.5)(12-2)} = 640.7\ ft-kips$$

Short-term dead load deformation:

$$I_e = (\frac{M_{cr}}{M_a})^3 I_g + \left[1-(\frac{M_{cr}}{M_a})^3\right] I_{cr} = (\frac{M_{cr}}{M_D})^3 I_g + \left[1-(\frac{M_{cr}}{M_D})^3\right] I_{cr} = (\frac{640.7}{723.1})^3 (69120) + \left[1-(\frac{640.7}{714.3})^3\right](26876.5)$$
$$= 43889.3 in^4$$

$$d_D' = \frac{I_g}{I_e} d_D = \frac{69120}{43889.3}(0.0529) = 0.0834\ ft$$

$$\theta_D' = \frac{I_g}{I_e}\theta_D = \frac{69120}{43889.3}(0.00415) = 0.00653$$

Short-term dead load + live load deformation:

$$I_e = (\frac{M_{cr}}{M_a})^3 I_g + \left[1-(\frac{M_{cr}}{M_a})^3\right] I_{cr} = (\frac{M_{cr}}{M_D})^3 I_g + \left[1-(\frac{M_{cr}}{M_D})^3\right] I_{cr} = (\frac{640.7}{1112.9})^3 (69120) + \left[1-(\frac{640.7}{1112.9})^3\right](26876.5)$$
$$= 31541.9 in^4$$

$$d_T' = \frac{I_g}{I_e} d_T = \frac{69120}{31541.9}(0.0745) = 0.163\ ft$$

$$\theta_T' = \frac{I_g}{I_e}\theta_T = \frac{69120}{31541.9}(0.00608) = 0.0133$$

Short-term live load deformation

$$d_L' = d_T' - d_D' = 0.0800\ ft$$

$$\theta_L' = \theta_T' - \theta_D' = 0.00680$$

Long term deformation factor for sustained load

$$\lambda = \frac{\xi}{1+50\rho'} = 2$$

The final total deformation = instantaneous deformation + long term deformation is

$$d_{LT}^{'} = d_{L}^{'} + \lambda_{\infty} d_{D}^{'} = 2.96 in$$

$$\theta_{LT}^{'} = \theta_{L}^{'} + \lambda_{\infty} \theta_{D}^{'} = 1.14^{o}$$

In comparison, finite element results for M_D, M_T (M_D and M_T here are for the whole section), d_D, d_T, θ_D and θ_T are 685.8 kips-ft., 1003.7 kips-ft., 0.0489 ft., 0.0567 ft., 0.00391, 0.00533, respectively. The reason for the difference between finite element results and the results derived from equations is the errors in the regression analysis. Figures 20 and 21 show that at small settlements, the curves have large slopes and thus more sensitive regression errors. In deformation calculation, using the effective width method is overly conservative. It predicted much larger values for deformation than using the total slab width and finite element method.

Long-term Deflection of Current LADOTD Approach Slab

In the long-term time-dependent deformation calculation, the AASHTO code method is used where no interaction between the soil and the slab is considered. As discussed earlier, in reality, when the approach slab is trying to deform more due to time-dependent effects, the soil will provide a support unless the differential settlement is very large where the soil and approach slab are not expected to be in contact. Therefore, the long-term deformation calculation shown in the calculation procedure is an upper bound and may be significantly different from the true values. However, to demonstrate the deformation problems of the current LADOTD slab (L = 40 ft. and h =1 ft.), the long-term deformations are given below. Again, these figures show that the 40 ft. slab could have very large long-term deflections and that may explain the observed failures in the field.

For comparison, the long term deflections of the redesigned slabs with different thicknesses are also shown here in figures A7 to A10. Again, the long-term deflection is calculated based on AASHTO code method without considering the soil and slab interaction.

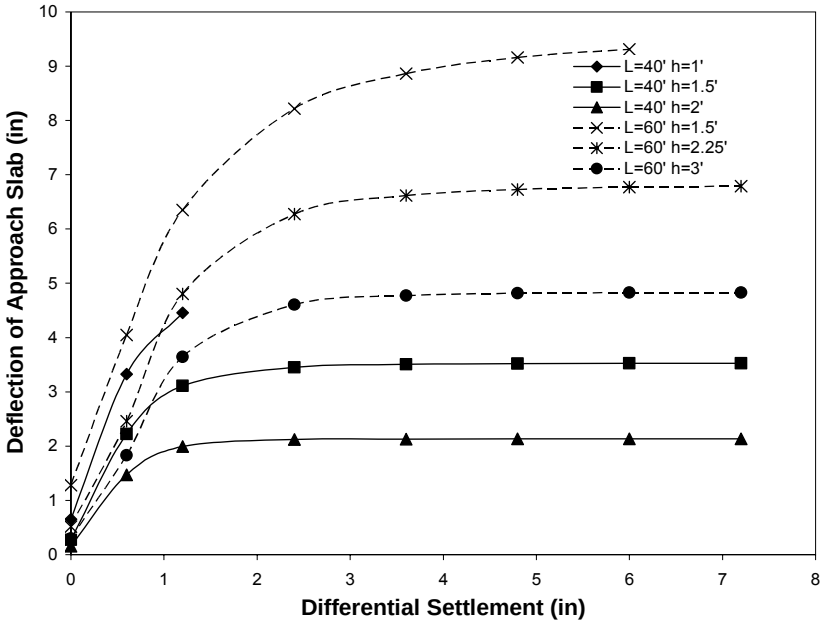

Figure A7
Long-term deflection of approach slab vs. differential settlement (effective width method)

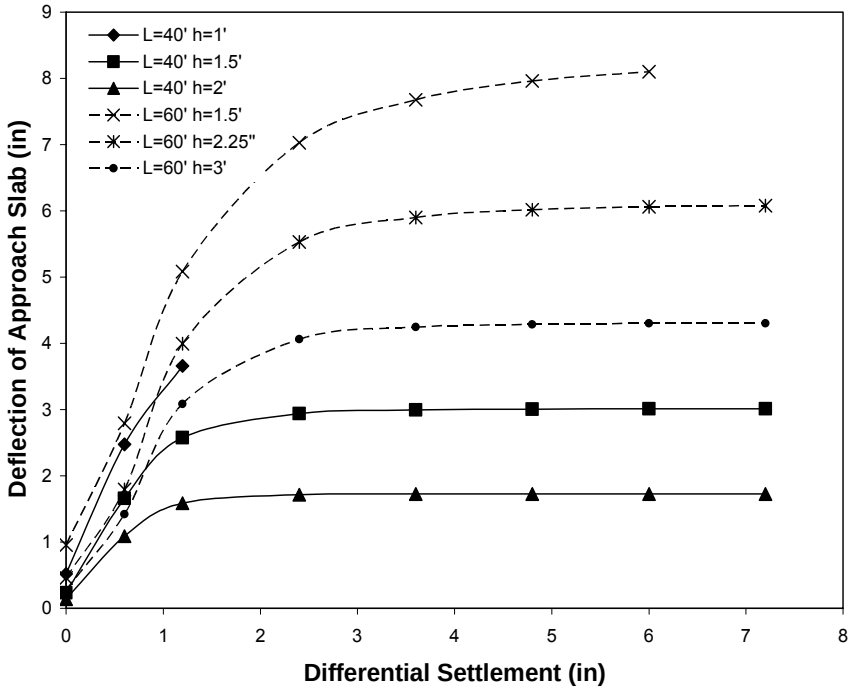

Figure A8

Long-term deflection of approach slab vs. differential settlement (total with method)

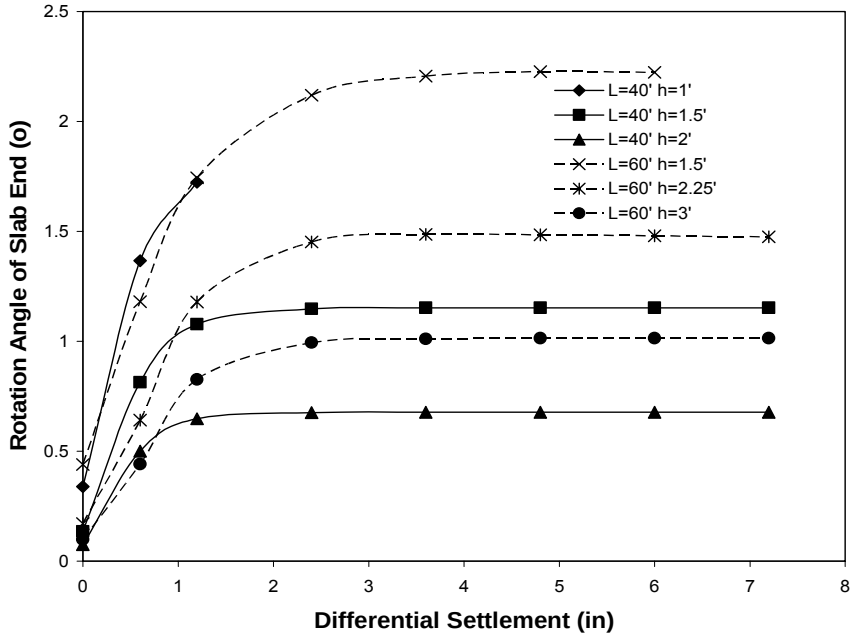

Figure A9

Long-term rotation angle of approach slab vs. differential settlement (effective width method)

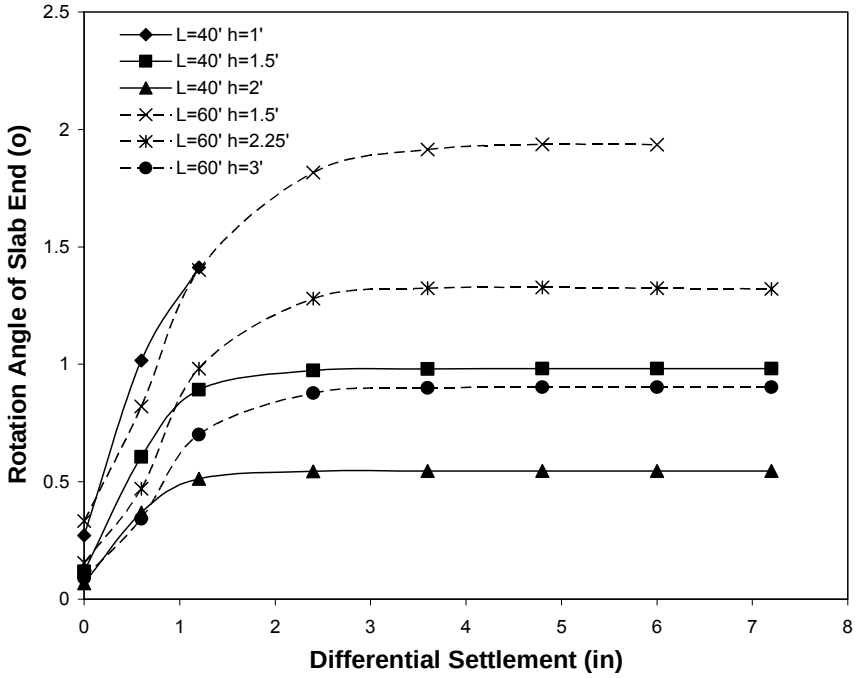

Figure A10

Long-term rotation angle of approach slab vs. differential settlement (total width method)

APPENDIX B

Special Study 1 – Skew Angle Effect

It is not unusual for bridges to end with large skews to pavements. To confirm the applicability of the previously derived equations to skewed approach slabs, skewed approach slabs with skew angles of 45^{o} for a few different span lengths under different differential embankment settlements were analyzed using the FE method. The geometry, material properties, and load condition of the FE model (figure B1) are the same as those used in normal (right) approach slab analysis, except the skewed angle. Flat approach slabs with different span lengths (40 ft. and 60 ft.) and different thicknesses (1 ft. and 1.5 ft. for 40 ft. long slabs and 1.5 ft. and 2.25 ft. for 60 ft. long slabs) were investigated. Two AASHTO design truckload HS20-44 were applied on the slab under different embankment settlements.

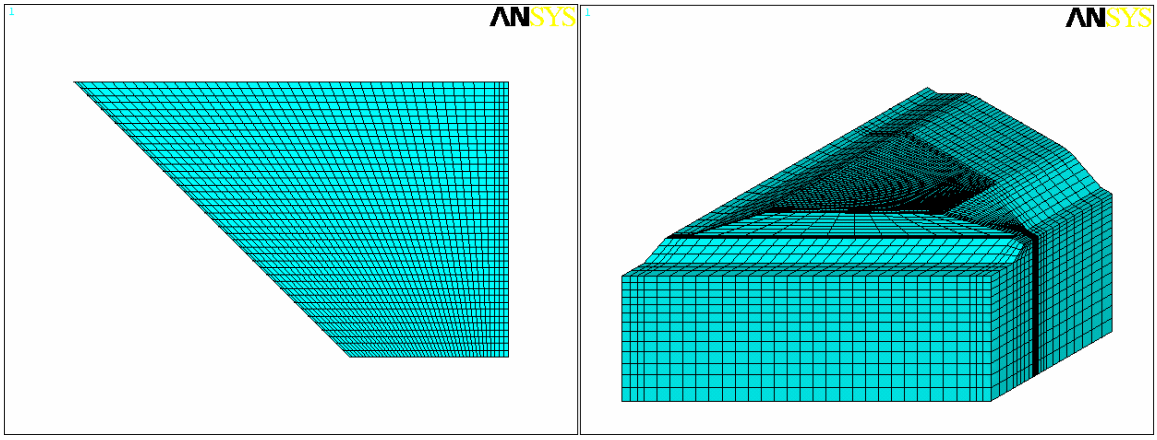

Figure B1
FE model of skewed approach slab

Figure B2 shows the stress distribution in a skewed slab under different embankment settlements. When the settlement is small, the slab is partially supported by the soil near the sleeper slab end and separates from the embankment soil near the abutment end. The performance of the slab under this condition is more like that of a triangular slab as shown in Figure B2(a). Although the maximum moment of the total section is in the rectangular part, the maximum stress is located in the triangular part. Therefore, using the moment per unit width to describe the internal force of the slab is more reasonable for design purpose. In the following study of skewed approach slabs, the moment per unit width is thus used instead of

the total moment of the section.

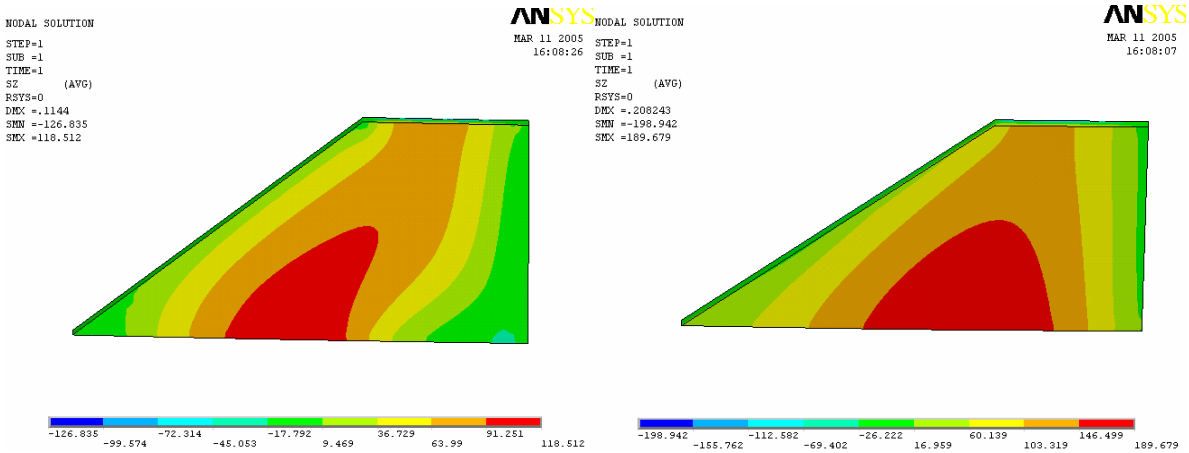

(a) Settlement = 0.5 in. (b) Settlement = 6 in.

Figure B2
Stress distribution of skewed approach slab

Figures B3 to B6 show the moment per unit width of a skewed approach slab with a span length of 40 ft. and 60 ft. under different settlements of embankment soil due to the dead load and total load, respectively. The span length L of the skewed slab used here represents the length of the slab along the mid-width line. In the previously derived equations (equations 3 to 11), the internal force and displacement of the approach slab considering the settlement effects are calculated by using a coefficient to multiply the corresponding value of a simply-supported beam. Therefore, in these figures, in addition to the moment predicted directly from the FE analysis that is labeled "FEM, SKEWED SLAB," two more calculations based on the derived equations were conducted. In the first one, the moment per unit width was obtained by using previously derived equations, but the M_0 (moment of a simply-supported beam) was based on a simply supported skewed slab using a finite element modeling since a direct calculation of M_0 for skewed slabs is not available. This calculation is labeled "EQUATION, SKEWED SLAB." In the second calculation, the unit width moment was calculated by using the derived equations, but the M_0 is based on an equivalent simply supported normal (right) slab where its span length is taken the same as the length along the mid-width line of the skewed slab. This calculation is labeled "EQUATION, RIGHT ANGEL SLAB." The displacement of the skewed approach slab due to the dead load and total load are shown in figures B7 to B10. Similarly, the displacement was calculated by

using the equations with d_0 based on a simply supported skewed slab and a simply-supported normal slab.

Figures B3 to B6 show that the moment of skewed approach slabs based on FEM is close to that obtained from equations based on the simply supported skewed slab, which indicates that the equations derived for normal approach slab can be used to calculate the internal forces of the skewed approach slab. However, the simply supported skewed slab is complicated, and a hand calculation for the internal force analysis is not available because of its irregular shape. An FE analysis is thus usually necessary. The moment obtained from the equations based on the equivalent simply supported normal slab is larger than that of the skewed slab moment from FE analysis, as shown in figures B3 to B6. Thus, it is conservative and more convenient to use the moment calculated from the equations based on an equivalent normal slab in skewed approach slab design.

The displacements of skewed slabs obtained from FE analysis and equations based on a *simply supported skewed slab* are close to each other, as shown in figures B7 to B10. This means that if the displacement of a simply supported skewed slab is known, the equations derived for normal approach slabs can also be used to analyze the displacement of skewed approach slabs. However, the displacement obtained from equations based on an equivalent *simply supported normal slab* is much smaller than that obtained from FE analysis of the skewed slab, which is caused by the big displacement of the long side of the skewed approach slab. Therefore, to use the developed equations, a nominal span length longer than that used for moment is needed.

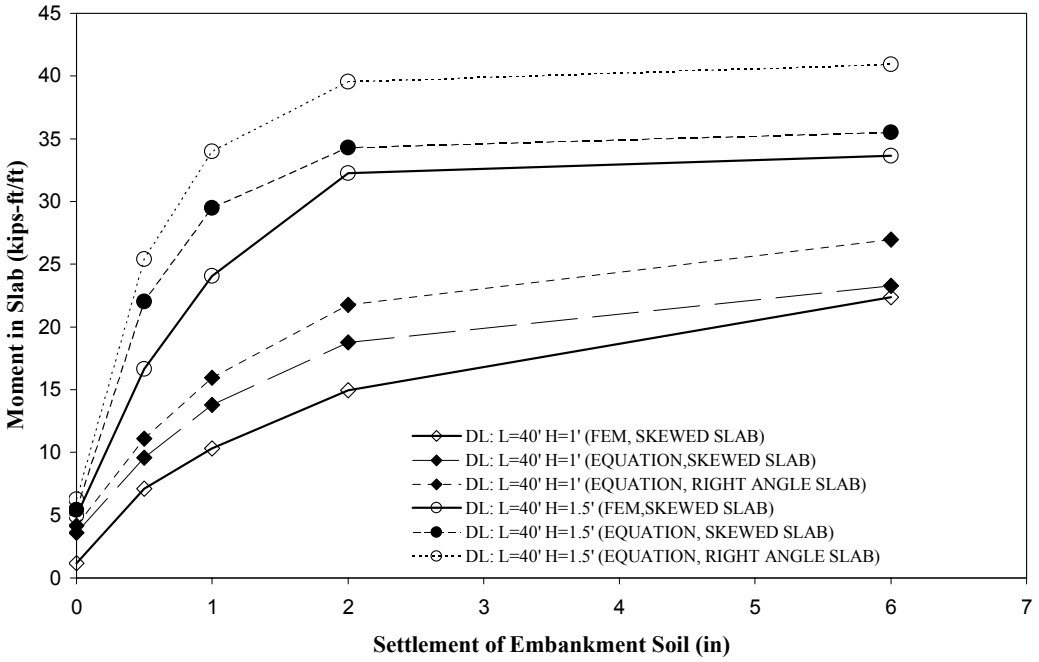

Figure B3
Moment of skewed slab with span of 40 ft. due to self weight vs. embankment settlement

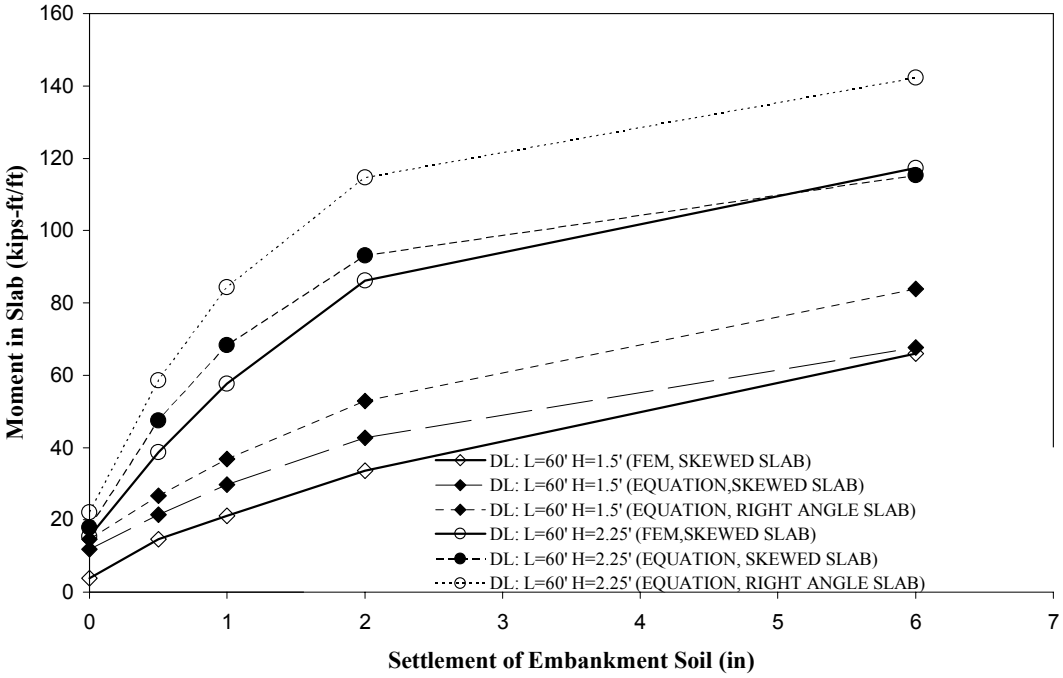

Figure B4
Moment of skewed slab with span of 60 ft. due to self weight vs. embankment settlement

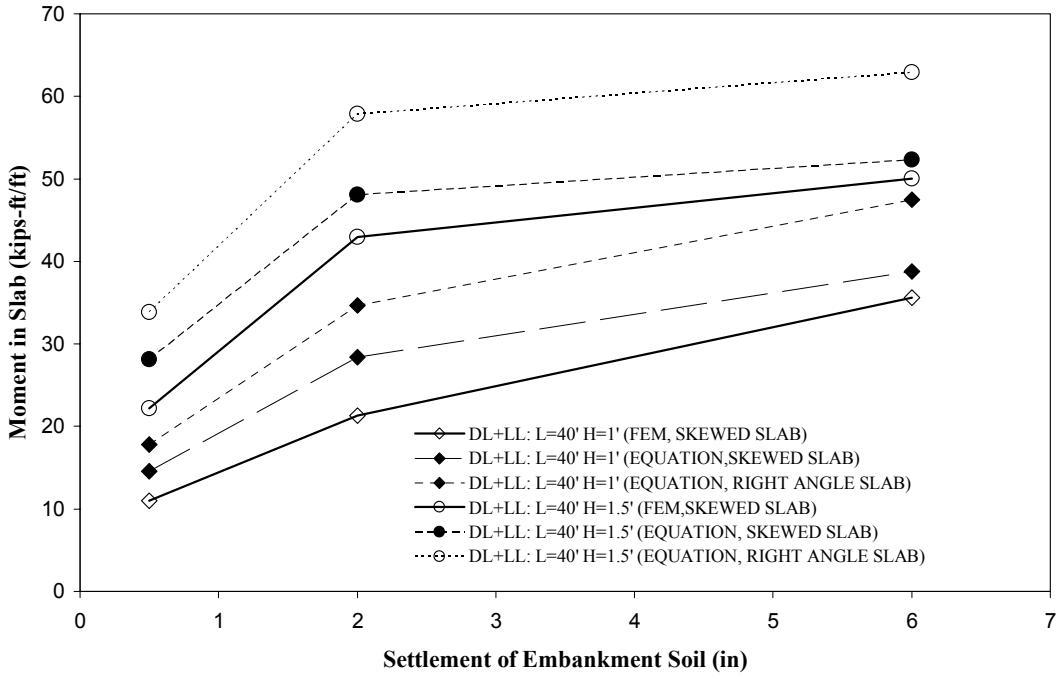

Figure B5
Moment of skewed slab with span of 40 ft. due to total Load vs. embankment settlement

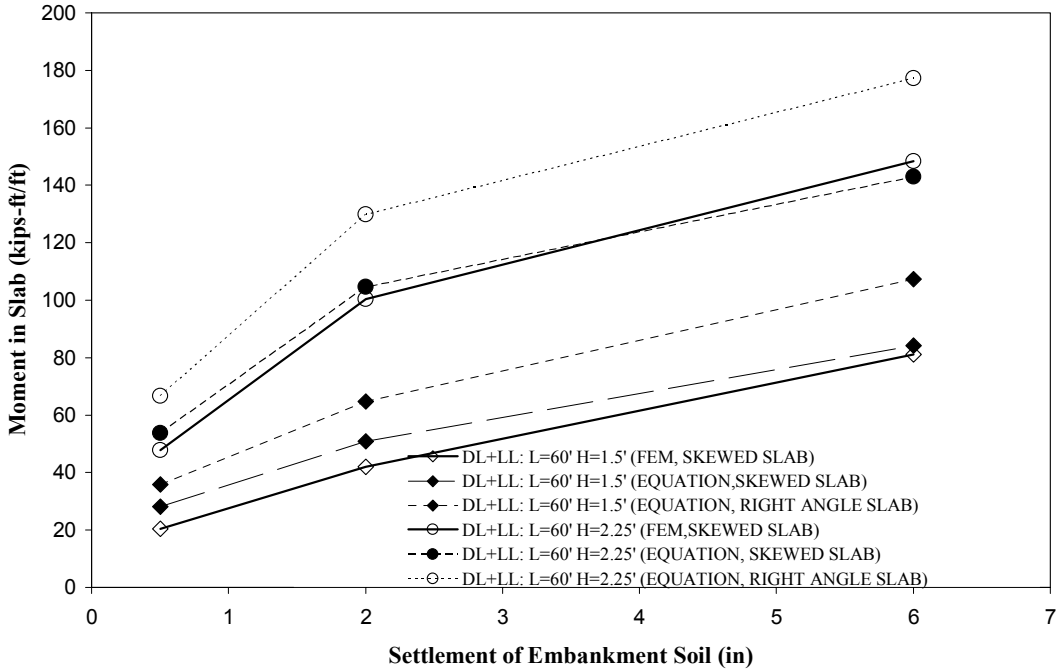

Figure B6
Moment of skewed slab with span of 60 ft. due to total load vs. embankment settlement

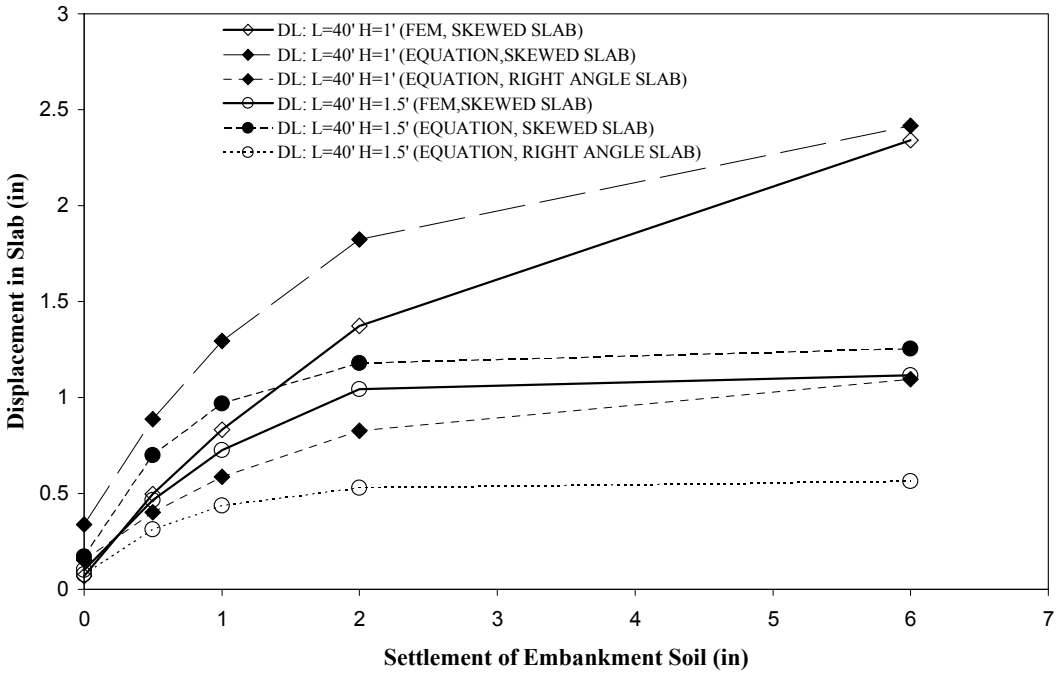

Figure B7
Displacement of skewed slab with span of 40 ft. due to self weight vs. embankment settlement

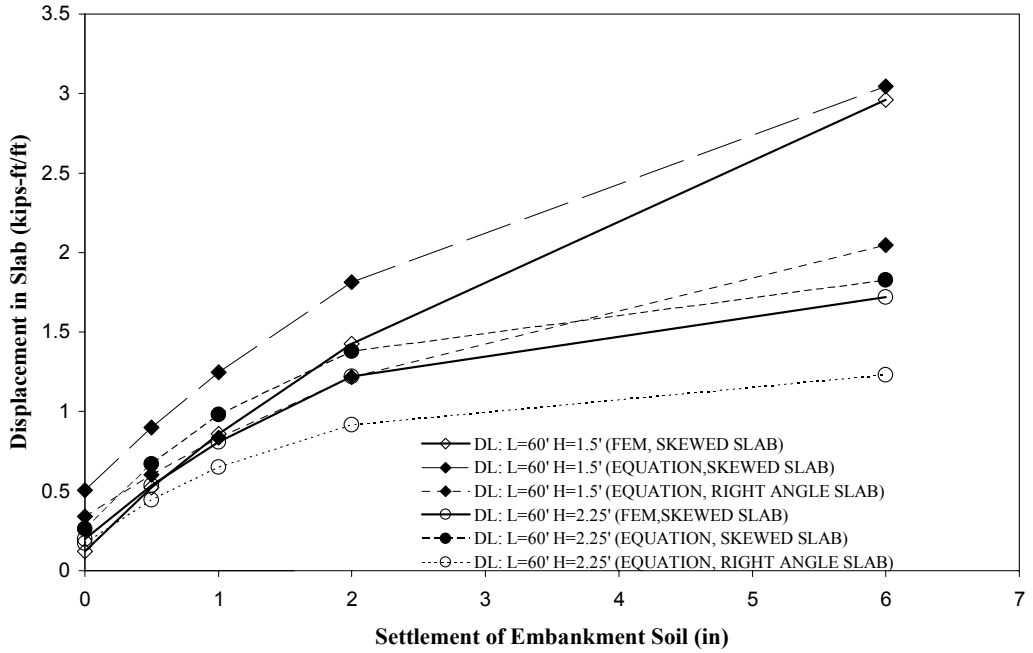

Figure B8
Displacement of skewed slab with span of 60 ft. due to self weight vs. embankment settlement

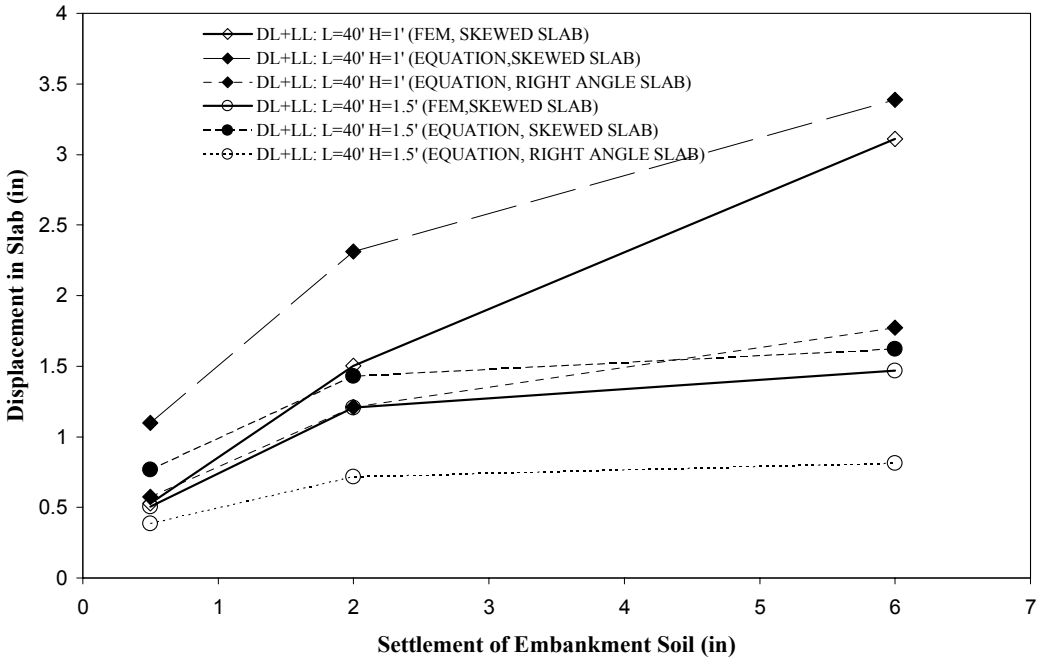

Figure B9
Moment of skewed slab with span of 40 ft. due to total load vs. embankment settlement

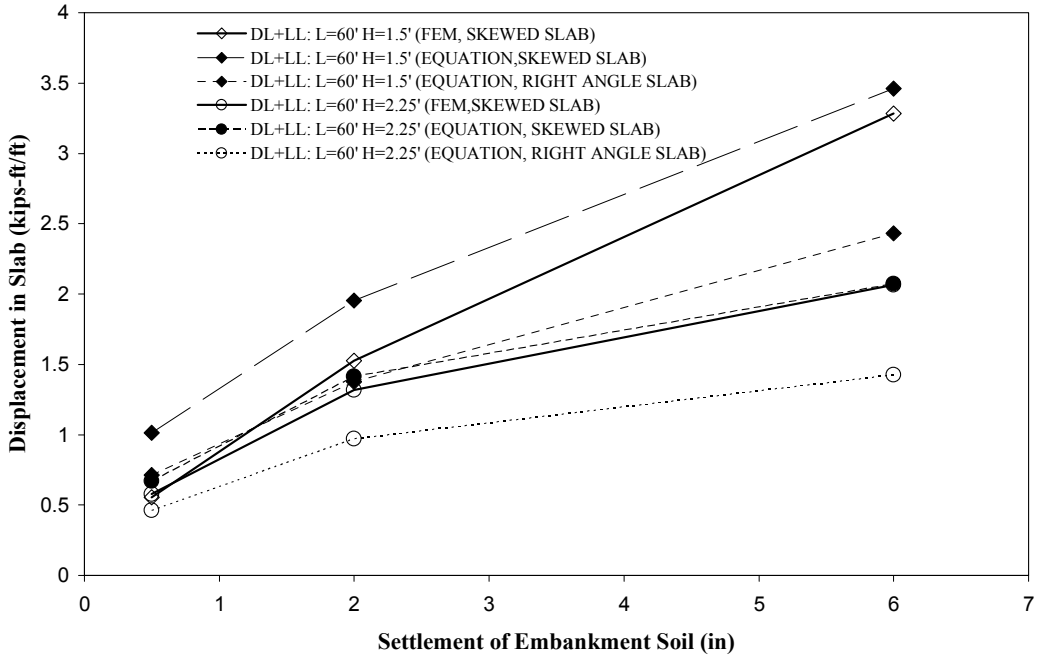

Figure B10
Moment of skewed slab with span of 60 ft. due to total load vs. embankment settlement

The comparison of results from FE analysis and the results calculated by using the previously derived equations indicates that the internal force and deflection of skewed approach slabs

can be obtained by using the equations derived for normal approach slabs, where M_0, d_0 and θ_0 are the internal forces and deformation of simply supported skewed approach slabs. Since the calculation of a simply supported skewed approach slab is more complicated than a simply supported normal slab, the FE method is also need to analyze the simply supported skewed slab, which makes the equation not convenient for design purpose. Therefore, the internal forces and deformation of skewed approach slabs are compared to those of simply supported normal slabs with the same nominal span. Results show that the internal forces of skewed slab are less than those obtained from equations using simply supported normal slab, which indicates that using the equations with M_0 of an equivalent normal slab to calculate skewed approach slab internal force is conservative.

Special Study 2 – Failure Modes-Mechanisms at Joint of Slab and Abutment

The approach slab can be considered as a simply supported slab; however, in Louisiana, the slab is often connected to the abutment wall by dowel bars and bolts (figure B11). The dowel steel bar is used to constrain the relative longitudinal displacement between the approach slab and abutment due to temperature change. The bolts are to hold the joint between approach slab and bridge deck in place during construction. When a finger joint is used between the approach slab and bridge deck, the steel bolts are usually placed in the abutment wall (figure B11) to support the joint during construction. However, the end of the approach slab at the abutment will rotate when the slab is subjected to some loads in the middle of the span, but the bars and bolts will prevent the rotation. Consequently, the steel bars and bolts will take some force when the joint is inclined to rotate, and a negative moment will form at the joint, which may be transferred to the bottom of the abutment. If the span length of the approach slab is large and the load or embankment settlement is significant, the steel rebars and bolts may yield and concrete may be damaged. The possible failure modes-mechanisms are investigated by using the FE model.

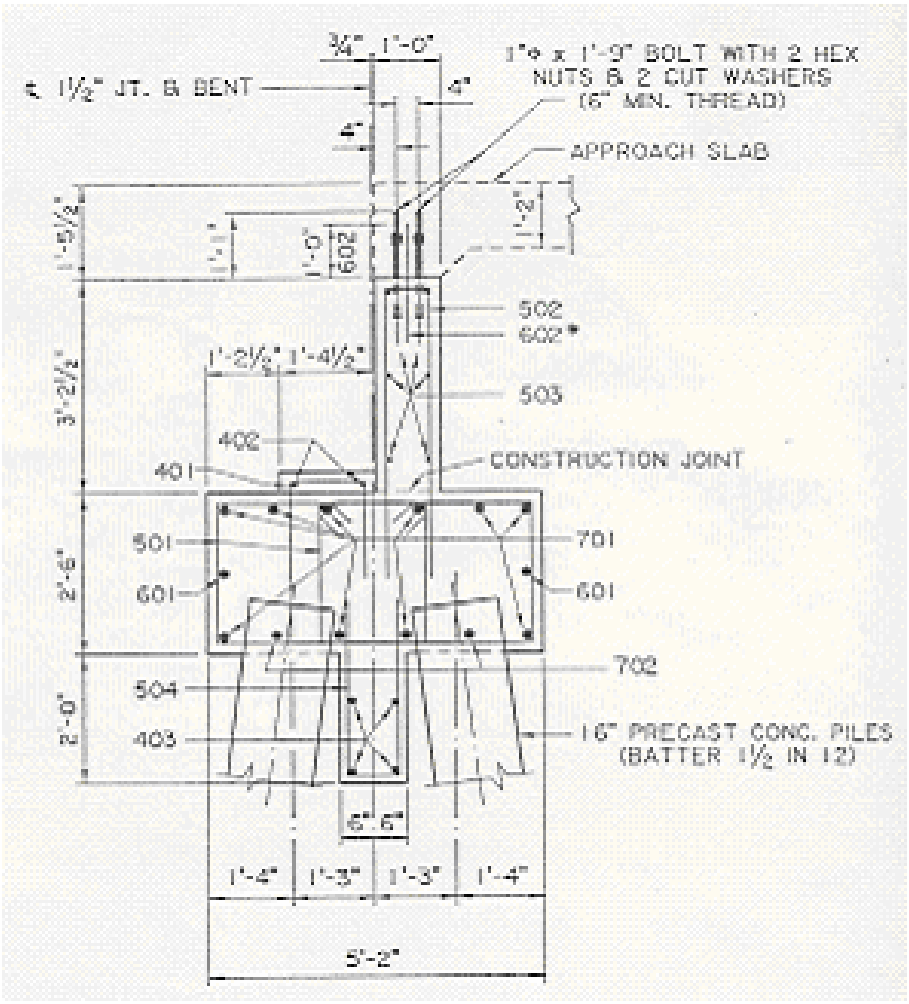

Figure B11
Detail of typical expansion joint

According to the commonly used approach slab and abutment joint (figure B11), 2 ft. long steel rebars spaced at 1 ft., and 2 or 4 steel bolts per girder line, are used to connect the slab to the abutment. A finite element model of approach slabs with the detailed joints, abutment, and embankment soil was used (figure B12). The material properties of the slab, abutment, and soil are the same as those used in the previous model. The elastic modulus of the steel rebars and bolts E is 29,000 ksi. The abutment, embankment soil, approach slab, and the interface of the approach slab and embankment soil are modeled using the same elements as in the previous analysis, while a link element is used to simulate the dowel bars and the bolts. The details of the approach slab and abutment joint are shown in figures B13 and B14.

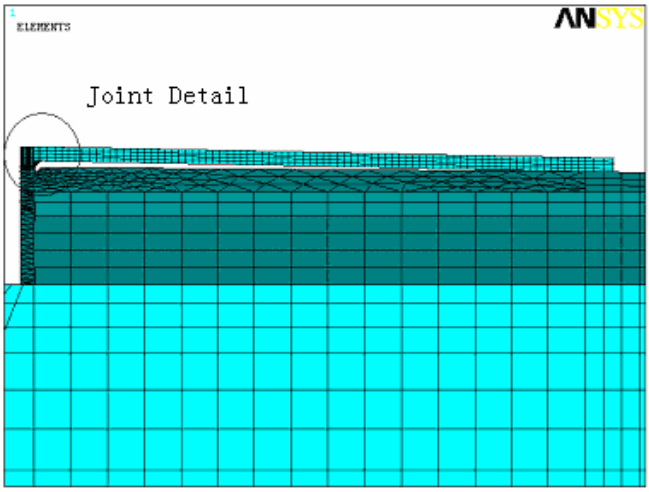

Figure B12
FE model used to analyze failure mechanism

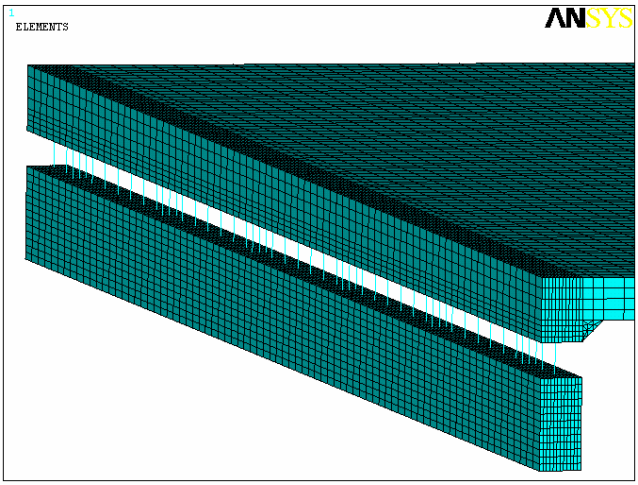

Figure B13
Detail of approach slab and abutment joint used in FE model

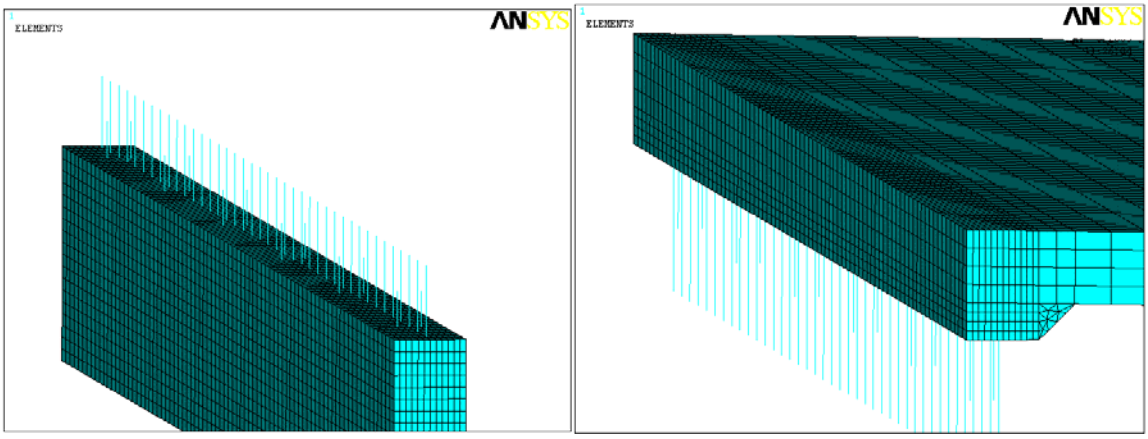

(a) Abutment (b) Approach slab

Figure B14
Detail of abutment and end of approach slab

Figures B15 and B16 show the stress distributions in the joint of abutment and approach slab, and Figure B17 shows the deformations of the joint under the embankment settlement of 0, 0.5, 2 and 6 in. In addition, tables B1 and B2 show the stresses in steel rebars and bolts as well as the stresses in the abutment wall and approach slab. The results in table B1 were obtained by applying only live load (truck load) on the approach slab while results in table B2 were reached by applying both live load and dead load. The former situation simulated the condition in which the steel rebars and bolts are subjected to only live load because when the approach slabs were cast, the concrete near the bolts and rebars was wet, and the dead load of the slab would not engage the bolts and steel rebars. The latter situation modeled the condition that the steel rebars and bolts are subjected to both live load and dead load. As the embankment soil settles, the dead load of the slab will transfer to the slab ends, which will engage the bolts and rebars. As shown in table B1, the stresses in steel rebars and bolts increase with the increase of the embankment settlements. When the embankment settlement reaches 6 in., the vertical stress at the abutment inner corner is 2.72 ksi and the tensile stress of abutment wall is 0.85 ksi, which means the concrete in the corner will be crushed and the wall will have cracks in its tension side. The steel rebars and bolts may yield in this condition.

The results show that when the embankment settlement is large, the stress in the dowel steel rebars will exceed the yield stress, indicating that the steel rebars can no longer take additional stress. In extreme case in practice, the steel rebars can be pulled out from the abutment and the concrete near the interface of approach slab and the abutment will be crushed.

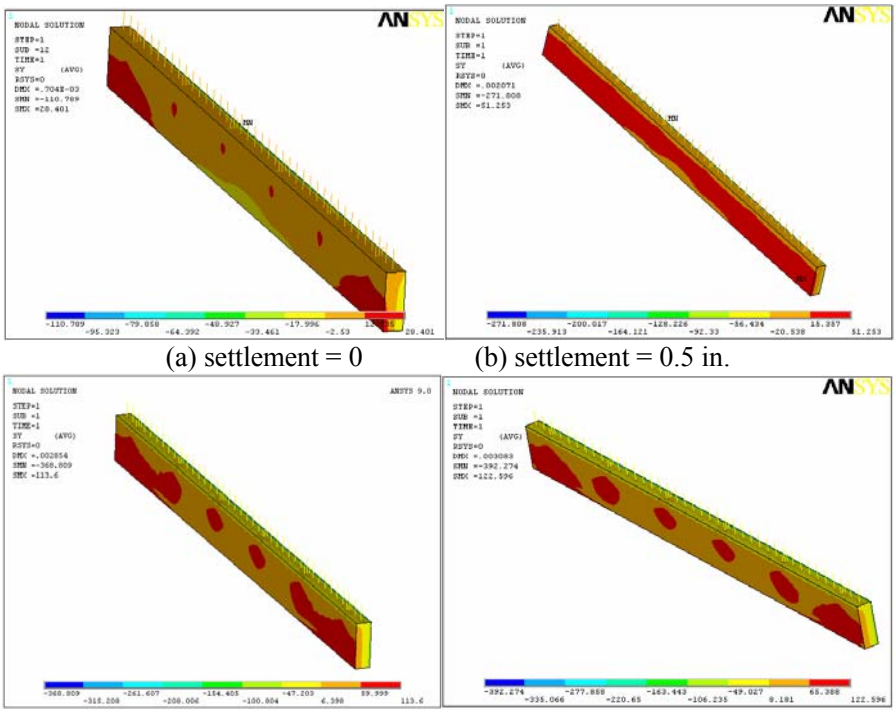

(a) settlement = 0 (b) settlement = 0.5 in.

(c) settlement = 2 in. (d) settlement = 6 in.

Figure B15
Stress distribution in abutment

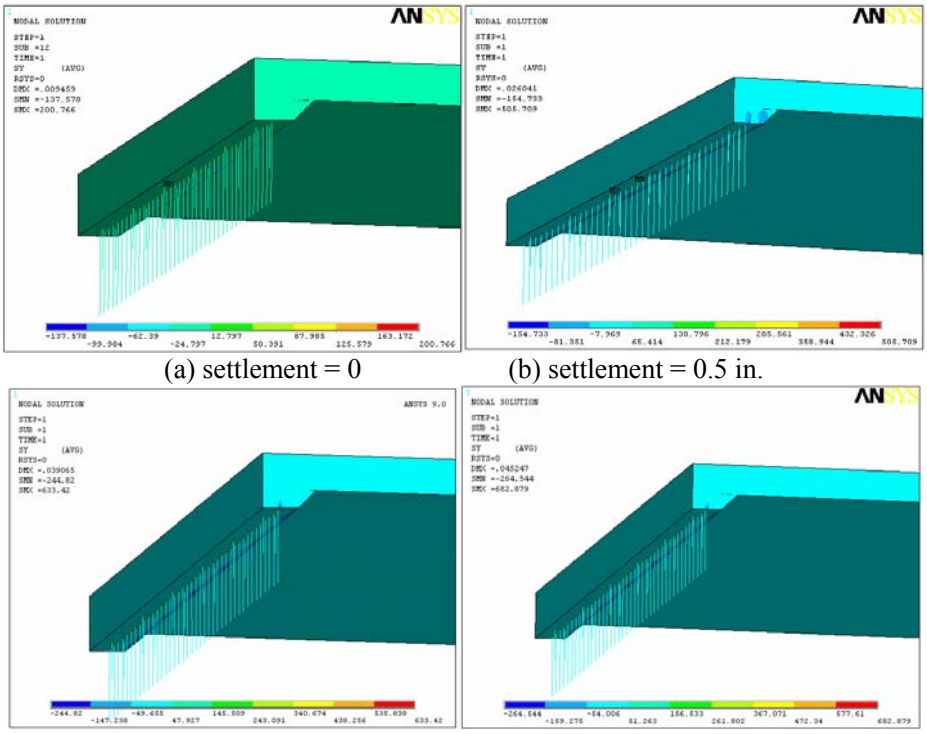

(a) settlement = 0 (b) settlement = 0.5 in.

(c) settlement = 2 in. (d) settlement = 6 in.

Figure B16
Stress distribution in approach slab

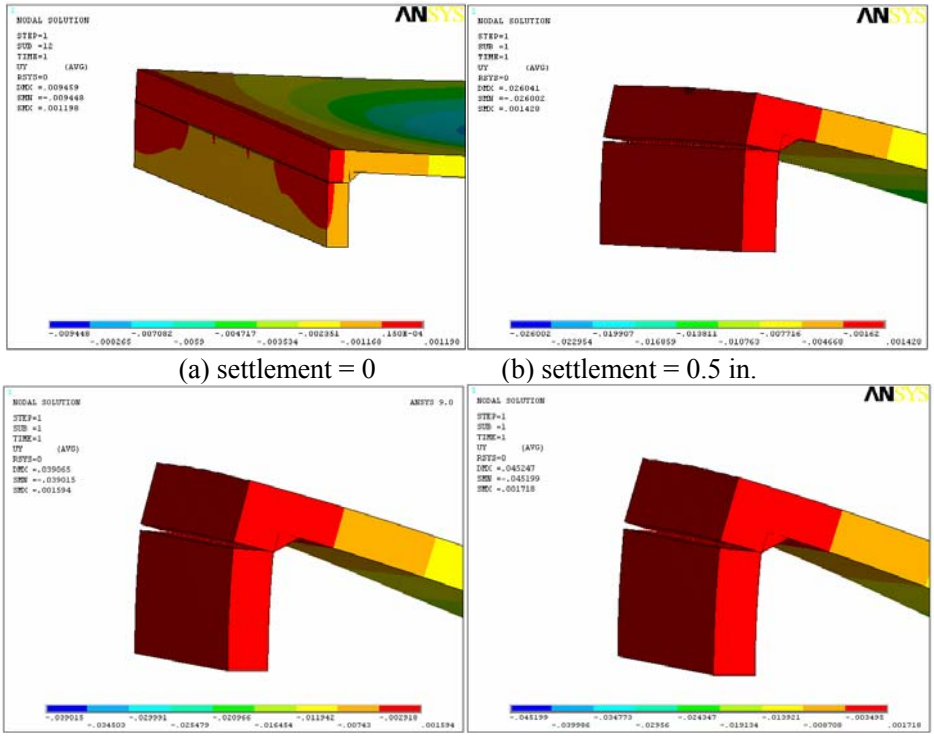

(a) settlement = 0 (b) settlement = 0.5 in.

(c) settlement = 2 in. (d) settlement = 6 in.

Figure B17
Deformation of the joint

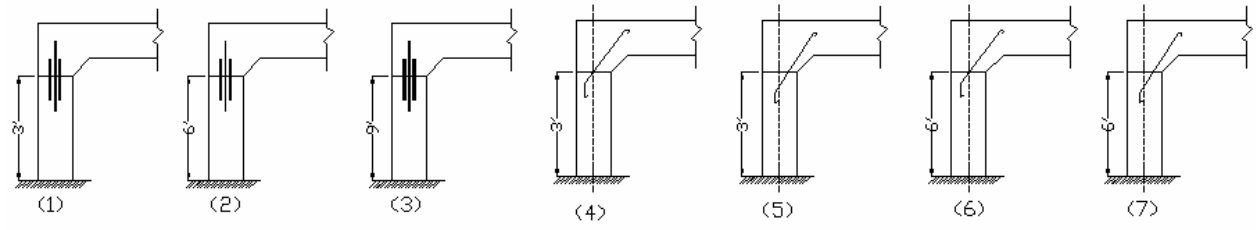

Figure B18
Different cases used in analysis

Table B1
Stress at the joint (case 1, approach slab subjected to live load)

Settlement (in)	Steel Bar	Bolt	Abutment		Approach Slab
	Stress (ksi)	Stress (ksi)	Tensile Stress (ksi)	Compressive Stress (ksi)	Contact Stress[(1)] (ksi)
0	10.17	10.72	0.20	0.77	0.96
0.5	25.21	27.00	0.36	1.89	1.08
2	49.00	45.57	0.79	2.56	1.70
6	52.96	49.13	0.85	2.72	1.84

Note: (1) The contact stress in approach slab at the joint is compressive stress.

Table B2
Stress at the joint (case 1, approach slab subjected to dead load & live load)

Settlement (in)	Steel Bar	Bolt	Abutment		Approach Slab
	Stress (ksi)	Stress (ksi)	Tensile Stress (ksi)	Compressive Stress (ksi)	Compressive Stress[(1)] (ksi)
0	19.05	20.47	0.28	1.48	0.96
0.5	37.58	40.63	0.52	2.87	1.60
2	65.31	70.77	0.94	4.94	2.85
6	117.38	109.78	1.91	6.07	4.07

Note: (1) The contact stress in approach slab at the joint is compressive stress.

Table B3
Stress and moment at the joint (settlement = 6 in., approach slab subjected to live load)

Different Case	Steel Bar	Bolt	Abutment		Approach Slab	Moment at Joint
	Stress (ksi)	Stress (ksi)	Tensile Stress (ksi)	Compressive Stress (ksi)	Contact Stress[(1)](ksi)	(kips-ft.)
(1)	52.96	49.13	0.85	2.72	1.84	575.32
(2)	37.70	39.80	0.54	2.69	1.58	461.12
(3)	36.72	39.08	0.55	2.72	1.57	415.00
(4)	58.78	-	0.74	2.43	2.31	363.34
(5)	54.98	-	0.31	2.66	2.17	209.27
(6)	56.44	-	0.71	2.31	2.22	362.60
(7)	53.92	-	0.24	2.56	2.13	201.21

Note: (1) The contact stress in approach slab at the joint is compressive stress.

Table B4
Stress and moment at the joint (settlement = 6 in, approach slab subjected to dead load & live load)

Different Case	Steel Bar	Bolt	Abutment		Approach Slab	Moment at Joint
	Stress (ksi)	Stress (ksi)	Tensile Stress (ksi)	Compressive Stress (ksi)	Contact Stress[(1)](ksi)	(kips-ft.)
(1)	117.38	109.78	1.91	6.07	4.07	1392.41
(2)	82.44	89.29	1.21	5.98	3.52	1124.00
(3)	81.90	88.69	1.22	5.99	3.95	1067.52
(4)	131.50	-	1.67	5.40	5.23	882.31
(5)	124.88	-	0.55	5.91	4.98	483.79
(6)	125.45	-	1.57	5.09	4.93	911.33
(7)	122.47	-	0.55	5.66	4.88	470.24

Note: (1) The contact stress in approach slab at the joint is compressive stress.

In tables B1 to B4, the negative moment at the joint as well as the stresses in steel rebars, bolts, abutment wall, and approach slab are listed for different cases shown in figure B18. In cases 1 to 3, vertical steel rebars and bolts are used with different abutment wall lengths. Tables B1 to B4 indicate that the longer (more flexible) abutment wall will reduce the stresses and the negative moment. As shown in figure B18, different abutment wall heights

are also investigated with steel bolts removed and only inclined steel bars are used. The inclined steel bars in cases 5 and 7 are much closer to the inner corner than the bars in cases 4 and 6. Tables B1 to B4 show that removing the bolts and using inclined bars will reduce the negative moment greatly, and that the closer the inclined bars are to the inner corner, the more the negative moment is reduced.

Based on the above investigation, a new style of approach slab and abutment joint is suggested as shown in figure B19. Inclined steel bar, which can prevent the relative longitudinal displacement between approach slab and abutment, while allowing rotation of the approach slab, can be used to replace the vertical bar.

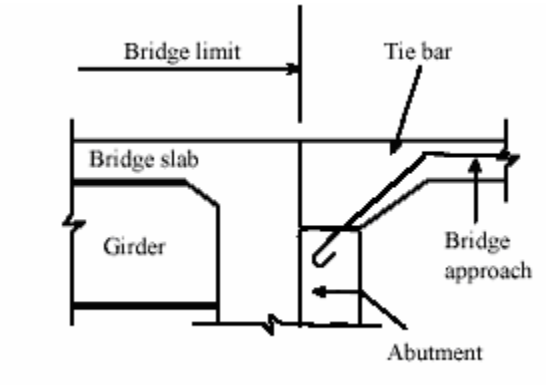

Figure B19
Proposed joint

Special Study 3 – HL93 Highway Load

Analysis of Flat Approach Slab Subjected to HL93 Highway Load

The previous analysis of flat approach slabs was based on AASHTO standard HS20-44 truckload. In this study, the investigation of approach slabs subjected to AASHTO LRFD HL93 highway load is conducted below.

For the flat approach slabs, equations were derived to simplify the calculation of internal forces and deformations based on the HS20-44 truckload in a previous study. The finite element method was used to investigate the applicability of the equations to LRFD HL 93

highway load. The geometries and the material conditions of the FE model are the same as those used in the analysis of approach slab subjected to HS20-44. The LRFD HL93 highway load, consisting of the lane load and the HS20-44 truckload, was applied on the approach slab.

A parametric study was conducted by changing the slab thickness and span length to investigate whether the previous equations are applicable to the HL93 highway load. The slab parameters, length (L) and thickness (h), were investigated in the parametric study for the following cases: (1) h was varied from 1 to 1.5 ft. for the fixed L = 40 ft.; and (2) h was varied from 1.5 to 2.25 ft. for the fixed L = 60 ft. For each case, settlement was varied from 0.5, 2, to 6 in.

The results of FE analysis for flat approach slabs under different settlements are shown in figures B20 to B23. Meanwhile, results obtained by using the equations derived for flat slabs subjected to HS20 truckload are also plotted to compare with the FE analysis. The M_0, d_0 used in the equations was calculated by applying HL 93 to the simply supported flat slabs. For the approach slab with a span length of 40 ft. and thickness of 1.5 ft., the internal moment of the slab calculated by using the equations is almost the same as those from FE analysis. These figures show that for different approach slabs with different dimensions under different embankment settlements, the moment and deformation obtained from equations are close to those from FE analysis. Based on the investigation of different cases of different flat approach slabs shown in these figures, we can conclude that the equations are applicable to flat approach slabs subjected to the LRFD HL93 highway load.

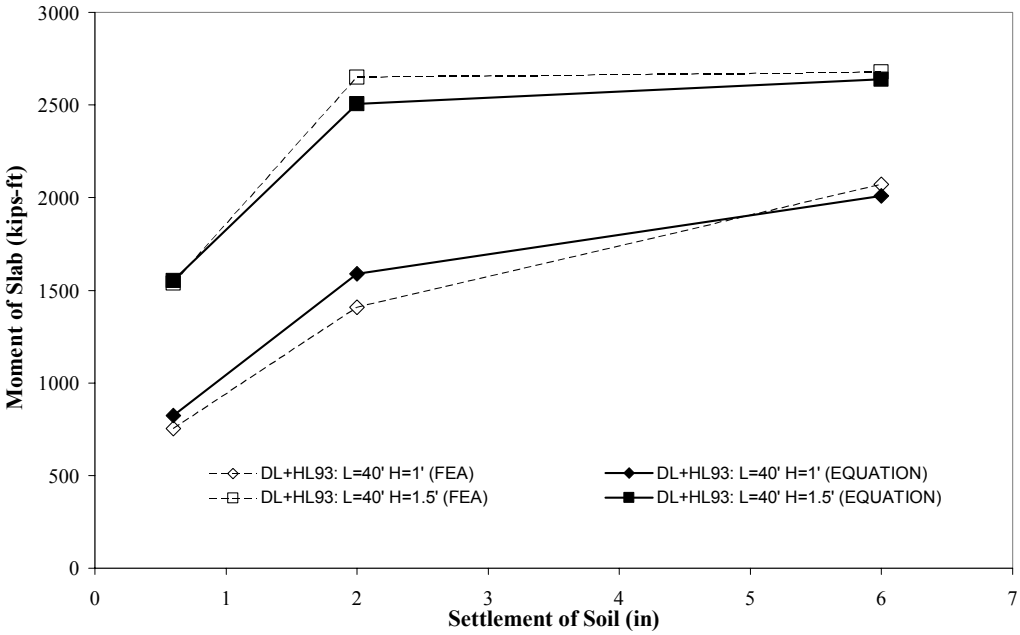

Figure B20
Moment of flat approach slab with span of 40 ft. vs. soil settlement

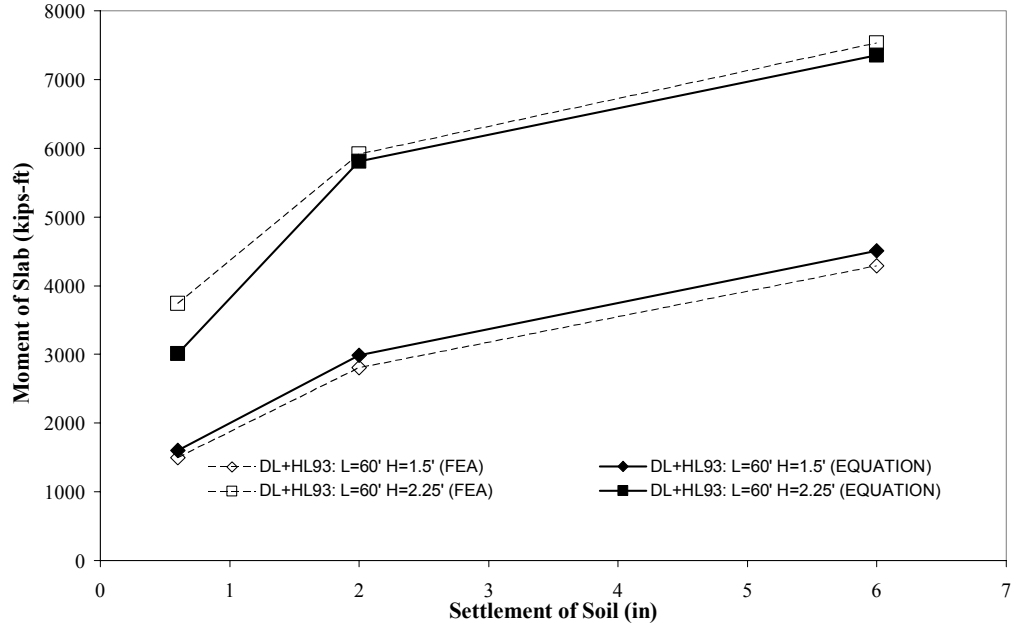

Figure B21
Moment of flat approach slab with span of 60 ft. vs. soil settlement

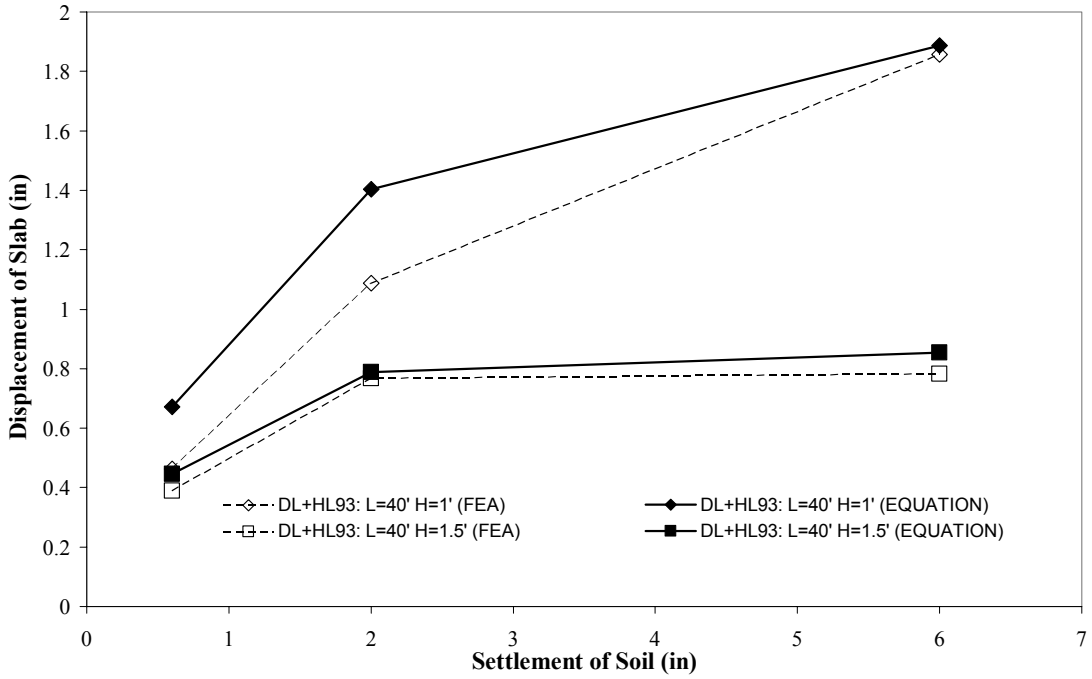

Figure B22
Displacement of flat approach slab with span of 40 ft. vs. soil settlement

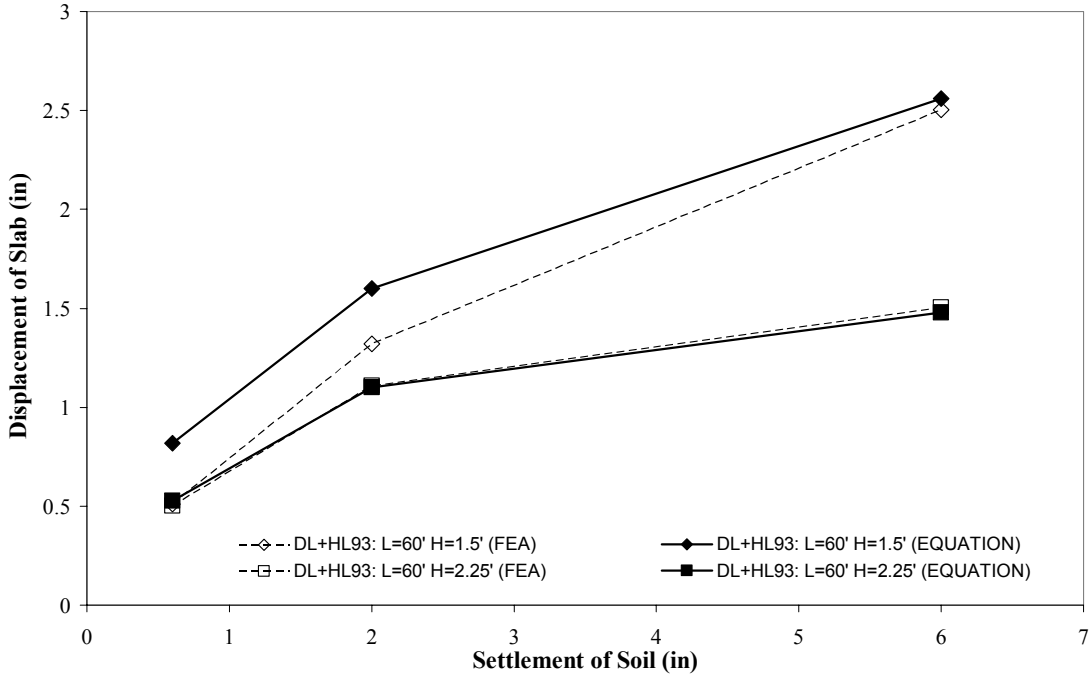

Figure B23
Displacement of flat approach slab with span of 60 ft. vs. soil settlement

Reinforcement Design of Flat Slab according to AASHTO LRFD Code

While the derived equations are applicable for both HS20 and HL93 highway loads, the internal forces are different. The results of reinforcement design for flat approach slab subjected to HL93 highway loads are listed in table B5.

Table B5
Reinforcement ratio of slab under different settlement (HL93)
(f'_c = 4000 psi and f_y = 60,000 psi)

Differential settlement (in)	40-ft. Slab			60-ft. Slab		
	ρ for thickness of 12 in.	ρ for thickness of 18 in.	ρ for thickness of 24 in.	ρ for thickness of 21 in.	ρ for thickness of 27 in.	ρ for thickness of 36 in.
0	0.0063	0.0025	0.0014	0.0035	0.0022	0.0014
0.6	0.0145	0.0081	0.0058	0.0060	0.0046	0.0036
1.2	NA(1)	0.0114	0.0074	0.0083	0.0065	0.0052
2.4	NA	0.0143	0.0080	0.0121	0.0093	0.0068
3.6	NA	0.0151	0.0081	0.0151	0.0110	0.0074
4.8	NA	0.0153	0.0081	0.0174	0.0120	0.0077
6	NA	0.0154	0.0081	0.0191	0.0126	0.0077
7.2	NA	0.0154	0.0081	NA	0.0130	0.0078

Note: (1) The required reinforcement ratio ρ exceeds the allowed maximum reinforcement of flexure, i.e., $\rho > \rho_{max} = 0.75\rho_b$, meaning that section dimension needs to be increased.

Analysis of Ribbed Approach Slab Subjected to HL93 Highway Load

For ribbed approach slabs subjected to HL93 highway load, 2, 3, and 4 beam alternatives for a given approach slab width of 40 ft. were studied, which corresponded to beam spacings of 32, 16 and 12 ft., respectively. For a ribbed slab with beam spaced at 32, 16, and 12 ft., the slabs with thickness of 14, 12 and 12 in. were used, respectively. For each case, settlement was varied from 0, 0.5, 1, 2, 3 to 6 in.

The results of internal moments, deformations and reaction forces of girder obtained from FE analysis are shown in tables B6 to B13. Since the analysis of ribbed slabs subjected to HS20-44 truckload in the previous study indicates that the internal forces of interior girder controls the beam design, only the internal forces of the interior girder are listed. The moments

shown in tables B8 to B13 can be used for ribbed approach slab reinforcement design.

Table B6
Deflection of beam (60')

Differential Settlement (in)	Beam Spaced at 32 ft.				Beam Spaced at 16 ft.				Beam Spaced at 12 ft.			
	DL		DL+HL93		DL		DL+HL93		DL		DL+HL93	
	Total Deflection (in)		Total Deflection (in)		Total Deflection (in)		Total Deflection (in)		Total Deflection (in)		Total Deflection (in)	
	at Mid-span	at End of Sleeper Slab	at Mid-span	at End of Sleeper Slab	At Mid-span	at End of Sleeper Slab	at Mid-span	at End of Sleeper Slab	at Mid-span	at End of Sleeper Slab	at Mid-span	at End of Sleeper Slab
0	0.072	0.084	0.107	0.102	0.074	0.088	0.112	0.100	0.074	0.090	0.111	0.102
0.5	0.288	0.096	0.349	0.110	0.285	0.098	0.349	0.112	0.274	0.101	0.338	0.116
1	0.445	0.099	0.542	0.116	0.428	0.107	0.530	0.120	0.403	0.111	0.506	0.125
2	0.643	0.113	0.840	0.127	0.562	0.123	0.782	0.135	0.480	0.123	0.715	0.142
3	0.674	0.118	1.037	0.137	0.566	0.125	0.872	0.147	0.481	0.124	0.756	0.149
6	0.675	0.119	1.094	0.142	0.566	0.126	0.875	0.150	0.481	0.126	0.761	0.151

Table B7
Deflection of beam (80')

Differential Settlement (in)	Beam Spaced at 32 ft.				Beam Spaced at 16 ft.				Beam Spaced at 12 ft.			
	DL		DL+HL93		DL		DL+HL93		DL		DL+HL93	
	Total Deflection (in)		Total Deflection (in)		Total Deflection (in)		Total Deflection (in)		Total Deflection (in)		Total Deflection (in)	
	at Mid-span	at End of Sleeper Slab	at Mid-span	at End of Sleeper Slab	At Mid-span	at End of Sleeper Slab	at Mid-span	at End of Sleeper Slab	at Mid-span	at End of Sleeper Slab	at Mid-span	at End of Sleeper Slab
0	0.099	0.106	0.120	0.131	0.105	0.105	0.014	0.115	0.109	0.109	0.137	0.120
0.5	0.326	0.113	0.378	0.123	0.324	0.114	0.380	0.123	0.318	0.119	0.372	0.129
1	0.518	0.120	0.597	0.129	0.504	0.124	0.586	0.132	0.486	0.131	0.568	0.140
2	0.813	0.133	0.959	0.142	0.768	0.144	0.911	0.149	0.724	0.153	0.867	0.161
3	1.024	0.146	1.248	0.155	0.923	0.162	1.149	0.167	0.820	0.168	1.069	0.181
6	1.138	0.159	1.690	0.183	0.944	0.169	1.325	0.191	0.823	0.170	1.153	0.193

Table B8
Internal force of beam spaced at 32 ft. (60')

Differential Settlement (in)	Moment (kip-ft.)		Reaction Force at Sleeper Slab End (kips)			
	DL	DL+HL93	Beam 1		Beam 2	
			DL	DL+HL93	DL	DL+HL93
0	135.8	275.1	5.0	4.3	5.3	3.9
0.5	757.9	1074.4	7.4	6.7	7.2	8.1
1	1085.1	1476.3	16.5	11.1	16.8	15.9
2	1466.3	2141.8	56.5	31.2	56.9	48.0
3	1533.6	2533.6	80.7	71.7	80.7	85.7
6	1532.9	2630.7	88.5	125.4	88.6	101.8

Table B9
Internal force of beam spaced at 32 ft. (80')

Differential Settlement (in)	Moment (kip-ft.)		Reaction Force at Sleeper Slab End (kips)			
	DL	DL+HL93	Beam 1		Beam 2	
			DL	DL+HL93	DL	DL+HL93
0	190.2	283.6	5.7	5.8	6.1	5.4
0.5	1056.5	1355.9	5.8	5.8	6.4	7.1
1	1520.0	2039.9	9.9	8.1	10.2	10.6
2	2165.9	2883.8	27.9	17.5	28.2	25.1
3	2613.0	3493.3	62.9	35.8	64.5	53.0
6	2845.9	4463.0	125.9	155.3	126.2	141.6

Table B10
Internal force of beam spaced at 16 ft. (60')

Differential Settlement (in)	Interior Beam							
	Moment (kip-ft.)		Reaction Force at Sleeper Slab End (kips)					
			Beam 1		Beam 2		Beam 3	
	DL	DL+HL93	DL	DL+HL93	DL	DL+HL93	DL	DL+HL93
0	121.5	218.8	3.4	2.1	5.1	8.4	3.7	1.7
0.5	627.9	922.6	5.0	5.2	6.6	6.8	4.8	5.4
1	874.2	1209.8	14.0	10.5	13.4	9.0	14.2	12.1
2	1086.4	1644.7	51.3	36.9	51.6	27.8	51.6	43.2
3	1098.3	1790.6	58.4	73.0	61.2	74.3	58.6	70.7
6	1099.2	1794.1	62.9	84.0	67.4	90.6	62.9	79.1

Table B11
Internal force of beam spaced at 16 ft. (80')

Differential Settlement (in)	Interior Beam							
	Moment (kip-ft.)		Reaction Force at Sleeper Slab End (kips)					
			Beam 1		Beam 2		Beam 3	
	DL	DL+ HL93	DL	DL+ HL93	DL	DL+ HL93	DL	DL+ HL93
0	172.6	276.2	3.9	4.1	6.3	7.0	3.9	4.3
0.5	894.7	1219.8	4.0	4.4	7.0	6.9	4.0	4.7
1	1256.9	1726.3	7.8	7.1	10.3	8.5	7.8	7.9
2	1751.1	2327.6	26.6	19.0	25.6	16.1	26.6	21.9
3	2034.5	2792.0	64.3	42.0	62.0	33.6	65.5	48.8
6	2069.4	3122.3	88.9	112.0	92.1	112.1	89.4	108.4

Table B12
Internal force of beam spaced at 12 ft. (60')

Differential Settlement (in)	Interior Beam									
	Moment (kip-ft.)		Reaction Force at Sleeper Slab End (kips)							
			Beam 1		Beam 2		Beam 3		Beam 4	
	DL	DL+ HL93	DL	DL+ HL93	DL	DL+ HL93	DL	DL+ HL93	DL	DL+ HL93
0	110.5	207.4	4.9	6.0	4.6	6.7	4.6	4.7	4.8	4.3
0.5	543.4	802.1	8.5	7.8	6.5	6.4	6.4	7.4	8.3	8.8
1	750.3	1048.5	20.7	14.5	14.9	9.6	15.0	12.8	20.8	19.6
2	867.4	1397.1	46.8	43.5	45.7	35.3	45.4	45.7	46.5	51.6
3	867.8	1437.9	48.3	70.4	49.1	63.9	49.1	61.2	48.0	54.5
6	867.9	1446.3	50.1	74.8	53.5	71.0	53.6	66.5	49.8	56.7

Table B13
Internal force of beam spaced at 12 ft. (80')

Differential Settlement (in)	Interior Beam									
	Moment (kip-ft.)		Reaction Force at Sleeper Slab End (kips)							
			Beam 1		Beam 2		Beam 3		Beam 4	
	DL	DL+ HL93	DL	DL+ HL93	DL	DL+ HL93	DL	DL+ HL93	DL	DL+ HL93
0	155.3	266.4	5.9	5.8	6.2	6.2	5.6	6.5	6.0	6.5
0.5	782.5	1093.9	7.4	7.3	6.6	6.1	6.9	7.7	7.8	8.4
1	1097.0	1520.7	13.2	11.1	10.3	8.3	10.2	10.3	13.5	13.7
2	1513.4	2036.6	37.2	25.4	27.4	17.0	27.7	22.9	37.2	33.8
3	1669.1	2406.1	68.4	52.3	63.6	40.3	62.9	51.2	68.3	67.3
6	1672.6	2508.3	73.9	96.9	74.3	90.1	74.0	88.5	74.7	85.0

Since the required reinforcement in exterior beams is less than that in interior beam, the exterior beam should be designed as the same as the interior beam according to the AASHTO code, which requires that exterior beams have strength no less than that of interior beams.

Reinforcement Design of Ribbed Slab according to AASHTO LRFD Code

Tables B8 to B13 show the results of the internal force analysis for ribbed approach slabs subjected to AASHTO LRFD HL93 highway load, considering the effects of different differential settlements. Checking the strength of the beam of the ribbed slabs was conducted according to the AASHTO LRFD Specifications (AASHTO LRFD 2004), namely, with load factors of 1.25 for dead load and 1.75 for live load. The results of reinforcement design of the beam are listed in tables B14 and B15.

Table B14
Design of beam (60')
(f_c'= 4000 psi, f_s = 60,000 psi)

Differential Settlement (in)	Beam Spaced at 32 ft.			Interior Beam Spaced at 16 ft.			Interior Beam Spaced at 12 ft.		
	Moment (kip-ft.)		# of #10 Bars	Moment (kip-ft.)		# of #10 Bars	Moment (kip-ft.)		# of #10 Bars
	DL	LL(HL93)		DL	LL(HL93)		DL	LL(HL93)	
0	135.8	139.3	3	121.5	97.3	2	110.5	96.9	2
0.5	757.9	316.5	7	627.9	294.7	6	543.4	258.7	5
1	1085.1	391.2	9	874.2	335.6	8	750.3	298.2	7
2	1466.3	675.5	14	1086.4	558.3	11	867.4	529.7	10
3	1533.6	1000.0	18	1098.3	692.3	13	867.8	570.1	10
6	1532.9	1097.8	19	1099.2	694.9	13	867.9	578.4	10

Table B15
Design of beam (80')
(f_c'= 4000 psi, f_s = 60,000 psi)

Differential Settlement (in)	Beam Spaced at 32 ft.			Interior Beam Spaced at 16 ft.			Interior Beam Spaced at 12 ft.		
	Moment (kip-ft.)		# of #11 Bars	Moment (kip-ft.)		# of #11 Bars	Moment (kip-ft.)		# of #11 Bars
	DL	LL(HL93)		DL	LL(HL93)		DL	LL(HL93)	
0	190.2	93.4	3	172.6	103.6	2	155.3	111.1	2
0.5	1056.5	299.4	6	894.7	325.1	5	782.5	311.4	5
1	1520.0	519.9	9	1256.9	469.4	8	1097.0	423.7	7
2	2165.9	717.9	12	1751.1	576.5	10	1513.4	523.2	9
3	2613.0	880.3	15	2034.5	757.5	12	1669.1	737.0	11
6	2845.9	1617.1	21	2096.4	1052.9	14	1672.6	835.7	12

Special Study 4 – Capacity Rating of Special Trucks

Analysis in Terms of Special Trucks

The objective of approach slab rating is to determine 1) the safe load-carrying capacity of the slab and 2) whether a specific overweight vehicle may cause damage to the slab. In this study, load rating is performed in accordance with the procedures given in the AASHTO Manual for Condition Evaluation of Bridges *[28]*; it is also conducted based on the standard AASHTO specifications and AASHTO LRFD (LRFR for rating, *[29]*) Specifications respectively.

Standard AASHTO and AASHTO LRFR equations and load factors are utilized respectively in the following rating procedure. For analysis in accordance with the Standard Specifications (STD, *[1]*), the load factors corresponding to the respective group loading are given in STD table 3.22.1A. For LRFD Specifications-based analysis, the factors defined in LRFD tables 3.4.1-1 and 3.4.1-2 were used with the load combination and corresponding limit state creating the maximum load effect *[2]*.

Generally, the rating of a bridge is controlled by the capacity of the component with the lowest rating. According to the AASHTO specifications, the following strength condition equation should be used to determine the load rating of the structure:

$$R.F. = \frac{\phi R_n - \sum[\gamma_D (DL)]}{\gamma_L (LL)(1+I)}$$

The coefficients Φ, γ_D, and γ_L may have different values depending on the type of loading rating (inventory or operating), and rating method (working stress or factored load). Load ratings using the factored load method are used in this study. The general rating formula reduces to the following form for factored load rating:

$$R.F. = \frac{\phi M_n - \sum \gamma_D M_D}{\gamma_L M_L (1+I)}$$

In this study, flat and ribbed approach slabs were rated by using trucks that may be more critical to the approach slab design. In the load rating procedure, the finite element analysis is

used to obtain the internal force caused by the rating load. Three special trucks provided by LADOTD are shown in figures B24 to B26.

The same FE model is used to analyze the internal force of the flat approach slabs subjected to different rating truck loads. For ribbed approach slabs, alternatives with 2, 3, and 4 beams for a given approach slab width of 40 ft. were studied, which corresponds to beam spacings of 32, 16 and 12 ft., with thicknesses of 14, 12 and 12 in., respectively. The internal moments of flat approach slabs with different dimensions are listed in table B16 while the moments of ribbed slabs are shown in table B17.

Load rating of the approach slabs (flat and ribbed), with reinforcement designed for AASHTO standard HS20 and AASHTO LRFD HL93 highway loads in a previous study, was conducted in accordance with standard AASHTO specifications *[1]* and AASHTO LRFR specifications *[29]*, respectively. A preliminary rating showed that the 12 in. thick flat slab and 32 ft. spacing ribbed slab cannot pass the rating. Therefore, they are not recommended for implementation and are not included in the rating tables.

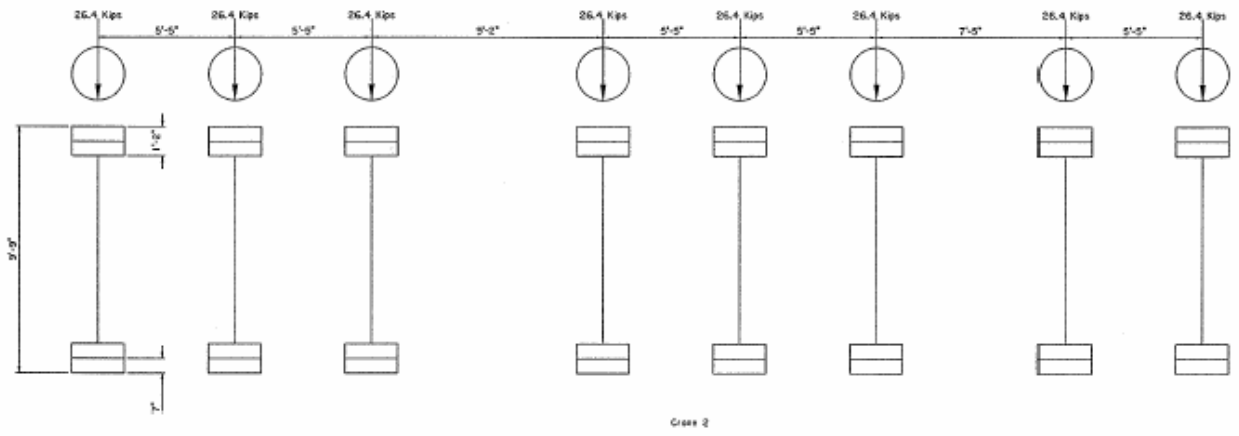

Figure B24
Rating truck 1: heavy crane

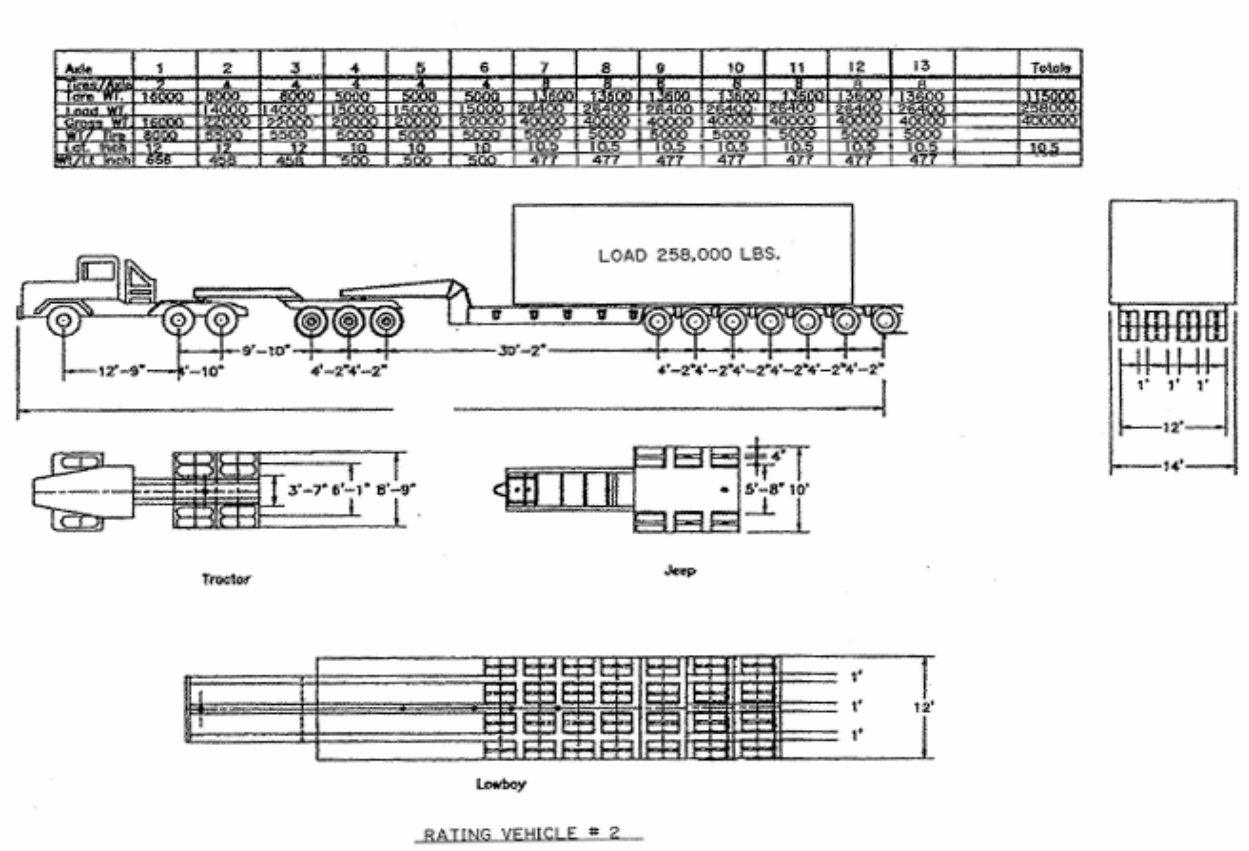

Figure B25
Rating truck 2

Axle	1	2	3	4	5	6	7	8	9	10	11	12	13	14	15	Total
Tires/Axle	2	4	4	8	8	8	8	8	8	8	8	8				
Tare Wt.	16000	12000	12000	7333	7333	7333	7333	7333	7333	7333	7333	7333				106000
Load Wt.		17500	17500	17222	17222	17222	17222	17222	17222	17222	17222	17222				190000
Gross Wt.	16000	29500	29500	24555	24555	24555	24555	24555	24555	24555	24555	24555				296000
Wt/ Tire	8000	7375	7375	3069	3069	3069	3069	3069	3069	3069	3069	3069				
Lot. Inch	12	14	14	7.5	7.5	7.5	7.5	7.5	7.5	7.5	7.5	7.5				
Wt/Lt in.	666	526	526	409	409	409	409	409	409	409	409	409				

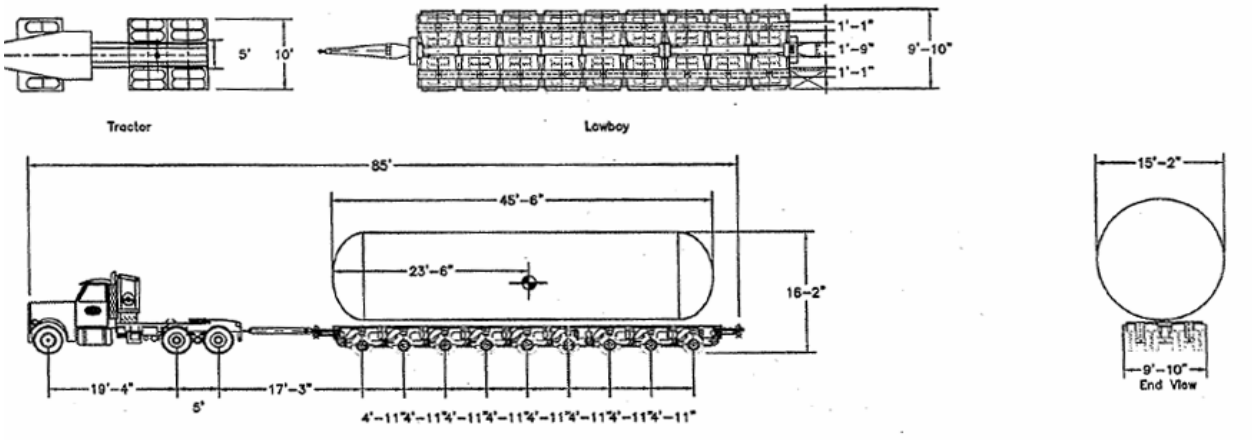

Figure B26
Rating truck 3: heavy tractor-trailer

Table B16
Internal force of flat approach slab subjected to rating truck

Truck Type	Moment of slab with L=40' H=1.5' (kips-ft.)	Moment of slab with L=40' H=2.0' (kips-ft.)	Moment of slab with L=60' H=1.75' (kips-ft.)	Moment of slab with L=60' H=2.25' (kips-ft.)
	DL+LL (DL: M=1697.9)	DL+LL (DL: M=2293.1)	DL+LL (DL: M=4429.1)	DL+LL (DL: M=5724.5)
Rating truck 1	2508.4	3098.6	5636.9	7519.4
Rating truck 2	3236.6	3831.9	6222.3	8611.6
Rating truck 3	2645.9	3236.3	5764.1	7746.5

Table B17
Internal force of ribbed approach slab subjected to rating truck

Truck Type	Moment of Interior Girder with L=60' Spacing=32' (kips-ft.)	Moment of Interior Girder with L=60' Spacing=16' (kips-ft.)	Moment of Interior Girder with L=60' Spacing=12' (kips-ft.)	Moment of Interior Girder with L=80' Spacing=32' (kips-ft.)	Moment of Interior Girder with L=80' Spacing=16' (kips-ft.)	Moment of Interior Girder with L=80' Spacing=12' (kips-ft.)
	DL+LL (DL: M=1532.9)	DL+LL (DL: M=1099.2)	DL+LL (DL: M=867.9)	DL+LL (DL: M=2845.9)	DL+LL (DL: M=2096.4)	DL+LL (DL: M=1672.6)
Rating truck 1	2802.6	1732.9	1372.6	4824.4	3065.4	2299.2
Rating truck 2	3527.3	2206.5	1782.6	5479.6	3718.0	2937.1
Rating truck 3	2896.5	1867.3	1484.8	4830.4	3233.1	2580.2

Rating according to Standard AASHTO Specification

The slab with a span length of 40 ft., thickness of 1.5 ft. and reinforcement designed for AASHTO LRFD HL93 truckload, was taken as an example.

Inventory rating: $\gamma_D = 1.3; \quad \gamma_L = 1.3 \times 1.67 = 2.17;$
(Operating rating: $\gamma_D = 1.3; \quad \gamma_L = 1.3; \quad$)

The compression distance: $a = \frac{A_s f_y}{\beta f_c b} = \frac{(0.0154)(18-3)(480)(60000)}{0.85(4000)(480)} = 4.08 \quad in$

The nominal moment capacity:

$$M_n = A_s f_y (d - \frac{a}{2}) = (110.88)(60000)(15 - \frac{4.08}{2}) = 86220288\ lb - in = 7185.0\ kips - ft$$

The moment due to dead load: $M_{DL} = 1697.9 \quad kips - ft$
The moment due to live load (rating vehicle 1): $M_{LL} = (2508.4 - 1697.9) = 810.5 \quad kips - ft$
The moment due to live load (rating vehicle 2): $M_{LL} = (3236.6 - 1697.9) = 1538.7 \quad kips - ft$
The moment due to live load (rating vehicle 3): $M_{LL} = (2645.9 - 1697.9) = 948.0 \quad kips - ft$

The rating factor (rating vehicle 1): $R.F. = \frac{\phi M_n - \sum \gamma_D M_D}{\gamma_L M_L (1+I)} = \frac{(1.0)(7185.0) - (1.3)(1697.9)}{(2.17)(1053.6)} = 2.18$
The rating factor (rating vehicle 2): $R.F. = \frac{\phi M_n - \sum \gamma_D M_D}{\gamma_L M_L (1+I)} = \frac{(1.0)(7185.0) - (1.3)(1697.9)}{(2.17)(2000.3)} = 1.15$
The rating factor (rating vehicle 3): $R.F. = \frac{\phi M_n - \sum \gamma_D M_D}{\gamma_L M_L (1+I)} = \frac{(1.0)(7185.0) - (1.3)(1697.9)}{(2.17)(1232.4)} = 1.86$

The load rating results for flat and ribbed approach slab are listed in tables B18 and B19.

Table B18
Rating result of flat approach slab (AASHTO standard)

Rating Vehicle	Approach slab with L=40' H=1.5'		Approach slab with L=40' H=2.0'		Approach slab with L=60' H=1.75'		Approach slab with L=60' H=2.25'	
	R.F		R.F		R.F		R.F	
	Inventory	Operating	Inventory	Operating	Inventory	Operating	Inventory	Operating
Rating truck 1	2.18	3.63	2.19	3.66	2.10	3.50	1.59	2.65
Rating truck 2	1.15	1.91	1.15	1.91	1.41	2.36	0.99	1.65
Rating truck 3	1.86	3.11	1.87	3.12	1.90	3.17	1.41	2.35

Table B19
Rating result of ribbed approach slab (AASHTO standard)

Truck Type	Interior Girder with L=60' Spacing=16'		Interior Girder with L=60' Spacing=12'		Interior Girder with L=80' Spacing=16'		Interior Girder with L=80' Spacing=12'	
	R.F		R.F		R.F		R.F	
	Inventory	Operating	Inventory	Operating	Inventory	Operating	Inventory	Operating
Rating truck 1	1.50	2.51	1.75	2.92	1.52	2.53	1.78	2.97
Rating truck 2	0.86	1.44	0.97	1.61	0.91	1.51	0.88	1.47
Rating truck 3	1.24	2.07	1.43	2.39	1.29	2.16	1.23	2.05

Rating according to AASHTO LRFR Specification

The LRFR adopts three levels of rating methodology. They are: dsign load rating, legal load rating, and permit load rating. While the provided trucks should fit in either the legal or permit truck, all the three levels of rating were conducted below.

(1) Design Load Rating

The currently used slab with span length of 40 ft., thickness of 1.5 ft. and reinforcement designed for AASHTO LRFD HL93 truckload, was taken as an example.

Inventory rating: $\gamma_D = 1.25; \quad \gamma_L = 1.75;$
(Operating rating: $\gamma_D = 1.25; \quad \gamma_L = 1.35; \quad$)

The compression distance: $a = \frac{A_s f_y}{\beta f_c b} = \frac{(0.0154)(18-3)(480)(60000)}{0.85(4000)(480)} = 4.08 \quad in$

The nominal moment capacity:

$$M_n = A_s f_y (d - \frac{a}{2}) = (110.88)(60000)(15 - \frac{4.08}{2}) = 86220288\ lb - in = 7185.0\ kips - ft$$

The moment due to dead load: $M_{DL} = 1697.9 \quad kips - ft$
The moment due to live load (rating vehicle 1): $M_{LL} = (2508.4 - 1697.9) = 810.5 \quad kips - ft$
The moment due to live load (rating vehicle 2): $M_{LL} = (3236.6 - 1697.9) = 1538.7 \quad kips - ft$
The moment due to live load (rating vehicle 3): $M_{LL} = (2645.9 - 1697.9) = 948.0 \quad kips - ft$

The rating factor (rating vehicle 1): $R.F. = \frac{\phi M_n - \sum \gamma_D M_D}{\gamma_L M_L (1+I)} = \frac{(1.0)(7185.0) - (1.25)(1697.9)}{(1.75)(1053.6)} = 2.68$
The rating factor (rating vehicle 2): $R.F. = \frac{\phi M_n - \sum \gamma_D M_D}{\gamma_L M_L (1+I)} = \frac{(1.0)(7185.0) - (1.25)(1697.9)}{(1.75)(2000.3)} = 1.41$
The rating factor (rating vehicle 3): $R.F. = \frac{\phi M_n - \sum \gamma_D M_D}{\gamma_L M_L (1+I)} = \frac{(1.0)(7185.0) - (1.25)(1697.9)}{(1.75)(1232.4)} = 2.29$

The load rating results for flat and ribbed approach slab are listed in tables B20 and B21.

Table B20
Rating result of flat approach slab (LRFR-design load)

Rating Vehicle	Approach slab with L=40' H=1.5'		Approach slab with L=40' H=2.0'		Approach slab with L=60' H=1.75'		Approach slab with L=60' H=2.25'	
	R.F		R.F		R.F		R.F	
	Inventory	Operating	Inventory	Operating	Inventory	Operating	Inventory	Operating
Rating truck 1	2.68	3.48	2.72	3.52	2.62	3.40	1.99	2.58
Rating truck 2	1.41	1.83	1.42	1.84	1.77	2.29	1.24	1.61
Rating truck 3	2.29	2.97	2.32	3.01	2.37	3.08	1.77	2.29

Table B21
Rating result of ribbed approach slab (LRFR-design load)

Truck Type	Interior Girder with L=60' Spacing=16'		Interior Girder with L=60' Spacing=12'		Interior Girder with L=80' Spacing=16'		Interior Girder with L=80' Spacing=12'	
	R.F		R.F		R.F		R.F	
	Inv.	Ope.	Inv.	Ope.	Inv.	Ope.	Inv.	Ope.
Rating truck 1	1.86	2.41	2.20	2.85	1.88	2.44	2.18	2.83
Rating truck 2	1.06	1.38	1.22	1.58	1.13	1.46	1.08	1.40
Rating truck 3	1.53	1.99	1.80	2.34	1.61	2.08	1.50	1.95

(2) Legal Load Rating

Operating rating: $\gamma_D = 1.25$; $\gamma_L = 1.8$;

The load rating results for flat and ribbed approach slab are listed in tables B22 and B23.

Table B22
Rating result of flat approach slab (LRFR-legal load)

Rating Vehicle	Approach slab with L=40' H=1.5'	Approach slab with L=40' H=2.0'	Approach slab with L=60' H=1.75'	Approach slab with L=60' H=2.25'
	R.F	R.F	R.F	R.F
	Operating	Operating	Operating	Operating
Rating truck 1	2.61	2.64	2.55	1.94
Rating truck 2	1.37	1.38	1.72	1.20
Rating truck 3	2.23	2.26	2.31	1.72

Table B23
Rating result of ribbed approach slab (LRFR-legal load)

Truck Type	Interior Girder with L=60' Spacing=16'	Interior Girder with L=60' Spacing=12'	Interior Girder with L=80' Spacing=16'	Interior Girder with L=80' Spacing=12'
	R.F	R.F	R.F	R.F
	Operating	Operating	Operating	Operating
Rating truck 1	1.81	2.14	1.83	2.12
Rating truck 2	1.03	1.18	1.10	1.05
Rating truck 3	1.49	1.75	1.56	1.46

(3) Permit Load Rating

Operating rating: $\gamma_D = 1.25$; $\gamma_L = 1.3$;

The load rating results for flat and ribbed approach slab are listed in tables B24 and B25.

Table B24
Rating result of flat approach slab (LRFR-permit load)

Rating Vehicle	Approach slab with L=40' H=1.5'	Approach slab with L=40' H=2.0'	Approach slab with L=60' H=1.75'	Approach slab with L=60' H=2.25'
	R.F	R.F	R.F	R.F
	Operating	Operating	Operating	Operating
Rating truck 1	3.61	3.66	3.53	2.68
Rating truck 2	1.90	1.91	2.38	1.67
Rating truck 3	3.09	3.12	3.19	2.38

Table B25
Rating result of ribbed approach slab (LRFR-permit load)

Truck Type	Interior Girder with L=60' Spacing=16'	Interior Girder with L=60' Spacing=12'	Interior Girder with L=80' Spacing=16'	Interior Girder with L=80' Spacing=12'
	R.F	R.F	R.F	R.F
	Operating	Operating	Operating	Operating
Rating truck 1	2.50	2.96	2.54	2.93
Rating truck 2	1.43	1.64	1.52	1.45
Rating truck 3	2.07	2.43	2.16	2.03

Research Dissemination

1. Cai, C. S., Shi, X. M., Voyiadjis, G. Z. and Zhang, Z. J. (2005) "Structural Performance of Bridge Approach Slab under Given Embankment Settlement." Journal of Bridge Engineering, ASCE, 10(4), 482-489.
2. Shi, X. M., Cai, C. S., Voyiadjis, G. Z., and Zhang, Z. J. (2005) "Design of Ribbed Concrete Approach Slab Based on Its Interaction with Embankment" *Transportation Research Record, J. of the Transportation Research Board,* National Research Council (in press, also presented).
3. Shi, X. M., Cai, C. S., Voyiadjis, G. Z. and Zhang Z. J. (2004) "Finite element analysis of concrete approach slab on soil embankment", Geo-Trans 2004, the Geo-Institute of the American Society of Civil Engineers, Los Angeles, CA, July 27-31, 2004, ASCE Geotechnical Special Publication no. 126, 393-402 (also presented).
4. Shi, X. M., Cai, C. S., Voyiadjis, G. Z., and Zhang, Z. J. (2004) "Determination of Interaction between Bridge Concrete Approach Slab and Embankment Settlement with 3D Finite Element Modeling" Presentation, ASCE/ACI Louisiana Civil Engineering Conference and Show, September 9th & 10th, at the Pontchartrain Center in Kenner, LA.